

https://dspace.org/

Thermodynamic and Kinetic Study of the Production of Carbon Nanotube Yarn from Chemical Vapour Deposition Reactor

Mahangani, Ndanganeni

2019

https://hdl.handle.net/10539/28780

Mahangani, Ndanganeni (2019) Thermodynamic and kinetic study of the production of carbon nanotube yarn from chemical vapour deposition reactor, University of the Witwatersrand, Johannesburg, <http://hdl.handle.net/10539/28780>

Downloaded from a DSpace repository. https://dspace.org/



Thermodynamic and Kinetic Study of the Production of Carbon Nanotube Yarn from Chemical Vapour Deposition Reactor

Ndanganeni Mahangani
1774947

A dissertation submitted to the Faculty of Engineering and the Built Environment, University of the Witwatersrand, Johannesburg, in fulfilment of the requirement for the Degree of Master of Science in Engineering.

Supervisor: Prof Michael O. Daramola
Co-Supervisor: Prof Sunny E. Iyuke

May 2019

DECLARATION

I declare that, this dissertation is my own and unassisted effort. It has been submitted for the degree of Master of Science at the University of the Witwatersrand, Johannesburg. I declare that it has never been submitted before for examination in other University for any other degrees.

_____

Signature of Student

_____ Day of _____

ABSTRACT

Overcoming the low production rate of carbon nanotubes (CNTs) could be instrumental to reducing their cost of production and enhancing its wide application. Understanding the kinetics of the production of yarn from CNTs, through kinetic model development could assist in the optimisation of the production and this makes the application of yarn as a replacement to filament in incandescent bulb promising.

In this study, kinetic of the production of CNTs, an intermediate in the production of yarn, is presented. Several experiments were conducted using Ferrocene as catalyst in a CVD reactor. The reaction of CH_4 on Ferrocene catalyst is via heterogeneous catalysis because methane is in gaseous phase and Ferrocene in solid phase. Langmuir Hinshelwood was used to develop a kinetic model based on these two- phase phenomena. The effect of CH_4 concentration was investigated as well. The derived kinetic model fits the experimentally measured data with 95% confidence interval.

Good quality CNTs were obtained at methane flow rate of 125 ml/min. The CNTs produced at this flow rate has high purity, low tube diameter and spinnable long array as compared to the one produced at 100 ml/min and 150 ml/min. Yarn was produced at this flow rate (125 ml/min) at a reactor temperature of 900, 950 and 1000^{o}C. Characterisation techniques such as Scanning Electron Microscopy (SEM), Transition Electron Microscopy (TEM), Energy-Dispersive X-ray (EDX), Gas Chromatography (GC) and Raman Spectroscopy were used to analyse the product from experiments. At all studied reactor temperatures CNT yarns were synthesised as observed in SEM images.

Four Probe method was used to measure the electrical conductivity of as-produced CNTs and yarn. By using the proposed CH_4 flow rate (125 ml/min) the produced CNT yarn was found to be metallic and electrically conductive. The studied electrical conductivity of as-produced

CNTs were found to be approximately 2 times higher than their yarn. Yarn produced at reactor temperature of 950^{o}C proved to have high quality and more electrically conductive than those produced at 900 and 1000^{o}C.

The thermodynamic properties of CNTs yarn were studied using TGA/DSC equipment. Polynomial models for predicting Specific heat capacities of yarns produced in this study were developed. The results showed that the temperature at which yarn is produced has an effect on a thermodynamic property such as heat capacities, enthalpy and entropy.

DEDICATION

This dissertation is dedicated to the memory of my sister, **Takalani Regina Mahangani**. I miss you every day and you are appreciated for your unconditional support you offered throughout my studies.

ACKNOWLEDGMENTS

I would like to thank my Supervisors, Prof Michael O. Daramola and Prof Sunny E. Iyuke for their support and their treasured knowledge and experience that motivated me to complete this study.

Thanks to the financial support offered by National Research Foundation (NRF).

I would also like to show gratitude towards the students and staff from the University of Witwatersrand for the support and creating a friendly working environment.

In addition, I would like to thank my family for love, encouragement, and support throughout the studies.

Last but not least, I would like to thank God Almighty for the gift of life that he gave to me.

PUBLICATIONS

1. **Mahangani, N.,** Aberefa, O., Igbokwe, E., Bodiba, V., Daramola, M.O., Iyuke, S.E. (2019). Production of CNT yarns for use as filaments in incandescent bulb: Kinetic study of the production of CNT. - Submitted.

2. **Mahangani, N.,** Igbokwe, E., Aberefa, O., Bodiba, V., Daramola, M.O., Iyuke, S.E. (2019). Production of CNT yarns from methane gas for use as filaments in incandescent bulbs: Thermodynamic properties of as-spun CNT yarns. – Submitted

3. Bodiba, V., Igbokwe, E., **Mahangani, N**., Aberefa, O., Daramola, M. O., & Iyuke, S. E. (2018, September). Production of CNT yarns for use as filaments in incandescent bulb: effect of carbon source and state of catalyst on production of CNTS. In IOP Conference Series: Materials Science and Engineering (Vol. 413, No. 1, p. 012027). IOP Publishing.

TABLE OF CONTENTS

DECLARATION i
ABSTRACT ii
DEDICATION iv
ACKNOWLEDGMENTS v
PUBLICATIONS vi
TABLE OF CONTENTS vii
LIST OF FIGURES x
LIST OF TABLES xiii
NOMENCLATURE xiv
CHAPTER ONE 1
1.0. Introduction 1
1.1. Problem Statement 2
1.2. Research Questions 2
1.3. Research Aim and Objectives 2
1.4. Expected Outcome 3
1.5. Dissertation Outline 3
CHAPTER TWO 4
2.0. Literature Review 4
2.1. Carbon nanotubes Structures 4
2.1.1. Single walled carbon nanotubes (SWCNTs) 6
2.1.2. Multi walled carbon nanotubes (MWCNTs) 7
2.2. Methods of Carbon Nanotube Production 7
2.2.1. Laser ablation 8
2.2.2. Arc Discharge method 10
2.2.3. Chemical Vapour Deposition 11
2.3. Catalysts for CNTs/ CNT yarn production 12
2.3.1. Supported Catalyst 12
2.3.2. Floating Catalyst 14
2.4. CNTs Purification 15
2.4.1. Physical purification method 16
2.4.2. Chemical Purification Method 17
2.4.3. Multi step purification method 19

2.5. CNT yarn Spinning Methods 20
2.5.1. Forest spinning 21
2.5.2. Direct Spinning 21
2.5.3. Surface based coagulation 22
2.5.4. Liquid-crystalline spinning 23
2.6. Characterisation Techniques 24
2.6.1. Thermal Gravimetric Analysis (TGA) 24
2.6.2. Scanning Electron Microscopy (SEM) 25
2.6.3. Transmission Electron Microscopy (TEM) 26
2.6.4. Raman Spectroscopy 26
2.6.5. Gas Chromatogram (GC) 27
2.6.6. Energy-dispersive X-ray spectroscopy (EDX) 28
2.6.7. Differential Scanning Calorimeter (DSC) 29
2.6.8. Four probe 30
2.7. Kinetic Study for Carbon Nanotube Production 30
2.7.1. Growth Mechanism 30
2.7.2. Kinetic Models 32
2.8. Thermodynamic Study for Carbon Nanoyarn 35
CHAPTER THREE 37
3.0. Methodology 37
3.1. Synthesis of CNT yarn using CVD reactor 37
3.2. Characterisation of CNTs and CNT yarn 38
3.2.1. Gas Chromatography 38
3.2.2. Transition Electron Microscope 39
3.2.3. Scanning Electron Microscope 39
3.2.4. Raman Spectroscopy 39
3.3. Thermodynamic Properties measurement of the CNT yarn 40
3.4. Measuring the electrical conductivity of the CNT yarn 40
CHAPTER FOUR 42
4.0. Production of CNTs and Kinetic study 42
4.1. Introduction 42
4.2. Experimental procedure and development of kinetic model 42
4.2.1. Experimental Procedure 42
4.2.2. Development of Kinetic Model 43
4.3. Results and discussion 46

4.3.1. SEM images of CNTs produced at a reactor temperature of 900°C 46
4.3.2. SEM images of CNTs produced at a reactor temperature of 950°C 47
4.3.3. SEM images of CNTs produced at a reactor temperature of 1000°C 49
4.3.4. Effect of methane flow rate on quality of CNTs obtained at 900°C 51
4.3.5. TEM images of CNTs produced at a reactor temperature of 950°C 53
4.3.6. TEM images of CNTs produced at a reactor temperature of 1000°C 55
4.3.7. Raman Spectrometer Results 57
4.3.8. Analysis by Gas Chromatogram 60
4.3.9. Kinetic Modelling 61
4.4. Summary 64
CHAPTER FIVE 65
5.0. Thermodynamic properties and electrical conductivity of CNT yarn 65
5.1. Introduction 65
5.2. Experimental procedure 66
5.3. Results and Discussion 66
5.3.1. Morphology of the produced yarn 66
5.3.2. Electrical conductivity 70
5.3.3. Thermodynamic Properties 73
5.4. Summary 77
CHAPTER SIX 78
6.0. Conclusion and Recommendations 78
6.1. Conclusion 78
6.2. Recommendations 79
References 80
APPENDIX 90
Appendix 1: SEM Images 90
Appendix 2: Calculating rate for kinetic model 94
Appendix 3: Data for production rate plot 98
Appendix 4: Data for Electrical Conductivity calculations and plot 99
Appendix 5: Sample Chromatogram 100
Appendix 6: Thermodynamic Properties of yarn 101

LIST OF FIGURES

FIGURE 2.1: GRAPHENE SHEET BEEN ROLLED TO FORM CNT (ADAPTED FROM: SHESHMANI ET AL.,2013) 5
FIGURE 2.2: SCHEMATIC ILLUSTRATION OF ZIG-ZAG, ARMCHAIR AND CIRAL CNTS. (RAHMANDOUST & OCHSNER,2011) 6
FIGURE 2.3:ATOMIC STRUCTURE OF CNTS (DRESSELHAUS ET AL.,2003) 7
FIGURE 2.4: LASER ABLATION (ADAPTED FROM: CHOUDHARY ET AL.,2013) 8
FIGURE 2.5: TEM RESULTS OF CNTS PRODUCED FROM CATALYST A) NI/Y B)NI/CO (USED WITH PERMISSION FROM: EKLUND ET AL., 2002) 10
FIGURE 2.6: SCHEMATIC ILLUSTRATION OF ARC DISCHARGE SET-UP (ADAPTED FROM: ARON & SHARMA, 2014) 10
FIGURE 2.7:SCHEMATIC ILLUSTRATION OF CHEMICAL VAPOR DEPOSITION (IYUKE ET AL.,2009) 11
FIGURE 2.8:MECHANISTIC MODEL OF CNTS FOREST BEEN DRAWN INTO YARN (ADAPTED FROM ZHANG ET AL., 2006) 12
FIGURE 2.9: FLOW CHART OF THE REPRESENTATIVE PROCEDURE FOR CNTS PURIFICATION BASED ON FUNCTION AND CHARACTERISTIC OF PURIFICATION METHOD (ADAPTED FROM HOU ET AL., 2008) 20
FIGURE 2.10:FOREST SPINNING (ADAPTED FROM:MIAO, 2013) 21
FIGURE 2.11:A SCHEMATIC DIAGRAM OF DIRECT SPINNING PROCESS (ADAPTED FROM: MOTTA ET AL., 2007) 22
FIGURE 2.12:SURFACTANT-BASED COAGULATION SPINNING (ADAPTED FROM: VIGOLO, 2000)23
FIGURE 2.13: LIQUID CRYSTALLINE SPINNING TECHNIQUE FOR CNT YARN (ADAPTED FROM:ERICSON, 2004) 23
FIGURE 2.14: SCHEMATIC ILLUSTRATION OF TG ANALYSIS 25
FIGURE 2.15: SCHEMATIC ILLUSTRATION OF SEM (ADAPTED FROM: RUSS, 2013) 25
FIGURE 2.16: SCHEMATIC ILLUSTRATION OF TEM (FRIEL, 2003). 26
FIGURE 2.17:TYPICAL RAMAN SPECTRA OF CNTS. 27
FIGURE 2.18: SCHEMATIC ILLUSTRATION OF GC (ADAPTED FROM MAPHUTHA, 2010). 28
FIGURE 2.19: TYPICAL EDX SPECTRA 28
FIGURE 2.20: SCHEMATIC ILLUSTRATION OF DSC SET-UP. 29
FIGURE 2.21: SCHEMATIC REPRESENTATIVE OF FOUR PROBE METHOD (UMMARTYOTIN ET AL.,2011) 30
FIGURE 2.22: CNTS FORMATION MECHANISM (ADAPTED FROM: KUMAR, 2011) 31
FIGURE 2.23: GRAPHS SHOWING, MOLAR HEAT SPECIFICATION AT DIFFERENT TEMPERATURES (NAN ET AL., 2009) 36
FIGURE 3.1:PROCESS FLOW DIAGRAM OF EXPERIMENTAL SET-UP FOR CNT YARN PRODUCTION. 37
FIGURE 4.1: CNTS PRODUCED AT METHANE FLOW RATE OF 100 ML/MIN (900^{O}C) 46
FIGURE 4.2: CNTS PRODUCED AT METHANE FLOW RATE OF 125 ML/MIN (900^{O}C) 47
FIGURE 4.3: CNTS PRODUCED AT METHANE FLOW RATE OF 150 ML/MIN (900^{O}C) 47
FIGURE 4.4:SEM IMAGE OF CNTS PRODUCED AT METHANE FLOW RATE OF 100 ML/MIN (950^{O}C) 48
FIGURE 4.5:SEM IMAGE OF CNTS PRODUCED AT METHANE FLOW RATE OF 125 ML/MIN (950^{O}C) 48

FIGURE 4.6:SEM IMAGE OF CNTS PRODUCED AT 150 ML/MIN METHANE FLOW RATE (950^{O}C) 49
FIGURE 4.7: SEM IMAGE OF CNTS PRODUCED AT 100 ML/MIN METHANE FLOW RATE (1000^{O}C) 50
FIGURE 4.8: SEM IMAGES OF CNTS PRODUCED AT 125 ML/MIN METHANE FLOW RATE(1000^{O}C) 50
FIGURE 4.9:SEM IMAGE OF CNTS PRODUCED AT 150 ML/MIN METHANE FLOW RATE (1000^{O}C). 51
FIGURE 4.10:TEM IMAGE OF CNTS PRODUCED AT METHANE FLOW RATE OF 100 ML/MIN (900^{O}C). 52
FIGURE 4.11: TEM IMAGES OF CNTS PRODUCED AT METHANE FLOW RATE OF 125 ML/MIN (900^{O}C). 52
FIGURE 4.12: TEM IMAGE OF CNTS PRODUCED AT METHANE FLOW RATE OF 150 ML/MIN (900^{O}C). 53
FIGURE 4.13: TEM IMAGE OF CNTS PRODUCED AT METHANE FLOW RATE OF 100 ML/MIN (950^{O}C). 54
FIGURE 4.14: TEM IMAGE OF CNTS PRODUCED AT METHANE FLOW RATE OF 125 ML/MIN (950^{O}C). 54
FIGURE 4.15: TEM IMAGE OF CNTS PRODUCED AT METHANE FLOW RATE OF 150 ML/MIN (950^{O}C). 55
FIGURE 4.16:TEM MAGE OF CNTS PRODUCED AT METHANE FLOW RATE OF 100 ML/MIN (1000^{O}C). 56
FIGURE 4.17: TEM IMAGE OF CNTS PRODUCED AT METHANE FLOW RATE OF 125 ML/MIN (1000^{O}C). 56
FIGURE 4.18: TEM IMAGE OF CNTS PRODUCED AT METHANE FLOW RATE OF 150 ML/MIN (1000^{O}C). 57
FIGURE 4.19:RAMAN SHIFT OF CNTS PRODUCED AT 900^{O}C AND METHANE FLOW RATE OF (A) 100 ML/MIN; (B)125 ML/MIN (C); 150 ML/MIN. 58
FIGURE 4.20:RAMAN SHIFT OF CNTS PRODUCED AT 950^{O}C AND METHANE FLOW RATE OF (A) 100 ML/MIN; (B) 125 ML/MIN; (C) 150 ML/MIN. 59
FIGURE 4.21: RAMAN SHIFT OF CNTS PRODUCED AT 1000^{O}C AND METHANE FLOW RATE OF (A) 100 ML/MIN; (B)125 ML/MIN; (C) 150 ML/MIN. 59
FIGURE 4.22: EXPERIMENTAL AND SIMULATED PRODUCTION RATE OF CNTS PRODUCED AT 900^{O}C 62
FIGURE 4.23: EXPERIMENTAL AND SIMULATE D PRODUCTION RATE OF CNTS PRODUCED AT 950^{O}C 63
FIGURE 4.24: EXPERIMENTAL AND SIMULATED PRODUCTION RATE OF CNTS PRODUCED AT 1000^{O}C 63
FIGURE 5.1:SEM IMAGE OF CNT YARN PRODUCED AT 900^{O}C 67
FIGURE 5.2: EDX SPECTRUM OF CNT YARN PRODUCED AT 900^{O}C 67
FIGURE 5.3:SEM IMAGE OF CNT YARN PRODUCED AT 950^{O}C 68
FIGURE 5.4:EDX SPECTRUM OF CNT YARN PRODUCED AT 950^{O}C 68
FIGURE 5.5:SEM IMAGE OF CNT YARN PRODUCED AT 1000^{O}C 69
FIGURE 5.6: EDX SPECTRUM OF CNT YARN PRODUCED AT 1000^{O}C 69
FIGURE 5.7:CURRENT-VOLTAGE RELATIONSHIP FOR CNTS AND CNT YARN PRODUCED AT 900^{O}C 70

FIGURE 5.8:CURRENT-VOLTAGE RELATIONSHIP FOR CNTS AND CNT YARN PRODUCED AT 950^{O}C 71
FIGURE 5.9:CURRENT-VOLTAGE RELATIONSHIP FOR CNTS AND CNT YARN PRODUCED AT 1000^{O}C 71
FIGURE 5.10: ELECTRICAL CONDUCTIVITY OF CNTS AND CNT YARN PRODUCED AT DIFFERENT TEMPERATURE 72
FIGURE 5.11: THERMOANALYTICAL CURVE OF YARN PRODUCED AT 900^{O}C 73
FIGURE 5.12: THERMOANALYTICAL CURVE OF YARN PRODUCED AT 950^{O}C 73
FIGURE 5.13:THERMOANALYTICAL CURVE OF YARN PRODUCED AT 1000^{O}C 74
FIGURE 5.14:SPECIFIC HEAT CAPACITIES OF YARN PRODUCED AT DIFFERENT REACTOR TEMPERATURE 75
FIGURE 0.1:CNTS PRODUCED AT METHANE FLOW RATE OF 100 ML/MIN AND 900^{O}C 90
FIGURE 0.2:CNTS PRODUCED AT METHANE FLOW RATE OF 125 ML/MIN AND 900^{O}C 90
FIGURE 0.3:CNTS PRODUCED AT METHANE FLOW RATE OF 150 ML/MIN AND 900^{O}C 90
FIGURE 0.4: CNTS PRODUCED AT METHANE FLOW RATE OF 100 ML/MIN AND 950^{O}C 91
FIGURE 0.5: CNTS PRODUCED AT METHANE FLOW RATE OF 125 ML/MIN AND 950^{O}C 91
FIGURE 0.6: CNTS PRODUCED AT METHANE FLOW RATE OF 150 ML/MIN AND 950^{O}C 91
FIGURE 0.7:CNTS PRODUCED AT METHANE FLOW RATE OF 100 ML/MIN AND 1000^{O}C 92
FIGURE 0.8:CNTS PRODUCED AT METHANE FLOW RATE OF 125 ML/MIN AND 1000^{O}C 92
FIGURE 0.9:CNTS PRODUCED AT METHANE FLOW RATE OF 150 ML/MIN AND 1000^{O}C 92
FIGURE 0.10:SEM IMAGE OF YARN PRODUCED AT 900^{O}C 93
FIGURE 0.11: SEM IMAGES OF YARN PRODUCED AT 950^{O}C 93
FIGURE 0.12:SEM IMAGE OF YARN PRODUCED AT 1000^{O}C 93
FIGURE 0.13: GAS CHROMATOGRAM OF EXPERIMENT AT 950^{O}C AND CH4 FLOW RATE OF 100 ML/MIN 100

LIST OF TABLES

TABLE 2.1: DIFFERENT CATALYSTS USED TO PRODUCE CERTAIN CNTS 14
TABLE 2.2:YARN CONDUCTIVITY BY DIFFERENT SPINNING METHODS 24
TABLE 3.1: SUMMARY OF THE EXPERIMENTAL CONDITIONS 38
TABLE 3.2: PRODUCT GASES RETENTION TIME 39
TABLE 4.1:I_D/I_G RATIO OF CNTS PRODUCED AT REACTOR TEMPERATURE OF 900^OC, 950^OC AND 1000^OC. 60
TABLE 4.2: GAS CHROMATOGRAM ANALYSIS OF THE OUTLET GAS FROM CVD REACTOR. 61
TABLE 5.1: AVERAGE HEAT CAPACITIES AND THERMODYNAMIC FUNCTION OF YARN PRODUCED AT 900^OC 76
TABLE 5.2: AVERAGE HEAT CAPACITIES AND THERMODYNAMIC FUNCTION OF YARN PRODUCED AT 950^OC 76
TABLE 5.3: HEAT CAPACITIES AND THERMODYNAMIC FUNCTION OF YARN PRODUCED AT 1000^OC 77
TABLE 0.1: FIGURE 2.22 DATA 98
TABLE 0.2:FIGURE 2.23 DATA 98
TABLE 0.3: FIGURE 2.24 DATA 98
TABLE 0.4:FIGURE 4.25 DATA AND CALCULATIONS 99
TABLE 0.5: DETAILED DATA FOR TABLE 5.1 101
TABLE 0.6: DETAILED DATA FOR TABLE 5.2 102
TABLE 0.7: DETAILED DATA FOR TABLE 5.3 104

NOMENCLATURE

CNTs - Carbon Nanotubes

CVD - Chemical Vapour Deposition

SWCNTs - Single Walled Carbon Nanotubes

MWCNTs - Multi Walled Carbon Nanotubes

DWCNTs – Double Walled Carbon Nanotubes

CH_4 – Methane

H_2 – Hydrogen gas

Ar – Argon

ΔH – Change in Enthalpy

ΔS – Change in Entropy

Cp – Heat Capacity

n – Chirality

Ch – Chiral Vector

^oC – Degrees Celsius

d – Diameter

nm – Nano Meters

Fe – Iron

β– heating rate

ρ – Resistivity

σ – Electrical Conductivity

Ω – Ohm's

TGA - Thermal Gravimetric Analyser

SEM - Scanning Electron Microscopy

TEM - Transmission Electron Microscopy

GC - Gas Chromatogram

EDX - Energy-dispersive X-ray spectroscopy

DSC - Differential Scanning Calorimeter

PID – Proportional Integral Derivatives

RPM – Revolution per minute

T - Temperature

Θ- Chiral Angle

RBM – Radial breathing mode

L – Length

R – Resistance

r – Reaction Rate

K – Chemical Equilibrium Constant

k – Reaction Constant

* - Catalyst activity

[A] – Concentration of ‘A’ Substance

ml/min – Millilitre per Minutes

A – Ampere

V – Voltage

I – Current

mW – Milliwatt

J – Joules

mg – milligram

G – Graphitisation

D – Defects

S/m – Siemens per meter

µm – Micrometer

ΔQ – Heat change

N_2 – Nitrogen gas

$C_{10}H_{10}Fe$ – Ferrocene

M – Motor

SS – Stainless Steel

ppm - Parts Per Million

GNF – Graphite Nano-fibre

CHAPTER ONE

1.0. Introduction

Iijima (1991) in his study discovered a long, thin cylinder of carbon called carbon nanotubes (CNTs). Due to outstanding physical and chemical properties that CNTs exhibit, they have attracted many researchers to research about their remarkable properties. Different kind of techniques have been used to synthesis CNTs (Iijima, 1991; Thess et al., 1996; Dillon et al. ,1997), but Catalytic Chemical Vapour deposition (CCVD) was found to be the cheapest way to produce CNTs of high quality and purity (Rafique & Iqbal, 2011). Several steps of CNTs synthesis in CCVD are acknowledged and can be outlined as follows: Decomposition of carbon precursor to generate carbon atom and carbon cluster, carbon atom and carbon cluster dissolution on the metallic nanoparticle, carbon precipitation from saturated metallic nano-particles and finally tubular carbon structure formation (Perez-Cabero et al., 2004).

CNTs building block can be spun into a yarn which has emerged as a high-performance material with exceptional properties derived from those of CNTs (Hernandez et al., 2006). One of many interesting properties of CNTs is its electrical conductivity. Research on CNT yarn shows that to obtain CNTs with excellent electrical conductivity comparable to the individual nanotubes, it is imperative to properly control the morphology of macro-scopic assemblies of CNTs (Xu et al., 2013). There are different types of CNTs, but they are normal categorised as either Single Walled Carbon Nanotubes (SWCNTs) or Multi Walled Carbon Nanotubes (MWCNTs), which differ in the arrangement of their graphene cylinders. MWCNTs have many layers while SWCNTs have one single layer of graphene (Iyuke et al., 2009). SWCNTs give a yarn of best electrical conductivity as compared to MWCNTs (Bettinger, 2004).

Since CNTs have excellent conductivity and are cost effective, they can outperform the existing conductors. CNTs are thus expected to be one of the most promising material in future electronic industries (Lekawa et al., 2014; Wei et al., 2004). However, the challenge of transferring excellent electrical conductivity of individual CNT to CNT macro-structure still stands (Miao,2013). A number of research studies have already been conducted with regards to the production of macroscopic CNTs like yarn but the kinetics and thermodynamic study of this production which will help in designing the production in a larger scale as well as helping

in operation at the continuous production still needs to be better understood. Therefore, this research focused on development of kinetic model and understanding thermodynamic of CNT yarn production in a CVD reactor using methane as carbon precursor and ferrocene as catalyst.

1.1. Problem Statement

With all the good property that CNTs has shown, the major problem is low production rate (See & Harris, 2007; Bepete et al., 2013; Segura-Cardenas et al., 2012). This problem is caused by the fact that there is little of understanding of growth mechanism of CNTs. Growth mechanism can help in understanding the requirements towards designing and operation of continuous mass production of CNTs and CNT yarn. In order to come up with viable continuous mass production of CNTs, kinetic studies of CNTs production have been widely studied. However, literature on kinetic modelling of CNT yarn production as opposed to CNTs is still scarce. In addition, literature on CNTs heat capacities and other thermodynamic parameters are insufficient and these quantities need to be reported in open literature. Heat capacities of CNT yarn are reflected to be more valued thermophysical measures that need to be understood when studying material (e.g. CNT yarn) because areas such as physics, chemistry and chemical engineering need this accurate heat capacity to obtain entropy, enthalpy, phase transition and energy balance of material.

Individual CNT has been conveyed to have high electrical conductivity by researchers and their yarn can be used as an incandescent lamp filament (Jiang et al., 2002). The challenge is to organise these building block (CNT) into macrostructure (CNT yarn) having similar property.

1.2. Research Questions

The goal of this research was achieved through answering the following questions:

i. What will be the rate of CNT yarn production using methane as feedstock?
ii. What will be the thermodynamic properties of CNT yarn?
iii. Will the conductivity of CNT yarn produced using methane be similar to that of individual CNT?

1.3. Research Aim and Objectives

The aim of this research was to improve the production of CNTs yarn to use in incandescent filament bulb through developing and understanding the kinetics and thermodynamic studies of their production. The aim was achieved through following specific objectives:

i. To produce and characterize CNT yarn using methane as feedstock

ii. To develop a kinetic model for carbon nanotube yarn produced in (i)

iii. To determine the thermodynamic parameters of CNT yarn produced in (i)

iv. To determine the conductivity of CNT yarn produced in (i) and compare it to that of the parent CNTs.

1.4. Expected Outcome

The expected outcomes from the research were:

i. Kinetic, thermodynamic and conductivity data on the produced yarn as a contribution to the existing body of knowledge in the field.

ii. A well-written dissertation on the findings as a reference document

1.5. Dissertation Outline

Chapter One:

This chapter gives the introduction of the study including the problem statement, the research objective and the expected outcomes.

Chapter Two:

This chapter considers the relevant literature with regards to this study. The structure of the carbon nanotubes, their growth mechanism and the formation of yarn is discussed. The thermodynamics study of CNTs is also prescribed.

Chapter Three:

The experimental procedures of CNTs yarn production and characterisation are explained in this chapter

Chapter Four:

This chapter explains the results and give summary of production of CNTs and their Kinetic study

Chapter Five:

This chapter give details about the produced yarn and their conductivity measurement and the thermodynamic properties

Chapter Six:

This is the final chapter that gives the conclusions and the recommendations from the study.

CHAPTER TWO

2.0. Literature Review

One of the allotropes of carbon is called carbon nanotubes. CNTs are made up of carbon atoms joined as a dense sheet then rolled up into a cylinder that has a diameter measuring in nanoscale (Iijima, 1991). CNTs are considered to be a sheet made up of graphene that is rolled-up to an arrangement of a tube e.g. a single walled nanotube (SWCNT) (Zhang & Li, 2009). When more than one graphene sheets are placed into one another the resulting tube is called multi walled carbon nanotube (MWCNT) (Zhang & Li, 2009). Since researchers have discovered that CNTs forest can be drawn into a microstructure made of pure CNTs, many possibilities have been unlocked in developing applications from these structures (Miao, 2013). This study focuses on producing Carbon nanotube yarn that will be used as a replacement for filament in an incandescent bulb.

2.1. Carbon nanotubes Structures

The dependency of nanotube properties on their shape is one of the fantastic phenomena that CNTs have. Nanotubes are long structure with the shape like that of a cylinder, having a diameter from one nanometre to a dozen of several nanometres with the length of up to numerous microns and it is made up of numerous plane hexagonal graphite that are rolled to form a tube. CNTs are the results of rolling up carbon atom of 2-dimensional layer in a hexagonal lattice that is bonded together called graphene in order to form a cylinder (Figure 2.1). The surface of the nanotube consists of cycles of hexagonal carbon (Dresselhaus et al., 2000; Saito et al., 1999; Zaporotskova et al., 2013).

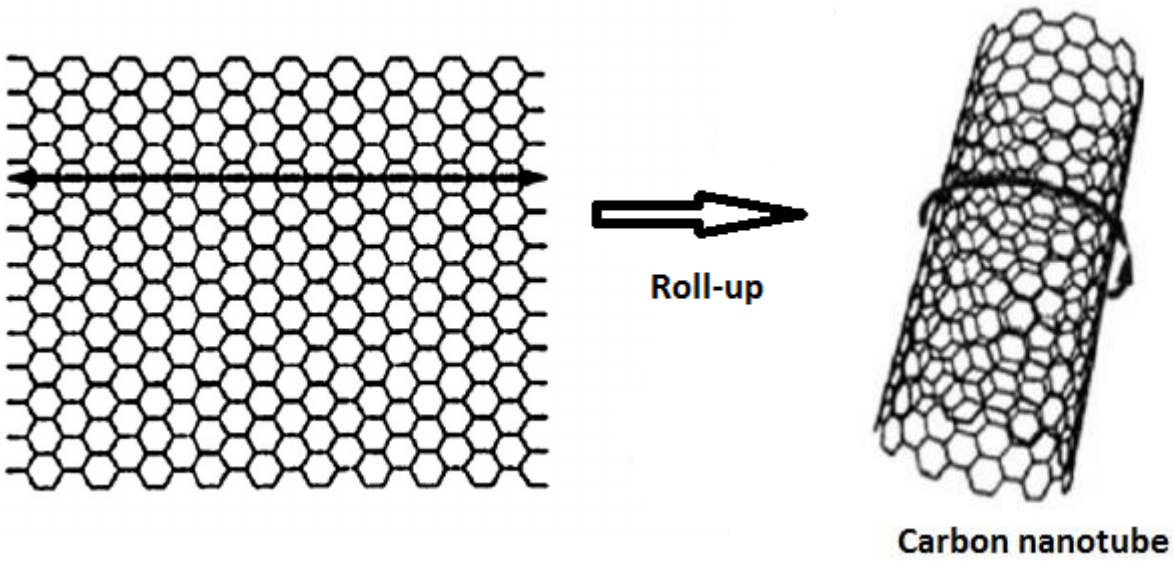


Figure 2.1: Graphene sheet been rolled to form CNT (Adapted from: Sheshmani et al.,2013)

The orientation of the mutual hexagonal network and the nanotube longitudinal axis govern the properties of nanotube structure called chirality. Two integers, *n* and *m*, are used to describe the chirality of a nanotube. These integers are the one that explains where the hexagonal network will match up with the hexagonal on the coordinated origin after rolling the graphene sheet to form a tube. Angle Θ is also exceptionally used to specify the chirality of the nanotube. This is the angle that is formed by the direction in which the graphene sheet is rolling and also caused by direction of 2 hexagons that are adjacent to each other. Hence Θ is called chiral or orientation angle. Graphene sheet has different options in which it can roll to form a nanotube. However, the rolling option that does not damage the structure of hexagonal network is the one that is of special interest. The chiral or oriental angles in the range of 0 to 30 degree are the ones that do not distort the hexagonal network.

These angles correspond to chiralities of *(n, n)* and *(n, 0)* respectively. The electrical properties of the nanotubes are determined by the chiral or orientation angle. The CNTs can either be metallic or semi-conductive.

There are numerous manners in which the graphene sheet can be folded to form carbon nanotube. The two common ones are the Zig Zag manner whereby (m ≠ 0, n = 0) armchair manner whereby (m = n ≠ 0) as shown in Figure 2.2. The Zigzag nanotube correspond to the chiral angle of 0 degree and the armchair nanotube correspond the chiral angle of 30 degree.

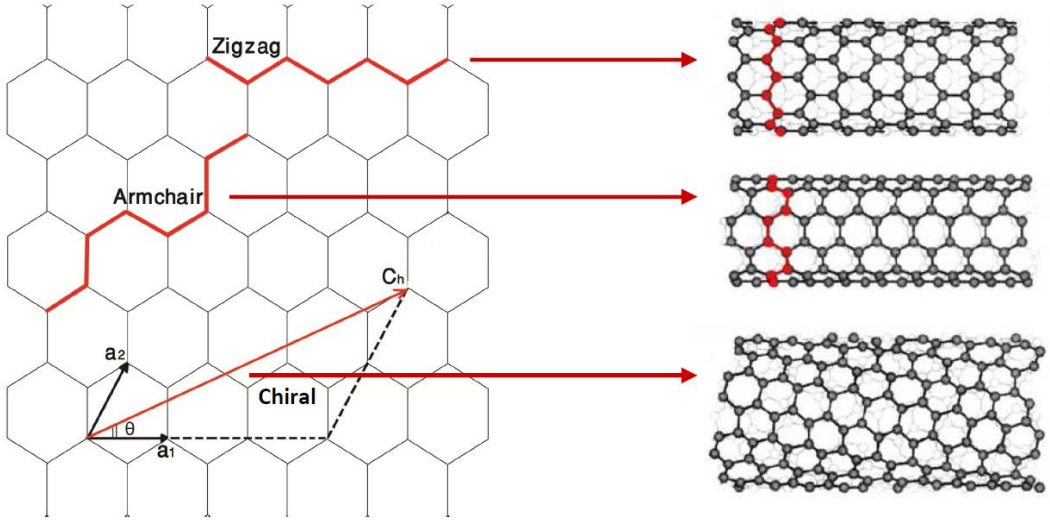


Figure 2.2: Schematic illustration of zig-zag, armchair and ciral CNTs. (Rahmandoust & Ochsner,2011)

The diameter of the nanotube as expressed in terms of integers n and m is given by:

$$d_t = C_h/\pi = 3^{1/2}a_{C-C}(m^2 + mn + n^2)^{1/2}/\pi \quad (0.1)$$

Whereby $a_{C\text{-}C}$ is the C to C distance of the nearest neighbour, C_h is the chiral vector length.

The chiral angle can be expressed by:

$$\theta = tan^{-1}[3^{1/3}/(m + 2n)] \quad (0.2)$$

Single wall Carbon Nanotube or Multi wall carbon nanotube with either closed or open termination may be produced depending on the reaction conditions. These are the two main types of CNTs. However, there are other type such as nanoknot and fullerite.

2.1.1. Single walled carbon nanotubes (SWCNTs)

Single walled carbon nanotubes are known to be a result of a single layer of graphite sheet rolling up to form a seamless cylinder (Figure 2.3). The length to diameter ratio of CNTs is generally about 1000 hence they are considered to be a 1-dimensional structure. The SWCNTs mostly have the diameter of about 1nm. There are two regimes that are separate in SWCNTs,

having different chemical and physical properties. Firstly, there is an end cap regime that has similar structure as the fullerene (C60) beside that it is cut into half, secondly there is a sidewall on the nanotube. The amazing electrical properties that SWCNTs possess that the MWCNTs do not possess makes them a very important type of CNTs. Carbon nanotube macrostructure such as yarn have high conductivity and are mostly used as conductors.

2.1.2. Multi walled carbon nanotubes (MWCNTs)

MWCNTs are considered to be a number of graphene sheet (Figure 2.3) that is placed into one another resulting in multiple layer of tubes. The properties, length and diameter of MWCNTs are different from those of SWCNTs (Iijima & Ichihashi, 1993). One type of MWCNTs called double walled carbon nanotubes (DWCNTs) have the similar properties as those of the SWCNTs. Depending on the reaction condition, DWCNTs can also be selectively synthesized (Flahaut et al., 2003)

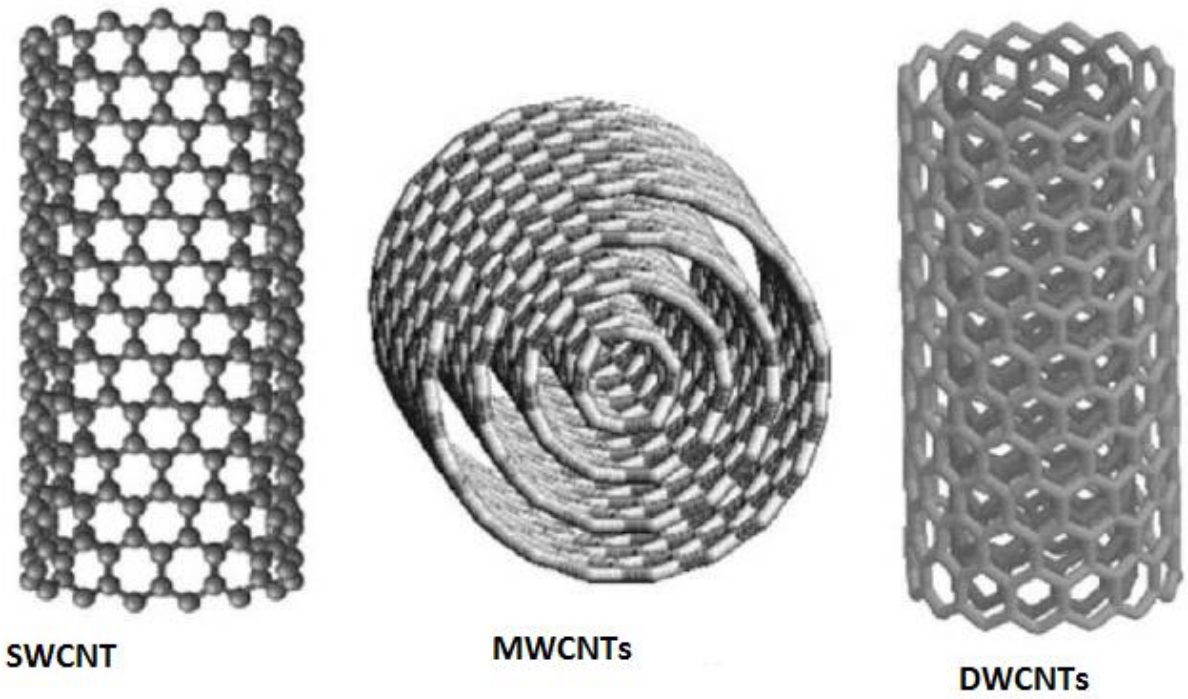


Figure 2.3:Atomic structure of CNTs (Dresselhaus et al.,2003)

2.2. Methods of Carbon Nanotube Production

There are different methods of producing CNTs as well as different post processing techniques which result in different individual structure and properties of CNTs, which results in different emerging properties of CNTs (Szabó et al., 2010). To produce CNTs of desired structures, different production methods have been developed for a specific CNTs product (Rafique,

2011). Three main methods of producing CNTs are chemical vapor deposition (Jose-Yecaman et al., 1993), laser ablation and arc discharge method (Iijima, 1991).

2.2.1. Laser ablation

One of the popular processes in the production of the carbon nanotube is the Laser Ablation. During this process target graphite is struck by a pulse laser in an inert gas environment, such as helium, at a very high reactor temperature. This way a graphite target is made to vaporize. The vaporized carbon will condense and the CNTs are usually developed at the cooler surface of rector as shown in Figure 2.4. In some applications, the surface of the reactor is cooled by cold water to collect the CNTs.

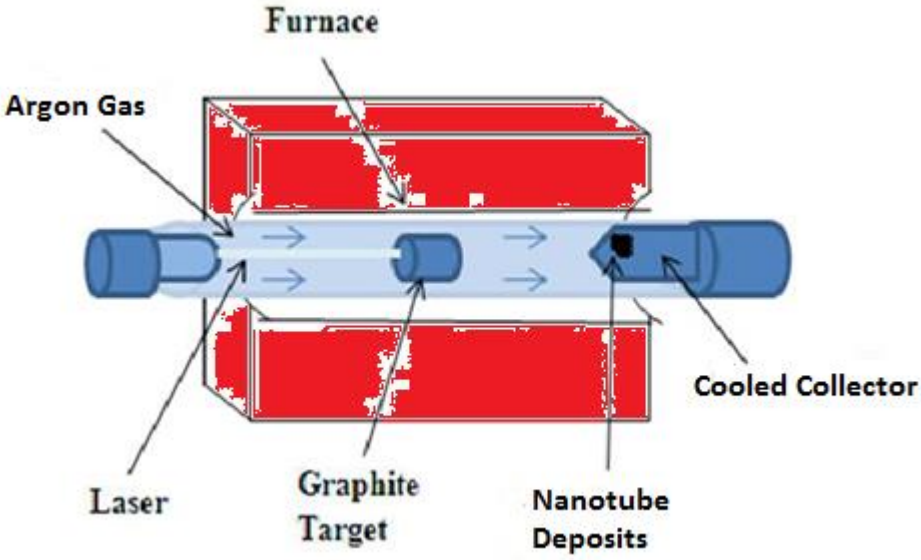


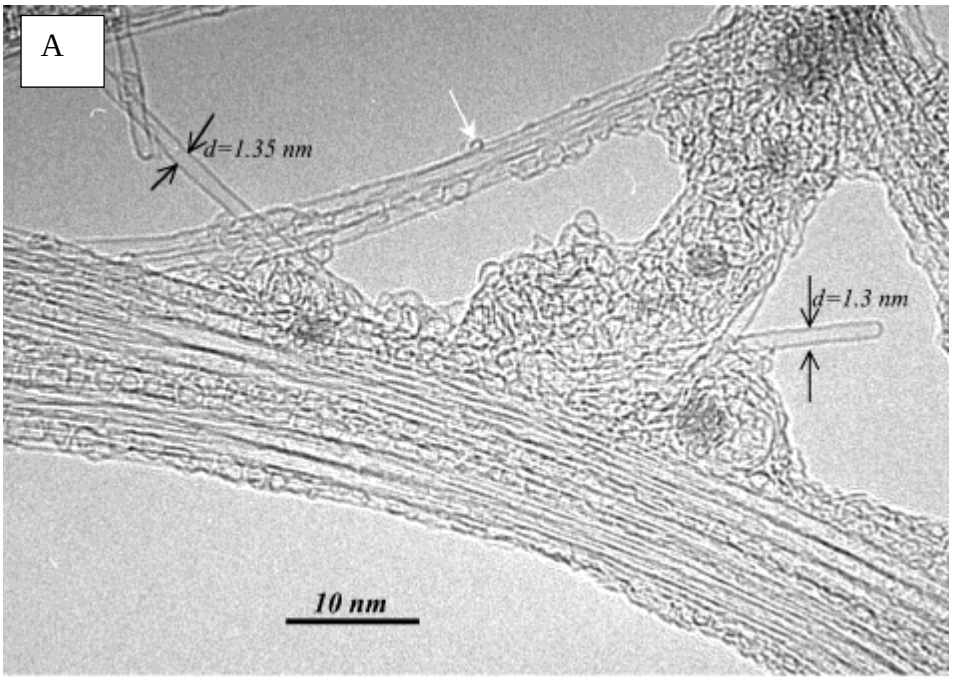
Figure 2.4: Laser Ablation (Adapted from: Choudhary et al.,2013)

Laser ablation method was discovered for the first time at the Rice University by Guo (Guo et al., 1995). It was a year later that this process was developed and effectively used for bulk production of the SWCNTs (Hafner et al., 1998). Rao et al (Rao et al., 1997) and other researchers improved this process by using laser of double beam. Laser ablation produces nanotubes with higher purity of about 90% pure and this purity is higher than the one produced from the arc discharge method. In addition, the structure of tube has better graphitization as opposed to the structure of nanotube from the arc process. However, one of the disadvantages of this process is the small carbon deposit.

Two most used carrier gases during the laser ablation process are H_2 and Ar. It is clear that any change in ambient gas conditions has a significant effect on the quality and quantity of the

product. A synthesis of CNTs on C/Ni/Y catalyst using He, Ar and N_2 atmosphere at a pressure of 50 – 500 Torr was studied by Munoz at al (Munoz et al., 2000). High yield of filamentous soot with a texture of web-like formation was observed when the reaction pressure was in the range of 200 to 500 Torr. The SWCNTs diameter was observed to be 10 to 20 nm with the length of more than 1 μm when using N_2 and Ar atmosphere. However, when using He as the carrier gas, there was no notable amount of SWCNTs or any filament material observed in the soot.

It was also proven that the Nd:YAG layer for the the production of SWCNTs and the CO_2 pulsed/continuous wave is capable of producing the CNTs at room temperature (Kokai et al., 1999, Maser et al., 1998). The target surface is heated up by the longer wavelength this phenomena act like a furnace. Eklind et al (Jounet et al., 1997) used pulsed laser vaporization (PLV) technique to do a large scale SWCNTs production by using the ultrafast (subpisecond) laser pulse for the first time. As shown in Figure 2.5, the produced SWCNTs had a huge diameter uniformity, which is approximately 1.3 nm for all the tubes.



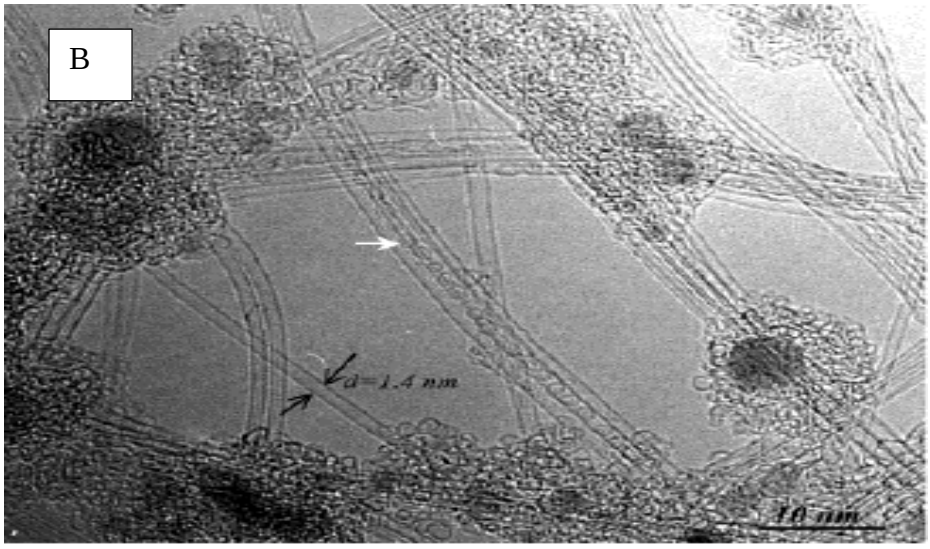


Figure 2.5: TEM results of CNTs produced from catalyst a) Ni/Y b)Ni/Co (used with permission from: Eklund et al., 2002)

2.2.2. Arc Discharge method

This method involves the use of two graphite electrodes of high purity (See Figure 2.6).

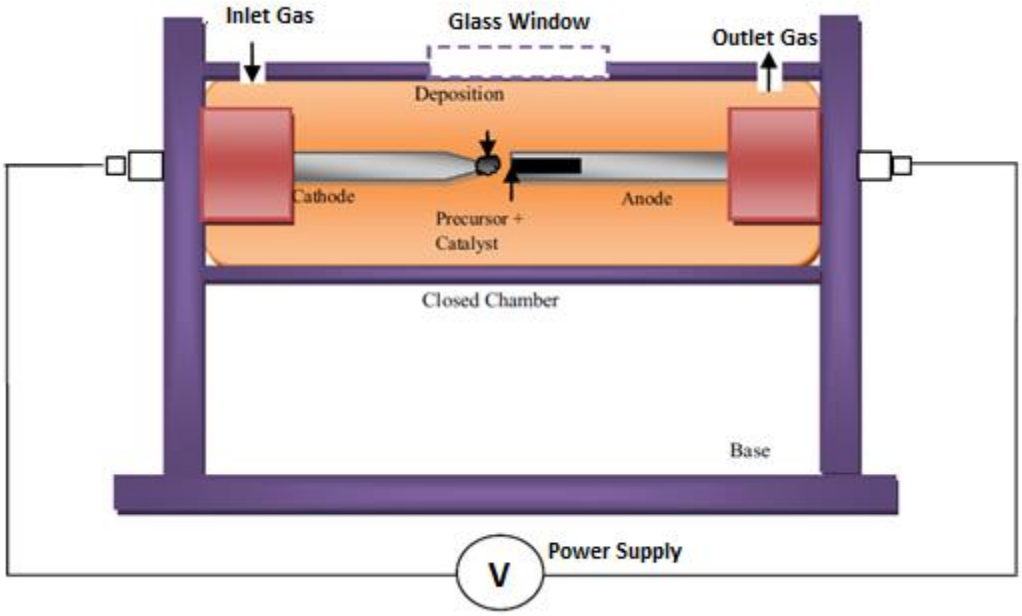


Figure 2.6: Schematic illustration of Arc Discharge set-up (Adapted from: Aron & Sharma, 2014)

Arc Discharge method was first used by Iijima (1991) to synthesize finite structure of carbon that has tube that are like needles. Bethume at al. (1993) filled the thin electrodes that had bored holes in it acting as anode, with a powdered pure metal mixed together as catalyst and also

graphite. A current of 95 to 105 A was used to vaporize the electrodes at a pressure of 100 to 500 Torr using Helium. A large-scale production of MWCNTs was reported by Ebbesen et al (1992) by utilising standard arc discharge technique.

A drawback of arc discharge is that, the method produces less CNTs. In addition, the arc discharge method normally gives impure material in large quantity.

2.2.3. Chemical Vapour Deposition

When comparing CVD method with arc discharges method and laser ablation method, it was found that CVD method has the advantage of mild operating condition, low cost than the other method and has controllable synthesis (Miao, 2013). It is also the most promising method of large-scale production (Zhang et al., 2011).

Chemical vapor deposition method was first introduced in 1959 (Li et al.,1999), but this method was only used in 1993 for production of CNT (Jose-Yecaman et al., 1993). Throughout the CVD method, metal catalyst or supported metal catalyst such as nickel, cobalt or iron is heated at a temperature of about 700^{o}C (Cantoro et al., 2006). Two gases pass through the chamber, one being a Carbon source and the other one is a carrier gas such as Nitrogen, Argon, or Hydrogen. A typical schematic set-up of CVD reactor is depicted in Figure 2.7.

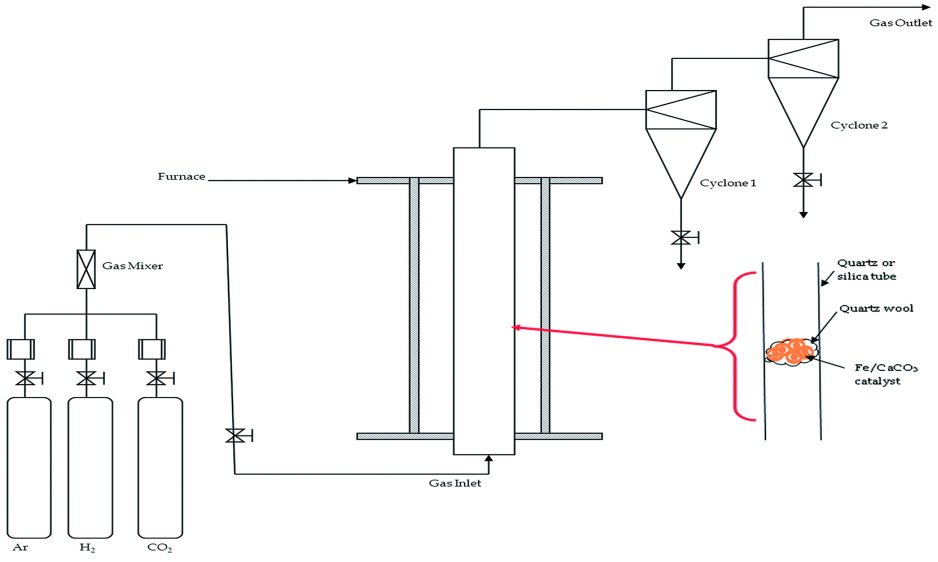


Figure 2.7: Schematic illustration of Chemical Vapor Deposition (Iyuke et al.,2009)

The production yield, which is the amount of CNTs formed in the converted carbon, can reach 90% (Dai, 2000). This method is well studied and offers satisfactory results on the industrial

scale. The chemical vapour method can give both single and multi-wall carbon nanotubes the good thing about CVD method is that the quality and quantity of CNTs can be controlled. In this study, CVD method was employed to produced CNTs that were spun into yarn. The CVD method was found to be the only one that can be easily scaled up and used for large production of CNTs in commercial production (Daenen et al., 2003).

2.3. Catalysts for CNTs/ CNT yarn production

Another way of exploring the CNTs excellent properties is by turning the CNTs microstructure into CNTs macrostructure such as the yarn. However, it is still a challenge to transfer the excellent properties of CNTs entirely into CNT macro structure. In order to successfully transfer the unique properties of CNT into their yarn, spinnable CNT forest must be produced first (lijima et al. 2011). When the CNT is super aligned, van der Waals force between the tubes makes the tubes to create continuous yarn by joining end to end as shown in Figure 2.8.

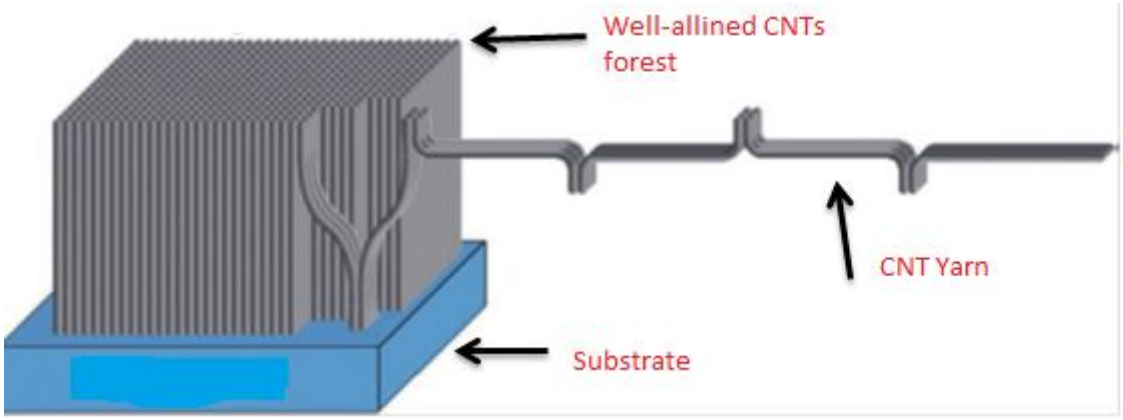


Figure 2.8 :Mechanistic model of CNTs forest been drawn into yarn (Adapted from Zhang et al., 2006)

It is clear that the reaction conditions during CNTs production have an effect on the alignment of the tube. Catalyst used during the production of CNTs is one of the factors that affect the alignment of CNTs forest. For CNTs production, normally nanoscale metal particles are desired for the decomposition of hydrocarbon at a low temperature as compared to the spontaneous decomposition of hydrocarbon that requires high temperature.

2.3.1. Supported Catalyst

During the production of CNT yarn, catalysts that are widely used are the transition metals such as Fe, Ni and Co because of the following two main reasons: 1). The carbon solubility in

these metals is high; 2). The rate of carbon diffusion in these metals is high. Ding et al (2008) discovered that the CNTs grown on Ni, Co and Fe are strongly adhered to the catalyst as compared to other transition metals. Therefore, these metals are efficient in producing CNTs with high curvature such as SWCNTs. However, the most studied catalyst out of all transition metals is the Fe catalyst. Fe based catalyst produces 2 times higher growth rate of super aligned CNTs forest than Ni and Co (Kim et al., 2002).

Different catalysts used during CNTs production result in different CNTs yield and purity. Suriani et al (2013) investigated the effect that the use of Co and Fe has on the structure of CNTs. They discovered that the use of Fe catalyst yields CNTs with smaller diameter as compared to the CNTs produced by using Co. However, the CNTs produced from the use of Fe was observed to have higher quality than those obtained using Co and the tubes has defects. The CNTs structure with good crystallinity is known to be produced from the use of Fe catalyst as compared to Co. The reason could be that iron catalyst has stable and also uniform catalytic activity when compared to other catalysts. Regarding the issue of growth rate, Lee et al (2002) found that Fe has lower growth rate when compared to Co and Nickel.

Siyakumar et al (2011) synthesized MWCNTs using methane as carbon source in a CVD reactor. Low-cost activated carbon was used as substrate for Iron and Nickel catalyst. Their results show that when using Fe as reaction catalyst, 98% conversion of methane was achieved whereas when using Nickel only 42% conversion of methane gas was obtained. These results show that for the production of CNTs using methane as carbon source, Fe catalyst is a good choice for efficient process.

Methane and acetylene were used to produce CNTs using Aluminium or Molybdenum to support Ni and Fe. During the experiment it was difficult to synthesize SWCNTs when using Ni supported catalyst. However, at the same reaction conditions, Fe based catalyst makes it easy for the SWCNTs to be synthesized (Shin et al., 2006). The reason behind this result could be the diffusivity of carbon atom into the metal particle, as it is easy for carbon atom to diffuse through Fe particle than it is in Ni particle as well as the solubility of carbon atoms in different catalyst.

The nature of CNTs desired can be synthesized by controlling the size of the particle for the catalyst and the chemical nature of catalyst. Single walled carbon nanotube may be selectively produced, and one may choose to selectively produce MWCNTs as indicated in Table 2.1.

Table 2.1: Different catalysts used to produce certain CNTs

Type of Catalyst	Carbon Precursor	Type of CNTs	References
Ni-Cu/Al203	CH_4	MWCNT & GNF	Blanchard et al. (1982)
Ni/MgO	CH_4	GNF	Philippe et al. (2007)
Ni/SiO2	CH_4	SWCNT & GNF	Perez-Cabero et al. (2003)
Ni/Al2O3	CH_4	GNF	Venegoni et al. (2002)
Fe-Mo	CH_4	SWCNT	Corrias et al. (2003)
Fe/SiO2	C_2H_4	MWCNT	Kunnii & Levenspiel. (1991)
Co/MgO	CO	CNT & GNF	Xiang et al. (2007)
Co/La2O3	C_2H_2	MWCNT	Kunnii & Levenspiel. (1991)

GNF – Graphite Nano-fibre

2.3.2. Floating Catalyst

Organometallocenes such as ferrocene, Iron carbonyl in a solid form have been widely used as catalyst for carbon nanotube production; because during reaction they release metal nanoparticles that efficiently catalyse the process of hydrocarbon decomposition. However, in order to effectively use the organometallic in the CNTs production, the floating catalyst method has to be employed (Govindara & Rao,2002; Ci et al.,2001) The floating catalyst method is the process whereby the complex of organometallic is injected into the hot tube together with the carbon precursor, thereby the metal nanoparticle reacts with the carbon precursor to form CNTs. Production of CNTs using Floating catalyst can synthesize continuously high purity CNTs and the equipment setup is fairly simple.

Mohlala et al (2005) synthesised MWCNTs using ferrocene and $Mo(CO)_5L$ (L = CO, BuNC) at a temperature range of 700 to 900^oC. The results show that at the same reaction condition, ferrocene produced CNTs whereas $Mo(CO)_5L$ did not produce any CNTs but only little carbonaceous matter. However, when ferrocene was mixed with $Mo(CO)_5L$ the results show formation of CNTs. In addition, the diameter of CNTs produced by ferrocene was smaller than the diameter of CNTs produced by the mixed catalyst. Carbon nanotubes can also be synthesized by liquid form floating catalyst such as ferric chloride (Khavarian et al, 2009).

Floating catalyst in a CVD reactor is recognized to be a process for industrial scale production. This research focused on producing CNTs using CVD reactor using a floating catalyst.

2.4. CNTs Purification

As-produced CNTs usually contain impurities such as amorphous carbon, residual catalyst and some other unwanted species. After the production of CNTs it is always advisable to separate those impurities from the CNTs. This process is called CNTs purification. These impurities that are rooted in the CNTs have significant impact on the properties of the CNTs. Most applications of CNTs depend mainly on the degree of purity of the material. The presence of impurities could affect the more detailed characterization of CNTs properties and also their potentials for future application. For example, in the excellent storage of gas and energy using CNTs, a very small amount of metal particles and debundling of the CNTs is desired to acquire a very high surface area (Mohanapriya & Lakshminarayanan, 2007; Duesberg et al., 2004). Similarly, catalysis and delivery of drugs applications entail the ability to access the central canal done by the opened tips, this process is made possible by removing the metal particles in the CNTs (Delpeux et al., 2005). Therefore, CNTs purification plays an important role in exploiting the excellent properties of the CNTs.

CNTs Purification Methods

There are two main categories of CNTs purification methods: chemical and physical method. Physical method involves separation of CNTs from impurities based on their differences in factors such as gravity, physical size, magnetic properties and aspect ratio etc. Generally, the physical method removes impurities such as graphitic sheet, carbon nanosphere, aggregates and also helps to separates CNTs with different lengths and diameter ratios. Physical separation method is usually less effective and is more complex. However, these processes are relatively mild, and they usually do not cause that severe damage to the tubes (Salernitano et al., 2007).

Chemical methods involve separation of CNTs from impurities by dissolution of the metallic impurities in acid and also due to the fact that the carbonaceous impurities can be oxidized much faster than the CNTs. The disadvantage of this process is that the chemical oxidation process sometimes causes defects on the surface of the tubes resulting in significant damages on the structure of the CNTs as well as the morphology of the CNTs.

2.4.1. Physical purification method

Physical properties and morphology such as magnetism, physical size, aspect ratio, solubility and gravity of CNTs differs from those ones of impurities. These differences are the one that make it possible to separate CNTs from impurities by using physical techniques. Physical purification method such as high temperature annealing, filtration and chromatography, have being widely studied.

Filtration

Uniform size such as diameter and lenths of CNTs is needed in order to fabricate CNTs-based nanodevices (Tagmatarchis et al., 2005). A membrane with pore size distribution that is narrow has been developed in order to separate the impurities fron CNTs as well as fractionating the CNTs by their lenth (Abetomarco et al., 1999). Abetemarco et al (1999) studied the membrane of different pore sizes for sequential filtration from the membrane with largest diameter to the ones in smallest diameter in cross flow system. In this manner oxidation treatment was not necessary. As a result, CNTs was trapped in the membrane that has small pore sizes whereas all other aggregated was trapped in the membrane that has large pore sizes. In this way filtration process successfully separates the large aggregates, CNTs and polyhedral nanoparticles from each other. In addition, separating CNTs according to their length was successful.

Sonication

One of the active processes in the removal of amorphous carbon impurities is known to be sonication. When high energy ultrasonic is used to treat CNTs in suitable solvents such as the O-dichlorobenzene and dichloromethane (Lu et al., 1996; Yang et al., 2006), interaction between molecules of solvent and the CNTs is possible during sonication leading to solubilisation. The effect of sonication in the structure of the CNTs was investigated and reported (Lu et al., 2006). As a result, it was discovered that high degree of defects for example, bucking and bending on the nanotubes was possible in the sonicated sample, whereas nanotubes thinning was a result of outer graphite layer that was gradually stripped off. The inner tubes were protected by a layer that was formed when the ultrasonication damage was mostly absorbed by the outer layer of the nanotubes. However, it was also found by Shelimov et al (1998) that the damage on the tube structure depend on the solvent that is used. This could be due to the difference in the resulting transfer of energy in the cavitation when using different solvents. The sonicated CNTs result in a shorter tube that caused by induced sonication cutting

of nanotubes, also the CNT tips appeared to be opened ((Lu et al., 2006) making this method to be not very effective.

2.4.2. Chemical Purification Method

Carbonaceous impurities that are rooted in the as-produced CNTs are mostly Carbon nanoparticles (CNPs) and amorphous carbon. These impurities have higher oxidation activity as compared to CNTs. High oxidative activity in amorphous carbon is due to their more structural defects and dangling bonds making them to be easily oxidized. Meanwhile the high reactivity demonstrated by the CNPs is due to their pentagonal carbon ring as well as their large curvature (Chang & Bard, 1991; Colbert et al., 1994). Chemical oxidation includes gas phase oxidation whereby gases like H_2O, air, Cl_2 and O_2 are used. In addition, liquid phase oxidation, such as acid treatment and refluxing, can also be used.

Gas phase oxidation

The structural defect densities of carbonaceous impurities are higher than those of the CNTs resulting in carbonaceous impurities to be more ready to act as site for the reaction of intercalated atom. Therefore, the difference in oxidation resistance between the carbonaceous impurities and the CNTs can easily be increased. To demonstrate the above statement, a study by Chen et al., (1996) showed a combination in purification processes comprising selective oxidation, with air at a temperature of 530^{o}C for a period of three days and bromination. It is clear that oxidation of sample without bromination occurs less freely than the one that is brominated. The purified sample results in both CNTs end opened, this was visualised using TEM studies, also the resulting yield using the above process ranged from 10 to 20 wt% with regards to the original mass sample of carbon. In addition to these results, they also found that the flow rate of the oxidant, the initial mass of the sample, the cathodic soot quality as well as the manner in which the carbon atom is packed are some of the crucial aspects that control the yield.

A study that shows optimum condition that successfully eliminate both spherical carbon and amorphous carbon impurities, with or without metal catalyst inside, at the same time protecting the SWCNTs was reported (Zimmerman et al., 2000). The purification process consists of a mixture of gases such as hydrogen chloride, chlorine and water vapour in order to eliminate the impurities. It is clear that the carbonaceous material was selectively removed because the yield and purity of SWCNTs was approximately 15 wt.% and 90 wt.%, respectively, with regards to their initial weight. Hydrogen chloride was needed in order to eliminate the

undesirable carbon. A nanotube hydroxy-chloride-functionalized cap was created when a chlorine gas interacts with the CNT cap. CNT cap that are more reactive was protected by the hydrogen chloride that is in the purification gas mixture, by stopping the hydroxyl group from producing a proton. One drawback about this process is that, a very small amount (approximately 5 mg) of CNTs was successfully purified each time. In addition, the reaction gases are very explosive and toxic which then restrict its practical application.

Liquid Phase oxidation

One of the commonly used reagents for purifying CNTs is the nitric acid. This acid has mild ability to oxidize and can remove the amorphous carbon selectively. Furthermore, this acid is inexpensive, effective in removal of metal catalyst and it does not introduce any secondary impurities into the sample. Concentrated nitric acid was used as one step method to purify SWCNTs that was produced using the laser ablation, as reported by Dujardin et al. (1998). Firstly, nitric acid was introduced into the as produced SWCNTs followed by sonication for a very few minutes, then magnetic stirring at a temperature of 120 to 130^{o}C for a period of four hours was used for refluxing. The amount of metal inside the sample was successful decreased to approximately 1 wt% and the yield was found to be between 30 to 50 wt% with respect to the raw sample. Hu et al. (2003) reported relationship, which is quantitative and systematic, between the sample purity and yield using NIR spectrometer at solution phase. It was discovered that the yield and purity resulted from purification of SWCNTs with nitric acid treatment depend mainly on the reflux time and nitric acid concentration.

In order to provide the stability and evenly disperse the catalyst nanoparticle in a support structure, the oxide support such as alumina and silica are normally used for growing the CNTs. This catalyst support, for example silica, can be dissolved easily in the present of Hydrofloric acid (HF) as an etching agent. A study by Engel-Herbert et al. (2007) showed that silica matrix can be completely removed from the CNTs yield using 5% liquid form HF for a period of 5 min. Smaller amount of amorphous carbon was also burned during HF oxidation given that the process was prolonged to about 60 min of time at a temperature of 550^{o}C. This method was also successful in separating and isolating the most dense CNTs bundles. In some studies, zeolite support was successfully removed from the carbon nanotubes using HF without causing any damage to the carbon nanotube structures (Igarashi et al., 2004; Colomer et al.1999).

2.4.3. Multi step purification method

Gas phase oxidation is best in removing impurities such as polyhedral carbon and amorphous carbon however it also damages some CNT and it fails in removing a large fraction of any graphite particles as well as the metal impurities (Zimmerman et al., 2000; Chiang et al., 2001). With all the advantages of Gas phase oxidation method, it also has a drawback that it cannot directly remove the metal particles and further process of acid treatment is needed in order to successfully remove the metal particles. Liquid phase oxidation method was developed in order to simultaneously remove both the carbonaceous impurities and the metal particles but the resulting CNTs from this process is always cut, opened and also damaged (Zhang et al., 2003). One process that is active in partly removing the isolated carbonaceous and metallic impurities is the physical purification process (Shelimov et al., 1998). However, this process leaves the amorphous and spherical particles stuck on the side of the tubes and also sometimes the metal particles are left encapsulated in the CNT (Jeynes et al., 2006).

As discussed above, it is a challenge to purify CNTs with just one method, therefore in order to achieve a desirable CNTs yield as well as the purity it is advisable to combine both the physical and the chemical purification method. Multistep purification method has also been extensively studied and reported. Depending on the degree of purity and the need of different CNTs, different type of multiple steps for purification has been reported. For example, when producing CNTs using either arc discharge or laser ablation there are some graphite particles that form. These graphite particles are difficult to remove when using chemical oxidation purification process; hence filtration method is adopted as one of the steps in multiple steps purification (Bandow et al. 2005; Kim & Luzzi, 2005). Moreover, it is well known that low temperature oxidation of carbons catalysed by metal particles extensively destroy SWCNT in the presence of oxygen as well as the other oxidizing gases. In order to avoid this difficulty, combination of acid treatment and gas phase oxidation purification steps were developed and widely studied (Ramesh et al., 2006; Delpeux et al 2005; Chen et al., 2002; Dillon et al., 1999).

Therefore, it is possible to obtain high yield and high purity CNTs by using multiple purification step by combining the advantages of both Physical and chemical purification method. Furthermore, one can control the morphology and structure of CNTs by choosing a suitable method of purification. Hou et al. (2008) summarized representative procedures that are based on the function as well as the characteristic of the purification as shown in Figure 2.9.

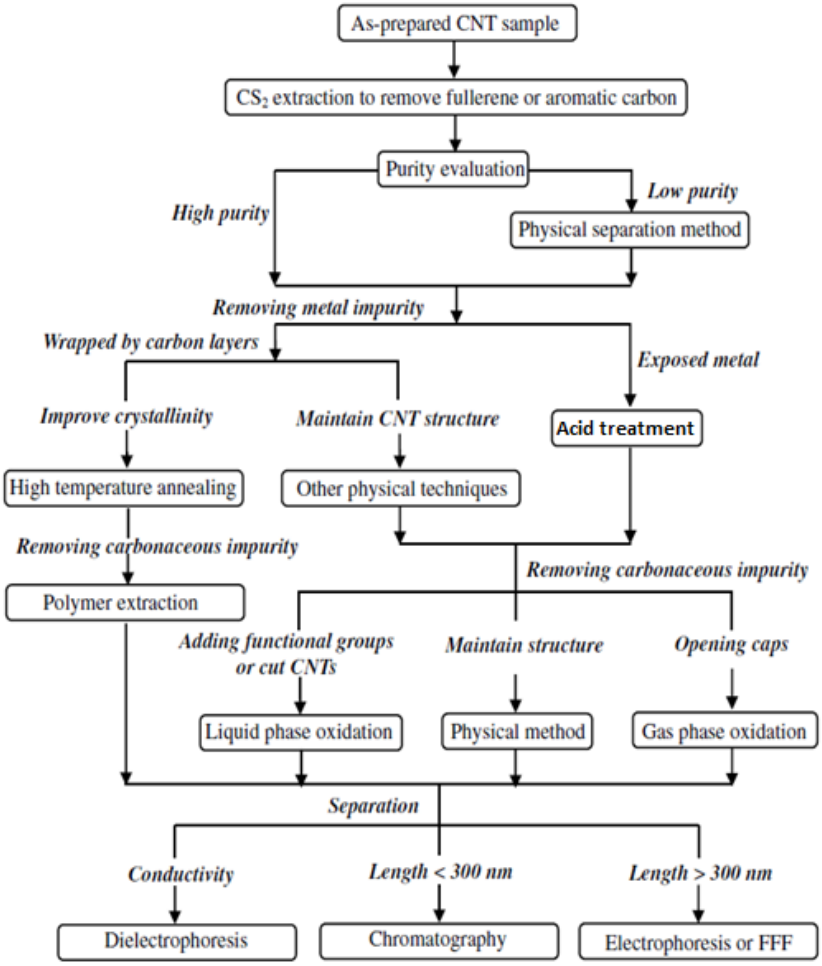


Figure 2.9: Flow chart of the representative procedure for CNTs purification based on function and characteristic of purification method (Adapted from Hou et al., 2008)

In summary, physical treatment is effective in removing the following impurities: metal particles, sorting CNTs by conductivity or length and also to some extent separating isolated carbonaceous particle by their sizes. Chemical oxidation is capable of removing amorphous carbon, and also adding functional groups, as well as the opening and/or cutting the tubes. Exposed metal particles can be effectively eliminated by using organic acid. Since this study concentrated on producing CNT yarn from direct spinning, there was no need for purification methods which saves both cost (for purchasing additional chemicals) and time.

2.5. CNT yarn Spinning Methods

CNTs have been shown to have extraordinary mechanical properties. It is highly expected that their macrostructure such as yarn will have the same properties as the individual CNT

There are four known methods for spinning CNTs into a yarn (Choo at al., 2012). That is: CNTs forest spinning (Zhang, 2014; Liu et al., 2009), direct spinning (Li, 2004; Motta et al., 2007). Surfactant-based coagulation spinning (Vigolo, 2000; Vigolo et al., 2002) and liquid-crystalline spinning (Ericson, 2004)

2.5.1. Forest spinning

The widely known method for making CNT yarn is to spin from vertical CNTs wafer (Fig. 2.10). This grown CNTs aggregates called forest is drawn then twisted to form yarn. Forest spinning was found to be unsuitable for continuous production because of limited size of wafer as well as the discontinuous process of CNTs production. This method also produces yarn of different properties based on where they are placed on the wafer (Zhang, 2014; Liu et al., 2009).

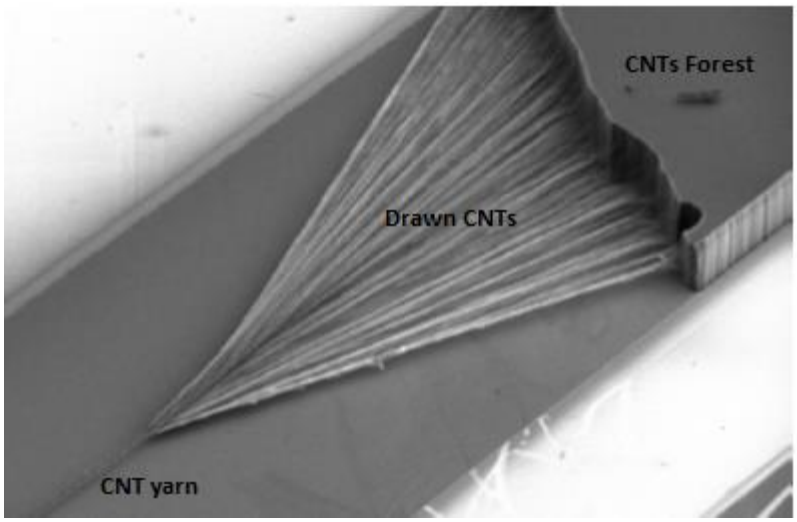


Figure 2.10:Forest spinning (Adapted from:Miao, 2013)

2.5.2. Direct Spinning

One of dry fabrication methods is direct spinning (Fig. 2.11), whereby a source of carbon, catalyst and a carrier gas are injected into a furnace at high temperature in order to produce CNTs in the furnace and a spindle is used to winds up the CNTs into CNT yarn coming down the bottom of the furnace (Li, 2004; Motta et al., 2007). The typical spinning rate that is used for this method is about 20-30 revs/min (Motta et al., 2007) making it suitable for mass production of CNT yarn, and better than other methods in this regard.

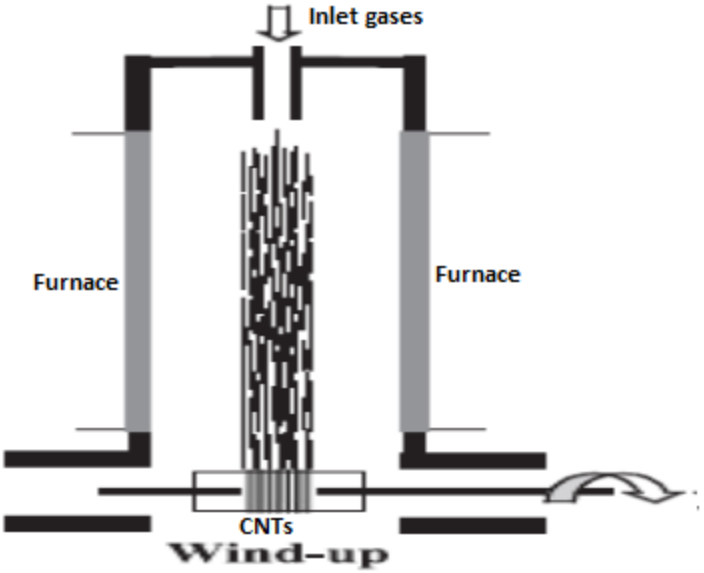


Figure 2.11:A schematic diagram of Direct Spinning process (Adapted from: Motta et al., 2007)

2.5.3. Surface based coagulation

In surfactant-based coagulation spinning, a Surfactants is used to disperse CNTs in it, and the polymer is used to coagulate the surfactant-stabilised CNTs solution. Polymer will then replace the surfactant that is in the dispersion solution (Fig 2.12). The role of the polymer is to bind CNTs together and form a yarn. Surfactant-based coagulation method has a CNTs content of about 60 wt% which is considered to be a high level that has not once reached by using other methods (Vigolo et al., 2002). The fact that the yarn produced this way has polymers amongst CNTs particles is an indication that this yarn has failed to overcome the limitations of composite materials.

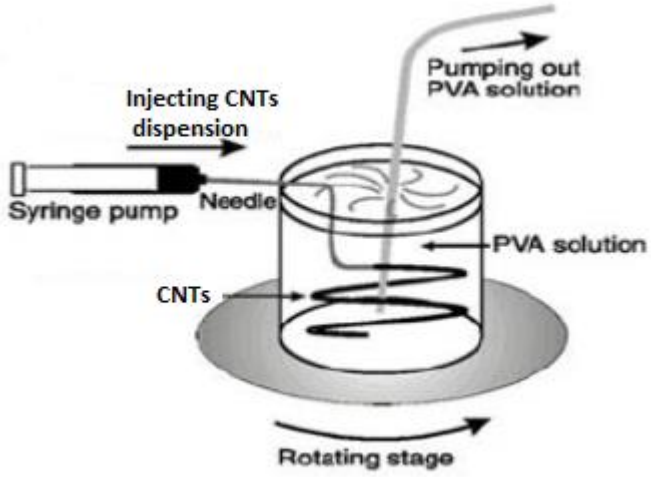


Figure 2.12:Surfactant-based coagulation spinning (Adapted from: Vigolo, 2000)

2.5.4. Liquid-crystalline spinning

One method of utilising CNTs solution to make a liquefied crystal at a certain condition as depicted in Figure 2.13 is called Liquid-Crystalline spinning (Ericson, 2004). CNT yarn formed by this method is highly oriented making it very advantageous. However, the resulted yarn has poor conductivity since they are just the collection of CNTs structure. Also, the speed of spinning is very slow (Ericson, 2004). This study focused on producing CNT yarn using direct spinning method.

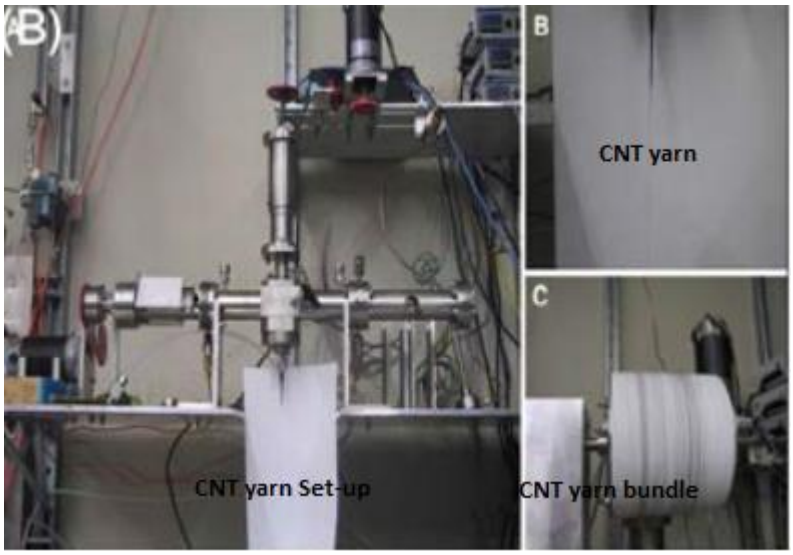


Figure 2.13: Liquid crystalline spinning technique for CNT yarn (Adapted from:Ericson, 2004)

As shown in Table 2.2, CNT yarn that is fabricated by direct spinning has higher electrical conductivity as compared to other methods.

Table 2.2:Yarn conductivity by different spinning methods

Spinning Method	**Electrical Conductivity [S/m]**	**References**
Coagulation Spinning	1×10^3	(Vigolo, 2000)
Liquid-crystalline spinning	3×10^4	(Ericson, 2004)
CNTs Forest spinning	1.1×10^5	(Zhang, 2004; Liu et al., 2004)
Direct Spinning	5×10^5	(Li, 2004; Motta et al., 2007)

2.6. Characterisation Techniques

Different characterisation techniques can be used to fully characterise the CNTs and CNT yarn. Depending on the information or properties of carbon nanotube needed, one may select an appropriate analytic tool to use. The following techniques have been broadly used successfully to give reliable result: Thermal Gravimetric Analysis, Scanning Electron Microscopy, Transmission Electron Microscopy, Raman Spectroscopy, Gas Chromatography, Energy-dispersive X-ray spectroscopy, Differential Scanning Calorimetry, Four probe etc.

2.6.1. Thermal Gravimetric Analysis (TGA)

TGA (Figure 8) is the thermal technique, whereby a sample mass is measured over time as the temperature of the sample is changing. Primary measurement in TGA is Temperature, mass and time, while other measurement may be derived from these 3 measurements. Information about the physical phenomena of sample is obtained from TGA measurement. These physical phenomena comprise desorption phase transition and absorption. Other information that the TGA measurement can give is chemical phenomena of the sample including thermal decomposition and chemisorption.

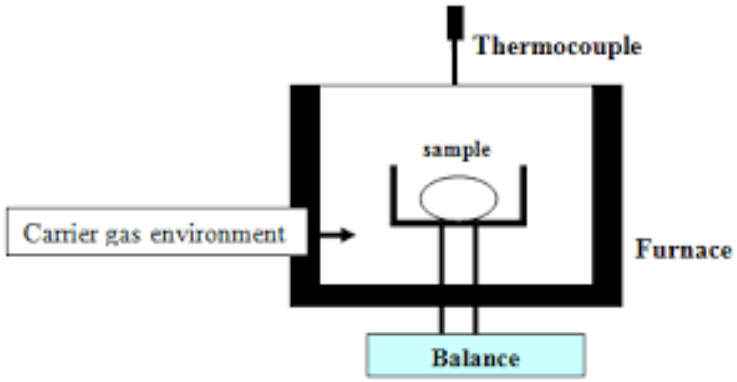


Figure 2.14: Schematic illustration of TG analysis

Generally, a TGA equipment consists of a programmable temperature control and a precision balance than has a sample pan situated inside a furnace (Figure 2.14). To start the thermal reaction, the temperature to the sample is normally increased at a constant rate. This thermal reaction occurs normally at inert gas such as N_2, Ar etc, and at different pressure. By analysing the characteristic of decomposition pattern, TGA can be used for characterisation of material. This technique is a useful method that is used to study CNTs and CNT yarn.

2.6.2. Scanning Electron Microscopy (SEM)

Another type of electron microscopy is called SEM. During this analysis an image of a sample is produced when the surface is scanned with an electron beam (Figure 2.15).

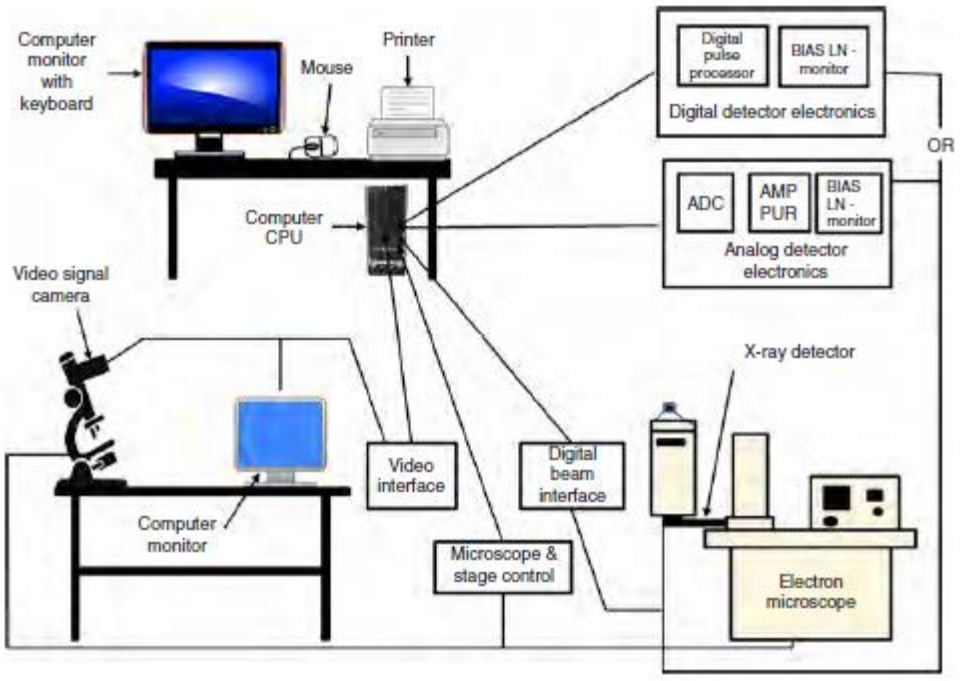


Figure 2.15: Schematic illustration of SEM (Adapted from: Russ, 2013)

The atoms in the sample interact with the electron, causing various signals containing sample's surface information such as topography and composition to be produced. The raster scan patten is used to scan the electron beam, combining this beam position and the detected signal cause an image to be produced. The resolution that can be achieved by the SEM equipment goes beyond 1 nanometre. SEM has a narrow electron beam and its micrographs have a field of large depth; these properties make it to produce a 3-dimensional appearance which is more important to understand the surface structure of carbon nanotubes.

2.6.3. Transmission Electron Microscopy (TEM)

TEM is also a type of microscopic technique, whereby image, an electron beam is generally transmitted through a specimen. See Figure 2.16.

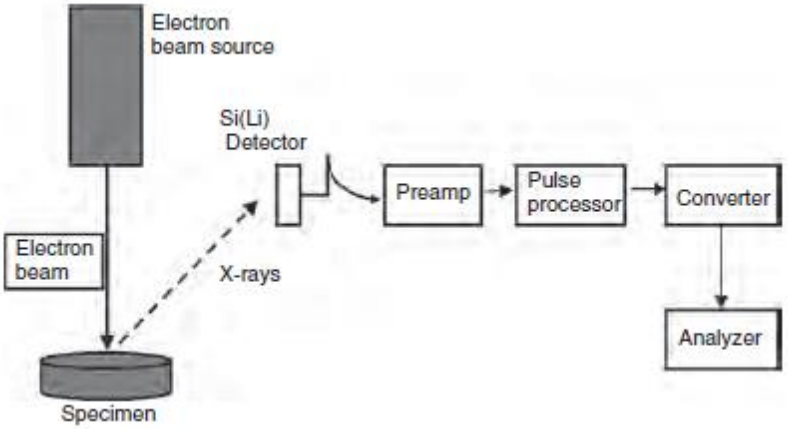


Figure 2.16: Schematic illustration of TEM (Friel, 2003).

A specimen usually consists of ultrathin section that is less than 100 nm thick or sometimes it is made up of a suspension on a grid. Formation of an image is the result of interaction between the sample and the electron when the beam is transmitted through the specimen. The resulting image will be magnified and focused on the device for image for example a fluorescene screen. TEM technique is an important method used in CNTs studies.

2.6.4. Raman Spectroscopy

This was named after the physicist who invented this technique, C. V. Raman (Raman & Krishma, 1928). Raman Spectroscopy is one of the scattering techniques that gives information about internal structure of crystals as well as the molecules. This technique is generally based on the Raman Effect. The Raman Effect state that the frequency resulted from monochromatic incident is totally different from frequency that resulted from small fraction of radiation that is

scattered. During Raman Spectroscopy analysis, monochromatic laser beam is used to illuminate sample, causing interaction between these beam and sample's molecules and a scattered light is then originated. The resulting scattered light has a frequency that is different from frequency of incident light hence this phenomenon is used to create a Raman Spectrum. A Raman Spectrum is generally offered as wavelength shift against intensity as shown in the Figure 2.17.

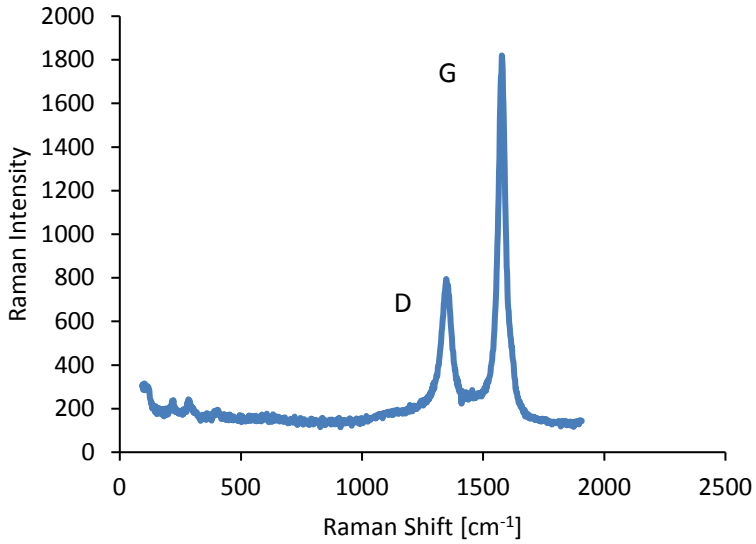


Figure 2.17:Typical Raman Spectra of CNTs.

The D band represents the degree of deformation of structure whereas the G band represents the graphitisation of the structure. Carbon nanotube is known to be Raman active, meaning it can be characterised by the Raman spectroscopy.

2.6.5. Gas Chromatogram (GC)

GC is the equipment that is used to separate and analysing gas mixtures to their discrete constituents. During GC analysis, a gas mixture is injected at the head of the column by micro-syringe, a carrier gas such as nitrogen or helium is used to carry the gases into the column wall. The progression of the gases inside the column depends entirely on the types of gas molecule and the material of stationary phase in the column. Due to different progression rate of different gases, the gas mixture is separated by the analyte mixture and gets to the detector at the different time (See Figure 2.18). The time at which each gas reaches the detector is recorded and depicted.

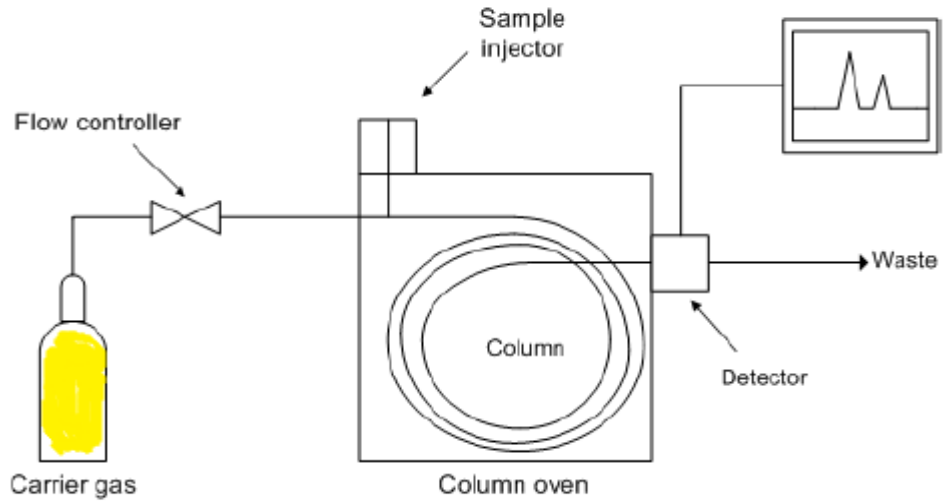


Figure 2.18: Schematic illustration of GC (Adapted from Maphutha, 2010).

2.6.6. Energy-dispersive X-ray spectroscopy (EDX)

This technique is used for elemental analysis of sample. This technique is based on a fundamental principle that each and every element that exists has a distinctive atomic structure, making it possible for the unique peak to show for different element on individual electromagnetic emission spectrum. (See Figure 2.19.)

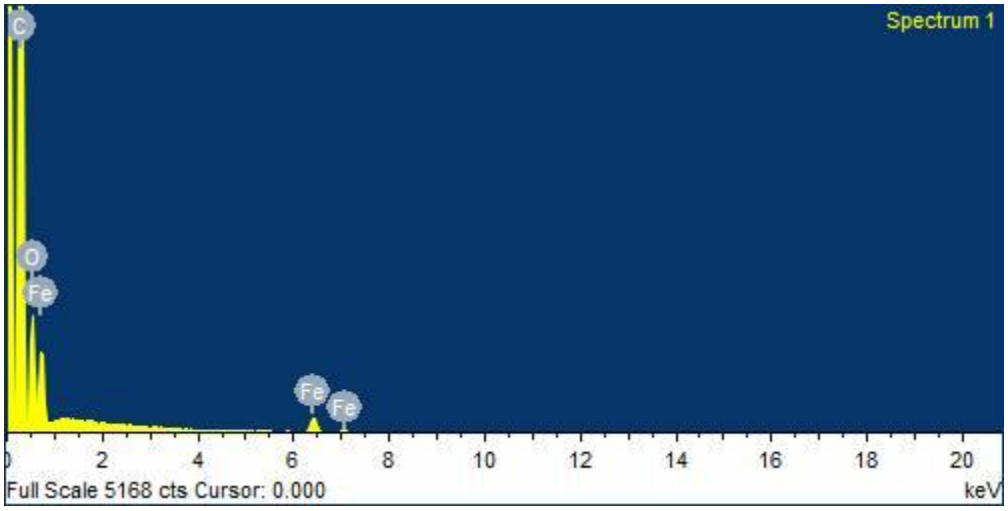


Figure 2.19: Typical EDX Spectra

What happens during this technique is that when the sample is bombarded by the electron beam the equipment detects the emitted x-ray by the sample to characterize the elemental composition of the volume being analysed. Small particle with the size that is as small as 1 µm can be analysed. EDX is a powerful tool in analysing the contamination in a sample. This

technique will be used in this study to determine the contamination of as-produced carbon nanotube.

2.6.7. Differential Scanning Calorimeter (DSC)

DSC technique (Figure 2.20) is a thermoanalytical method used to measure the difference amount of heat that is needed to raise temperature of sample being analysed.

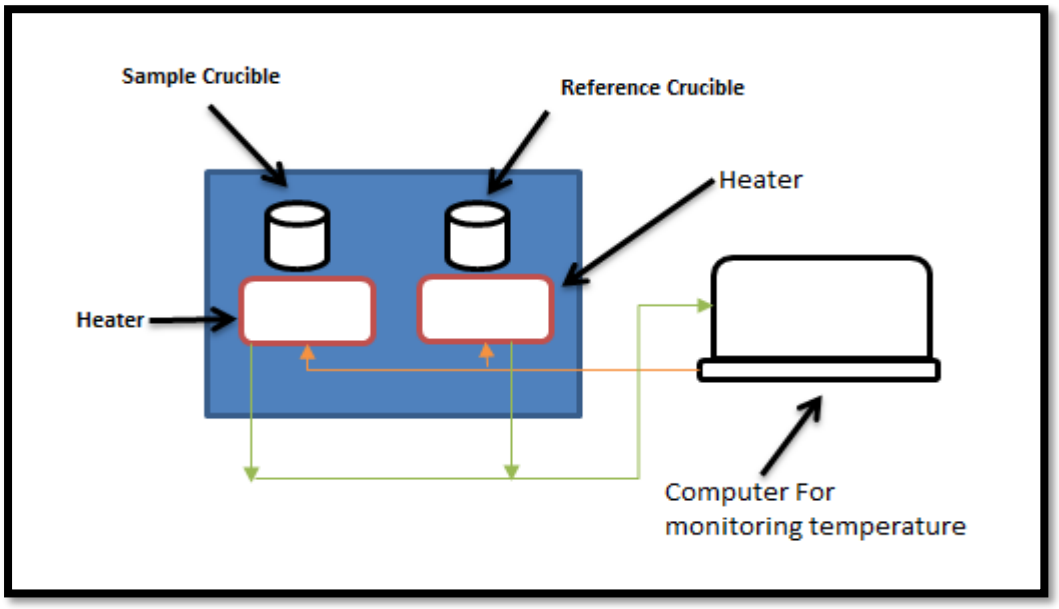


Figure 2.20: Schematic illustration of DSC set-up.

Schematic illustration shown in Figure 2.20 is a DSC equipment available at the University of the Witwatersrand coal lab. During this analysis, the temperature of the sample in increased linearly as a function of time. The reference sample is used to compare the difference in the heat required to raise the temperature. DSC technique is used mainly when studying phase transition of material. For example, the melting point of sample, glass transition temperature and/or exothermic decomposition. This technique follows the principle that during physical transformation of the sample such as phase transition either less or more heat will be required to flow through the sample than the reference to maintain both the sample and reference at the same temperature. The amount of heat required to flow through the sample depends on whether the process that is taking place is exothermic or endothermic. As an example, during crystallization process of a sample, less heat will be required since this is exothermic process. However, when a sample is moving from solid to liquid state, more heat is required because absorption of heat by sample is essential as it will be undergoing endothermic process. In this

study this DSC technique was used to measure the heat capacities of both the CNTs and CNT yarn.

2.6.8. Four probe

Four probe (See Figure 2.21) is an electrical impedance method of measuring resistivity of material. This method uses separation of pair of electrodes that carry current and detect voltage to give accurate measurement. Voltage and current electrodes reduce the contact and leads resistance from the sample measurement. This procedure has an advantage of giving measurement that is very precise such as low resistance values. This method was used in this study to measure the conductivity of CNTs yarn.

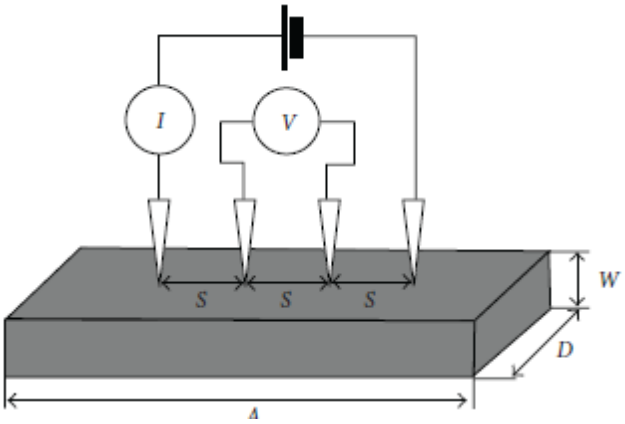


Figure 2.21: Schematic representative of Four Probe method (Ummartyotin et al.,2011)

2.7. Kinetic Study for Carbon Nanotube Production

2.7.1. Growth Mechanism

In order to control reaction condition, to obtain product as quick and economical as possible, kinetic studies of the reaction should be studied. CNTs growth is studied using kinetic model based on the rate of their chemical reaction.

There are different types of growth models that have been developed and are based on qualitative and experimental studies (Agboola et al., 2007. The following mechanisms, for CNTs growth, have been widely accepted (Kumar, 2011):

(1) When a hydrocarbon vapour interaction with a hot metal catalyst, it undergoes decomposition to form carbon and hydrogen species. Carbon species get adsorbed and dissolved into the surface of the metal particle whereas hydrogen species get detached off the catalyst. Carbon species will reach carbon solubility limit then start to

precipitate and crystallise in the form of cylinder network called carbon nanotubes (Kumar, 2011).

(2) The process of hydrocarbon decomposition is an exothermic reaction because it releases heat to the metal exposed surface whereas the carbon crystallisation is an endothermic reaction because it absorbs heat from metal precipitation zone. This is evident that there is some thermal gradient within a metal atom, and this makes the process to go on (Kumar, 2011). Two general cases for growth mechanism exist (Fig. 2.22). Figure 2.22a represents a case whereby the interaction between catalyst and support is weak and hydrocarbon vapor will decompose on top of metal catalyst.

(3) Carbon species will diffuse through towards the bottom of metal species and CNT will then precipitate out across the metal bottom pushing the whole catalyst unit off a substrate as shown in Figure 2.22ai. On condition that the metal's top surface is still available for more hydrocarbon decomposition, concentration gradient happens at the metal permitting carbon atoms to diffuse hence CNT remains to grow even longer as shown in Figure 2.22aii. The moment the metal particle become fully covered with excess carbon, its catalytic activity come to an end and the growth of CNT stops as depicted in Figure 2.22aiii. This growth mechanism is known as tip-growth model.

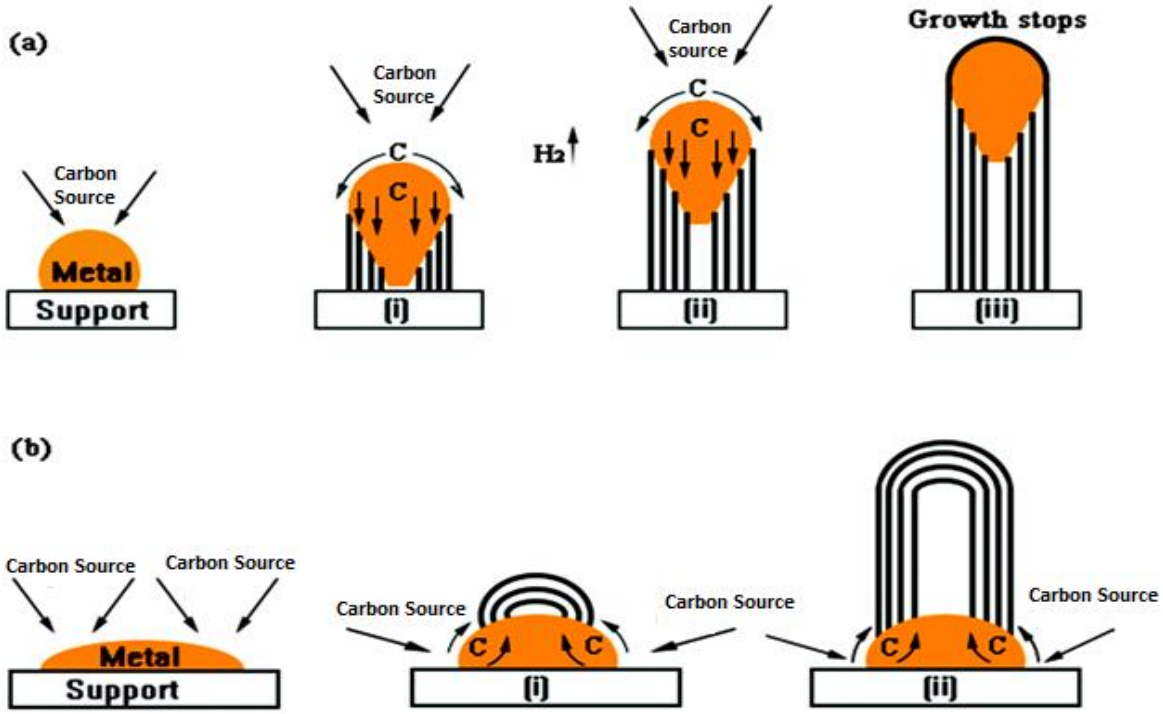


Figure 2.22: CNTs formation mechanism (Adapted from: Kumar, 2011)

(4) The second case as shown in Figure 2.22b happens when the interaction between catalyst and support is strong. Firstly, hydrocarbon will decompose, and carbon will start to diffuse through the metal particle as explained in tip growth method. However, in this method CNT crystallisation cannot push metal particle off support. Instead carbon will crystallize like a hemispherical dome which later prolongs up as unbroken graphitic cylinder as shown in Figure 6bi. Later the process of hydrocarbon decomposition proceeds on the lower surface of the metal as shown in Figure 6bii, followed by as-dissolved carbon that is diffusing upward. This case is known as base-growth model (Kumar, 2011).

2.7.2. Kinetic Models

A number of kinetic models for the production rate of CNTs has been proposed. Cabero (2004) in his study explained growing mechanism of CNTs using kinetic approach. The author produced CNTs in a thermo-balance using acetylene as carbon source and iron catalyst supported in silica. The author studied the influence of operating condition of the CNTs formation rate.

The author then developed a model that considers the formation of carbon, CNT nucleation and growth. The author expressed carbon concentration at the surface of metallic catalyst C_B, using first-order kinetics as follows:

$$\frac{dC_B}{d_t} = k_B(c_s - c_B), \quad (1)$$

where the constant k_B shows the segregation diffusion coefficient of metallic catalyst surface and Cs and C_B represent the saturated carbon atoms and the carbon concentration at the surface of metallic catalyst respectively.

Catalyst deactivation rate was stated as:

$$-\frac{da}{dt} = k_d a - k_r(1 - a) = k_G(a - a_S), \quad (2)$$

Deactivation and regeneration kinetic constants are denoted by k_d and k_r, respectively. a_s represents catalyst residual activity;

$$k_G = k_d - k_r. \quad (3)$$

Then carbon formation rate with respect to time was expressed as:

$$r_C(t) = rC_0[a_S + k_G \propto \exp(-k_G t) - k_B \beta \exp(-k_B t)], \quad (4)$$

Whereby;

$$\propto = [k_B(1 - a_S)]/[k_G(k_B - k_G)], \quad (5a)$$

$$\beta = (k_B - k_G a_S)/[k_B(k_B - k_G)], \quad (5b)$$

rC_0 denotes the maximum rate that CNT particles can be produced when catalyst is not deactivating

Kim et al (2005) investigated temperature-dependent of CNTs. They used CVD method with Ferrocene acting as catalyst as well as acetylene as carbon precursor. They discovered that as the growth temperature increased the length of CNT also increased. The authors proposed mechanism that Carbon atoms dissolved throughout a metal catalyst as follows: Carbon atom get saturated in the metal particle and form intermediate before they precipitate into CNTs as described in the following equation:

$$C_{free} + C_{sat} \overset{k_1}{\rightarrow} C_{excess}, \quad (6a)$$

$$C_{excess} \overset{k_{-1}}{\rightarrow} C_{free} + C_{sat}, \quad (6b)$$

$$C_{excess} \overset{k_d}{\rightarrow} C_{sat} + CNTs, \quad (6c)$$

Where C_{free} is carbon that is still in gas phase. C_{sat} is the carbon that is saturated in a metal nano particles. k_1, k_{-1} and k_d represent the equilibrium constant for forward, reverse and CNTs growth reactions respectively.

They assumed that the intermediate atom, C_{excess}, is in equilibrium with C_{sat} and $C_{free,}$ the equilibrium constant was then expressed as:

$$K = \frac{[C]_{excess}}{[C]_{free}[C]_{sat}} = \frac{k_1}{k_{-1}} \quad (7)$$

Then the rate for CNTs growth was finally expressed as follows:

$$\frac{d[CNT]}{dt} = k_d[C]_{excess} = k_d K[C]_{excess}[C]_{sat}$$
$$= \left(K[C]_{free}\right)k_d[C]_{sat} = Ak_d[C]_{sat}. \quad (8)$$

Simate et al (2014) investigated the effect of carbon source on the production rate of CNTs. They produced CNTs using carbon dioxide as carbon precursor and iron supported by calcium carbonate as catalyst using CVD reactor at constant temperature set at 800°C. They found out that an increase in CO_2 concentration increased the production rate of CNTs until concentration

up to 5000 ppm then CNTs production rate start to decrease again. Their model development started at the decomposition of CO_2 into carbon and oxygen following this reaction:

$$CO_2 \rightarrow C + O_2 \quad (9)$$

However, they considered the so called "initial stage" for the splitting of CO_2 that result in producing carbon monoxide (CO) and oxygen (O_2) as shown in reactions below:

$$2CO_2 \rightarrow 2CO + O_2 \quad (10)$$

Then CO will then further decompose into Carbon and CO_2 as shown below:

$$2CO \rightarrow C + CO_2 \quad (11)$$

They then reported that when CO_2 comes into contact with hot metal catalyst the following reactions takes place:

$$CO_{2(gas)} \rightleftharpoons CO_{2(ads)} \quad (12)$$

Then decomposes reversibly into CO and oxygen as shown in reaction below;

$$CO_{2(ads)} \rightleftharpoons CO_{(ads)} + O_{(ads)} \quad (13)$$

Then the reaction rate for reverse and forward reaction was formulated as shown below:

$$R_{forward} = k_1[CO_{2(ads)}] \quad (14a)$$

$$R_{reverse} = k_{-1}\left[CO_{(ads)}\right][O_{(ads)}\ ] \quad (14b)$$

CO will then further decompose into Carbon and Carbon dioxide

$$2CO_{(ads)} \rightleftharpoons C_{(ads)} + CO_{2(ads)} \quad (14c)$$

The rate equation for the forward and reverse reaction was then expressed as follows:

$$R_{forward} = k_2[CO_{(ads)}]^2 \quad (15a)$$

$$R_{reverse} = k_{-2}\left[C_{(ads)}\right][CO_{2(ads)}]\ ] \quad (15b)$$

Whereby k_2 and k_{-2} denote rate constants for forward and reverse reactions at equilibrium.

The resulting carbon atom on the metallic nanoparticle then crystallises and form CNT as shown below:

$$C_{(ads)} \rightarrow CNT \quad (16)$$

The final CNT production rate was proposed as follows:

$$\frac{d[CNT]}{dt} = k_3\left[C_{(ads)}\right]. \quad (17)$$

It should be emphasized that out of all kinetic models that are in the open literature none of them deals with the production of CNT yarn as opposed to CNTs. This study was focusing on the production of CNT yarn using methane as carbon precursor and the kinetic model for this production was developed.

2.8. Thermodynamic Study for Carbon Nanoyarn

Thermodynamic functions such as heat capacities of CNT yarn are reflected to be more valuable thermophysical measures that need to be understood when studying material (e.g. CNT yarn). Many scientific areas such as Chemical engineering physics and chemistry need accurate heat capacity in order to obtain entropy, enthalpy, phase transition and energy balance. Harutyunyan et al. (2009) studied the thermodynamics of the catalytic growth of CNTs via endothermic reaction. They monitored reaction enthalpy progression during the process of CNTs production using methane gas as carbon precursor. The authors found that, though methane vapour decomposition reaction is considered to be endothermic reaction, an exothermic reaction is superimposed to promote CNTs growth. They proposed that the resulting heat liberated is due to the radiative heat transfer coming from the surrounding as well at the decomposition reaction of secondary hydrocarbon that has formed at the surface of the catalyst and carbon hydrogenation or oxidation reaction. Their finding shows that the CNTs growth process is an exothermic reaction. In addition, they proposed that the main contributor of this liberated heat is because of the radiative heat transfer from the surroundings as well as the dehydrogenation reaction of formed secondary hydrocarbons on the catalyst surface and the carbon hydrogenation or oxidation processes. Their finding implies that the CNTs growth process enthalpy is exothermic.

Kabo et al. (2016) studied Thermodynamic Properties and Similarity of Stacked-cup MWCNTs and Graphite. They measured eat capacity of MWCNTs using adiabatic calorimeter. This was done in a temperature range between 5 to 370 Kelvin and the resulting heat capacities were reported. The determined energy of combustion for MWCNTs using combustion calorimetry, and the enthalpy of combustion was found to be 0.6 ± 0.9 kJ·mol^{-1}. They also

reported that the thermodynamic properties of MWCNTs at temperature less than 200 K are close to those of the graphite.

Nan et al. (2009) in his demonstrated that CNTs are stable at the temperature between 25-600 °C as shows in the Figure 2.23. This molar heat capacities of SWNTs and MWNTs were measured using adiabatic calorimeter at temperatures between 78 and 398 K.

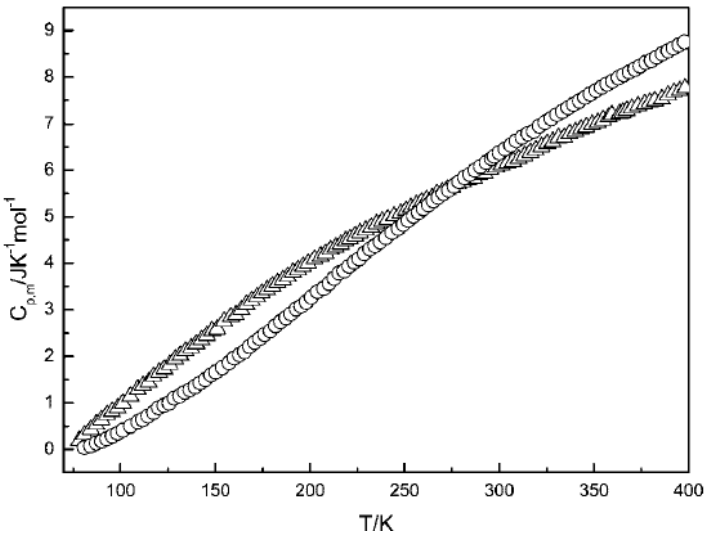


Figure 2.23: Graphs showing, molar heat specification at different temperatures (Nan et al., 2009)

Thermodynamic study of CNT yarn using methane as carbon precursor and ferrocene as catalyst is not available in the open literature. This study concentrated on determining thermodynamic parameters such as Heat flow, heat capacities, entropy and enthalpy for CNT yarn produced in CVD reactor.

CHAPTER THREE

3.0. Methodology

3.1. Synthesis of CNT yarn using CVD reactor

For this study, a catalytic CVD reactor equipped with a motor was used for direct spinning of CNTs to CNT yarn. The diameter of a stainless steel (SS) tube used as a reactor was 50 mm with a length of 1050 mm and placed vertically in an electric furnace as shown in Figure 3.1. The reactor temperature was monitored with PID controller that is built in the reactor and PT100 thermocouple was used to measure the temperature in the reaction zone. The speed of the motor was kept constant at 10 rpm for all the experiments. The motor speed was also monitored using PID controller built within the reactor.

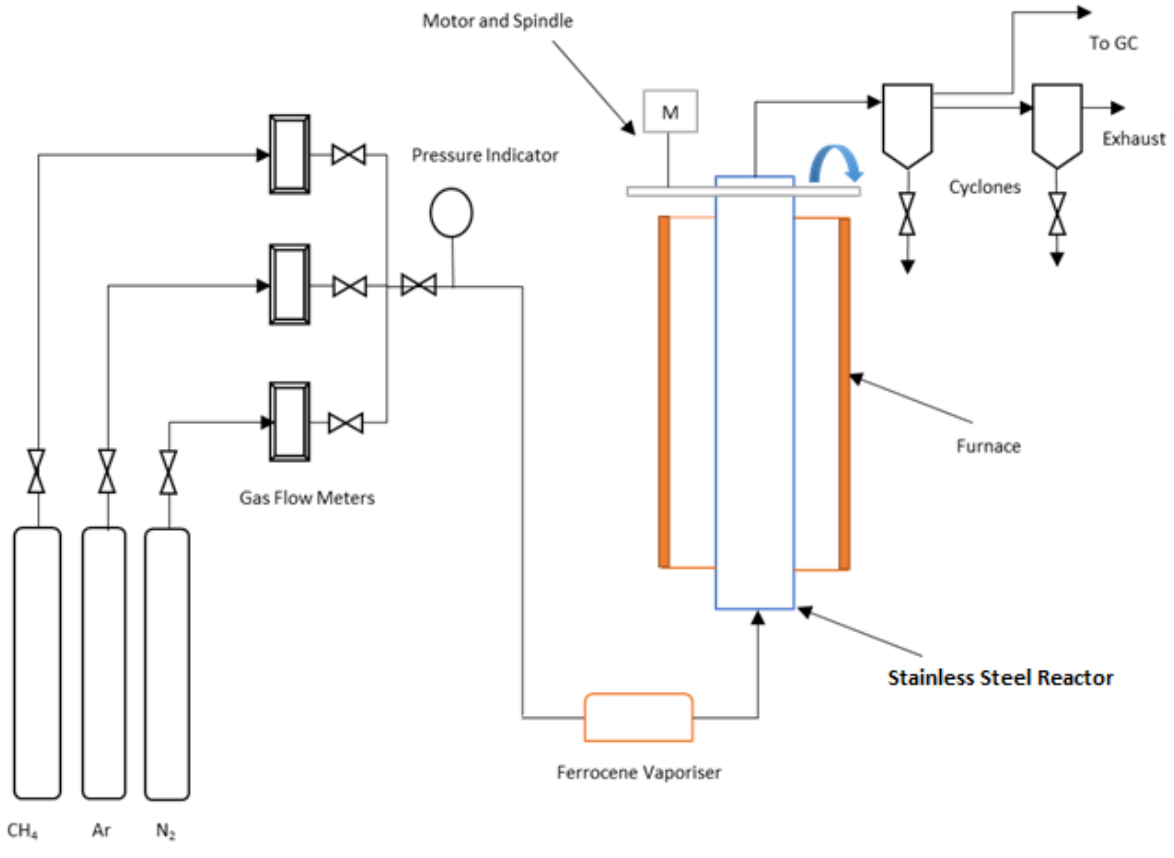


Figure 3.1:Process flow diagram of experimental set-up for CNT yarn production.

Before each experiment, Nitrogen (N_2) gas was used to detect leaks, purge the system and also create inert environment inside the reactor. During the production process, Methane gas was

used as a carbon source and Ferrocene ($C_{10}H_{10}Fe$) was used as a catalyst. The catalyst amount that was used during the production of CNT yarn was kept at approximately 10 g and vaporised at a temperature of 250^{o}C in a vaporiser that is attached to the reactor. The vaporised ferrocene was carried to the reaction zone using argon as a carrier gas together with methane for the production of CNT yarn. All gases that were used for these experiments were Ultra High Purity (UHP) gases purchased from AFROX Ltd. The catalyst was supplied by Sigma Aldrich and used as-purchased with no further preparation or enhancement. In order to determine the kinetic study, methane flow rate was varied from 100 ml/min to 150 ml/min at a constant temperature of 900^{o}C. The duration of each experiment was kept constant at 15 min. Similar experiment was repeated at reactor temperature of 950^{o}C and 1000^{o}C. CNTs and yarns were collected from the spindle after each experiment. Table 3.1 summarises the experimental condition that was considered in this study.

Table 3.1: Summary of the experimental conditions

Experiment No.	CH_4 Flow Rate [ml/min]	Reaction Temperature [^{o}C]	Time of reaction [min]	Motor Speed [rpm]
1	100	900	15	10
2	100	950	15	10
3	100	1000	15	10
4	125	900	15	10
5	125	950	15	10
6	125	1000	15	10
7	150	900	15	10
8	150	950	15	10
9	150	1000	15	10

3.2. Characterisation of CNTs and CNT yarn

The amount of CNTs and CNT yarn produced was measured gravimetrically using electronic precision balance.

3.2.1. Gas Chromatography

During the reaction, the gaseous portion of the product was collected using gas sampling bag and analysed using Bruker 430 Gas Chromatogram (GC) equipped with a thermal conductivity detector to determine the composition of the gases. Argon was used as the carrier gas and the pressure was kept at 400 kPa during the gas analysis cycle. The oven was kept at an initial temperature of 50^{o}C for a period of 5 minutes before ramping program was started. The

temperature in the column was increased at a rate of 10^{o}C per minutes until it reached the maximum temperature of 150^{o}C. The injector temperature was set at 140^{o}C. The GC oven was retained at this temperature for duration of 12 minutes. The full cycle took 14 minutes to complete. Table 3.2 summarises the approximate retention times of product gases.

Table 3.2: Product gases retention time

Gas	Approximate time[min]
H_2	0.4
CH_4	0.7-1
Ar	0.5

3.2.2. Transition Electron Microscope

The structure of the tube was determined using High Resolution Transition Electron Microscope (HRTEM), Joel JEM-2100, operated at 200 kV acceleration voltage. Methanol of 5 ml was added to the sample before it was placed into a sonic bath for a period of 10 min. The resulting suspension was then dropped onto copper grid that had lacey carbon film which was sited on the microscope.

3.2.3. Scanning Electron Microscope

The CNTs and CNT yarn surface morphology was checked using FEI Quantra 200 Scanning Electron Microscopy operated at 30kV and also equipped with Energy Dispersive X-Ray Spectroscopy for determining elemental composition. A small amount of each sample was placed onto the double-sided tape and mounted on the aluminium stub. The mounted samples were coated with two layers of gold-palladium with a thickness of 10 nm on each sample before characterisation.

3.2.4. Raman Spectroscopy

Raman spectra of CNTs were acquired by means of a 514.5 nm line of a Lexel Model 95 SHG argon ion laser with a Horiba LabRAM HR Raman spectrometer which was equipped with an Olympus BX41 microscope attachment. A 100x objective lens was used to focus incident beam onto the sample. In order to prevent localised heating, the power at the sample was kept as low as approximately 0.5 mW. 600 lines per mm grating were used to disperse the backscattered light onto a nitrogen liquid cooled charged coupled device (CCD) detector and LabSpec v5 was used to acquire data.

3.3. Thermodynamic Properties measurement of the CNT yarn

The thermal stability and heat flow of CNT yarn was obtained by thermogravimetric analyser equipped with Differential Scanning calorimeter (TGA/DSC), model SDTQ600. A platinum crucible was used to load sample and another empty platinum crucible was used as a reference. The sample was heated from an ambient temperature to 900ºC at a heating rate of 5ºC per minute. During the process, nitrogen was passed through the system at a constant flow rate of 50 ml per minute. Each experiment took about 3 hours to complete.

The heat capacity (C_P) of the sample was determined by the dimensional relationships, dividing the heat flow by the rate of heating the sample using equation (1) (Perry,1950):

$$\frac{\Delta Q/\tau}{\Delta T/\tau} = \frac{\Delta Q}{\Delta T} = C_P \quad (1)$$

Specific heat capacity ($C_{p,m}$) can be expressed in terms of heat flow acquired straight from DSC curve using formula [2]:

$$C_{p,m} = \frac{1}{m}\frac{\Delta Q}{\Delta T} = \frac{1}{m}.C_p \quad (2)$$

Whereby m is the initial sample mass, ($\frac{\Delta Q}{\tau}$) is the heat flow obtained from DSC Curve and($\frac{\Delta T}{\tau}$) is the heating rate.

The following thermodynamic functions of CNT yarn were also calculated:

Enthapy Change:

$$\Delta H = H[T] - H[25] = \int_{25}^{T} C_{p,m}\,dT \quad (3)$$

Entropy Change:

$$\Delta S = S[T] - S[25] = \int_{25}^{T} \frac{C_{p,m}}{T}\,dT \quad (4)$$

Whereby 25ºC was the initial sample temperature

3.4. Measuring the electrical conductivity of the CNT yarn

High Field Cryogen Free Measurement System supplied by Cryogenic Ltd was used to conduct Four-probe method test for each sample of CNT yarn. Small quantity of each sample was attached to a double-sided tape and mounted onto the sample holder. A 5 x 5 mm substrate was used to support the mounted sample. The four corners of the mat were applied by a conductive silver paint to offer contact between the sample holder and the mat. Before the sample holder was mounted on a resistivity probe, the paint was first allowed to dry. The resistivity probe

with the sample was then connected to a four-terminal configuration. A voltage of 0-2 V was passed through each sample at room temperature during the measurements.

The electrical conductivity was calculated using the following formulas:

The I-V curve obtained during measurements of each sample was utilised to estimate the resistivity according to ohm's law as follows:

$$R(\Omega) = \frac{1}{gradient} \quad (5)$$

Equation (6) was used to calculate the resistivity of each sample:

$$\rho(\Omega.m) = \frac{RA}{L} \quad (6)$$

Equation (7) is then used to calculate the electrical conductivity of CNT yarn

$$\sigma\ (S/m) = \frac{1}{\rho} \quad (7)$$

Whereby *R* is the sample resistance, *L* represent the length of the mat *A* is the cross-sectional area of the mat, **ρ** represent the resistivity of the sample and σ shows the electrical conductivity of the sample.

CHAPTER FOUR

4.0. Production of CNTs and Kinetic study

4.1. Introduction

Carbon nanotubes (CNTs) applications has been extensively explored due to their extraordinary physical, chemical and electrical properties. Despite the outstanding properties of carbon nanotubes, the major challenge is to organize this nanoscale structure into macroscale structure such as yarn that have the same properties as the individual CNT. CNTs alignment is one of the main important factors in obtaining a yarn with similar properties (Zhang et al., 2006), because individual CNT has intrinsic one-dimensional nature (Jiang et al., 2011; Jakubineck et al., 2012). With all the different types of CNTs production methods, the challenge of low CNTs production rate still exists (Bepete et al., 2013; Segura-Cardenas et al., 2012; See & Harris, 2007). The low production rate could be due to the little understanding of growth mechanism of CNTs. A number of kinetic models for the production rate of CNTs have been proposed (Gokcen et al., 2002; Hsieh et al., 2009; Philippe et al., 2009). Several steps of CNTs synthesis in CVD are acknowledged and can be outlined as follows: decomposition of carbon precursor to generate carbon atom and carbon cluster, carbon atom and carbon cluster dissolution on the metallic nanoparticle; carbon precipitation from saturated metallic nanoparticles and finally, tubular carbon structure formation (Perez-Cabero et al., 2004). To maximize the continuous production of CNTs in a large scale, kinetic studies of the production of CNTs have been widely studied. However, the kinetic model of CNTs produced from methane is not yet reported in open literature till date to the best of my knowledge. This Chapter focuses on the production of CNTs and their kinetic modelling as the intermediate in the production of yarn.

4.2. Experimental procedure and development of kinetic model

4.2.1. Experimental Procedure

CNTs were produced in a CVD reactor using Methane as Carbon precursor and Ferrocene was used as a catalyst. Various Characterisation method was used to identify CNTs. For detailed Experimental; procedures please refer to Chapter 3, Section 3.1 and Section 3.2.

4.2.2. Development of Kinetic Model

During the experiment, carbon source (CH_4) was in gas phase and ferrocene was in solid phase. It can then be concluded that, the reaction is heterogeneous catalysed as opposed to homogenous catalysed whereby the reactants and the catalyst are in the same phase. During heterogeneous catalysis, three reaction steps take place; adsorption of reactants onto the catalyst followed by the surface reaction of the adsorbed reactants and finally desorption of product off the surface of the catalyst.

The following assumptions were considered when modelling:

- Desorption of carbon atom, from catalyst particle, to form CNTs is the rate limiting step
- The adsorption process is very fast and quasi-equilibrium controls it
- The initial active site of the catalyst $[*]_0$ is equal to $6.18\ x\ 10^{-7} mol/min.mg$ which is the actual active site of $Ni_{20}/AlPO_4$-P.

Below is the mechanism of methane decomposition in the presence of ferrocene catalyst to form carbon nanotubes.

Initially CH_4 will adsorb on the surface of the Catalyst (Ferrocene) as follows:

$$CH_4 + * \underset{k_{-1}}{\overset{k_1}{\leftrightarrow}} CH_4* \quad (1)$$

The reaction rate for the forward and reverse reaction of equation (1) is as follows:

$$R_{forward} = k_1[CH_4]\,[*] \quad (2)$$

$$R_{reverse} = k_{-1}[CH_4*] \quad (3)$$

Where CH_4* represent methane chemisorbed on a surface site of the catalyst nanoparticle, * denotes the active site of the catalyst and [*] indicate surface concentration. k_1 and k_{-1} correspond to rate constants for adsorption and desorption respectively.

It is assumed that the adsorption process is very fast and quasi-equilibrium controls it, hence the rate of forward reaction is equal to the rate of reverse reaction.

From equation (2) & (3):

$$\text{Net rate} = 0 \quad (4)$$

Therefore;

$$k_1[CH_4]\,[*] = k_{-1}[CH_4*] \quad (5)$$

The equilibrium constant for the reaction is defined as follows:

$$K_1 = \frac{k_1}{k_{-1}} = \frac{[CH_4^*]}{[CH_4][*]} \quad (6)$$

The adsorbed methane onto the catalyst particle will further decompose into carbon atom and hydrogen. Hydrogen atom will combine with another hydrogen atom forming hydrogen gas as shown in equation (7):

$$CH_4* \underset{k_{-2}}{\overset{k_2}{\leftrightarrow}} C* + 2H_2 \quad (7)$$

The reaction rate for the forward and reverse reaction of equation (7) is as follows:

$$R_{forward} = k_2[CH_4*] \quad (8)$$

$$R_{reverse} = k_{-2}[C*]\,[H_2]^2 \quad (9)$$

Where C* represent Carbon atom chemisorbed on a surface site of a catalyst nanoparticle, k_2 and k_{-2} are rate constants for adsorption and desorption reactions respectively.

Since equation (7) is an equilibrium reaction the rate of forward reaction is equal to the rate of reverse reaction (quasi equilibrated)

From equation (8) & (9):

$$\text{Net rate} = 0 \quad (10)$$

Therefore;

$$k_2[CH_4*] = k_{-2}[C*]\,[H_2]^2 \quad (11)$$

The equilibrium constant for the reaction is defined by the following equation:

$$K_2 = \frac{k_2}{k_{-2}} = \frac{[H_2]^2[C^*]}{[CH_4^*]} \quad (12)$$

Carbon atom adsorbed on the surface of the catalyst will diffuse into the catalyst combining with another carbon atom in the particle and forming CNT as shown below:

$$C* \xrightarrow{k_3} CNT + * \quad (13)$$

This reaction is the rate determining step (Simate et al. 2014)

The rate of reaction for reaction (13) could be expressed as follows:

$$r = k_3[C^*] \quad (14)$$

Total site balance on the catalyst surface is shown in equation (15):

$$[*]_0 = [CH_4^*] + [C^*] + [*] \quad (15)$$

From equation (12):

$$CH_4^* = \frac{[H_2]^2[C^*]}{k_2} \quad (16)$$

From equation 6:

$$[*] = \frac{CH_4^*}{[CH_4]k_1} \quad (17a)$$

Combining equation (16) and equation (17) gives:

$$[*] = \frac{[H_2]^2[C^*]}{k_1k_2[CH_4]} \quad (17b)$$

Substitute (17b) and (16) into (15)

$$[*]_0 = \frac{[H_2]^2[C^*]}{k_2} + [C^*] + \frac{[H_2]^2[C^*]}{k_1k_2[CH_4]}$$
$$= [C^*]\left[\frac{[H_2]^2}{k_2} + 1 + \frac{[H_2]^2}{k_1k_2[CH_4]}\right] \quad (18)$$

Simplifying equation 18 gives:

$$[C^*] = \frac{[*]_0}{\frac{[H_2]^2}{k_2}+1+\frac{[H_2]^2}{k_1k_2[CH_4]}} \quad (19)$$

Substitute equation (19) into (14) gives:

$$r = \frac{k_3[*]_0}{\frac{[H_2]^2}{k_2}+1+\frac{[H_2]^2}{k_1k_2[CH_4]}} \quad (20)$$

Simplifying equation (20) gives:

$$\frac{d[CNT]}{dt} = \frac{K_1K_2k_3[CH_4][*]_0}{K_1[CH_4][H_2]^2+K_1K_2[CH_4]+[H_2]^2} \quad (21)$$

Equation (21) is the kinetic model equation that can be used to predict the production rate of CNTs produced using methane as carbon precursor.

4.3. Results and discussion

4.3.1. SEM images of CNTs produced at a reactor temperature of 900ºC

The SEM image in Figure 4.1 shows the carbon nanotubes produced at methane flow rate of 100 ml/min. The image shows a few carbon nanotubes and more of amorphous carbon. The carbon nanotubes in Figure 4.2 are produced at methane concentration of 125 ml/min. The image shows a number of CNTs in the midst of amorphous carbon and catalyst impurities. Figure 4.3 shows carbon nanotubes produced at 150 ml/min methane flow rate. There are some forms of long CNTs, and the amorphous carbon as shown in the image. When comparing the CNTs produced at reactor temperature of 900^{o}C, it can easily be seen that more CNTs are produced at methane flow rate of 125 ml/min (Fig 4.2) than 100 (Fig 4.1) and 150 ml/min (Fig 4.3). These could be due to the fact that, the flow rate of 100 ml/min is not enough for CNTs production because of less concentrated carbon available in the feed, and the flow rate of 150 ml/min results in high superficial velocity in the reactor and the residence time of methane in the reactor is not enough for proper formation of CNTs.

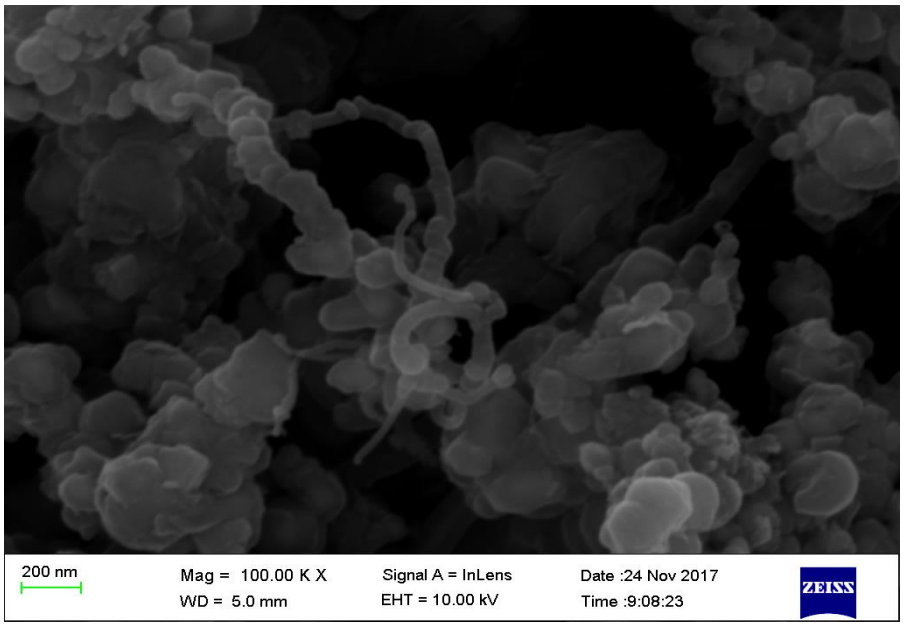


Figure 4.1: CNTs produced at methane flow rate of 100 ml/min (900^{o}C)

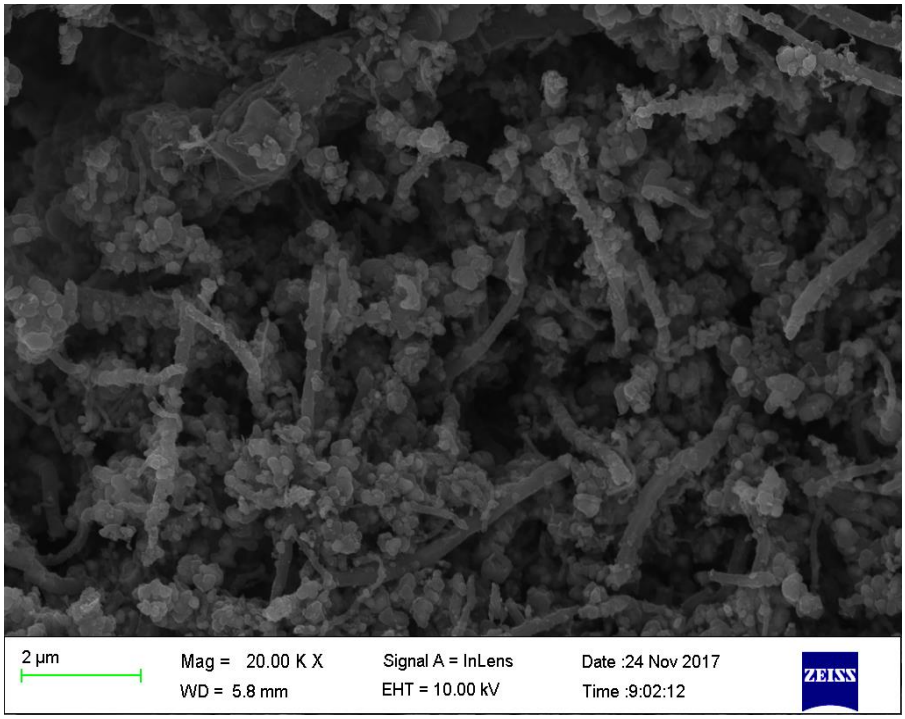


Figure 4.2: CNTs produced at methane flow rate of 125 ml/min (900^{o}C)

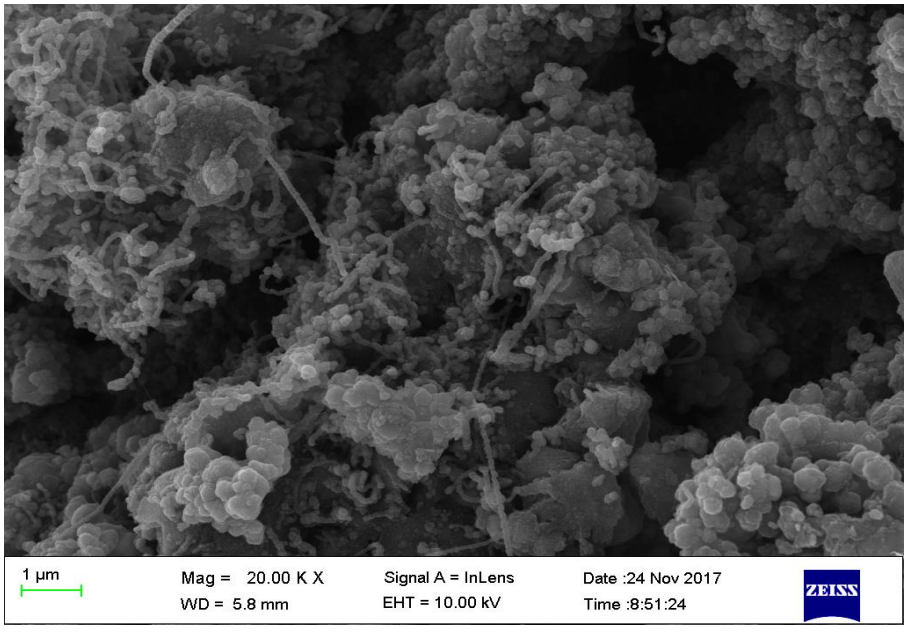


Figure 4.3: CNTs produced at methane flow rate of 150 ml/min (900^{o}C)

4.3.2. SEM images of CNTs produced at a reactor temperature of 950^{o}C

Figure 4.4 shows the carbon nanotubes as well as the amorphous carbon that were obtained when the methane flow rate was at 100ml/min. Figure 4.5 shows less amorphous carbon and a lot of long and aligned carbon nanotubes that were produced at a flow rate of 125 ml/min of

methane gas. The carbon nanotubes that were produced at methane concentration of 150 ml/min are shown in Figure 4.6. These carbon nanotubes have less amorphous carbon as well. This is an indication that, increasing the reactor temperature from 900 to 950^{o}C resulted in the formation of a well aligned CNTs with less amorphous carbon. Furthermore, CNTs produced at methane flow rate of 125 ml/min (Fig 4.5) have better quality as compared to CNTs produced at methane flow rate of 100 (Fig 4.4) and 150ml/min (Fig 4.6).

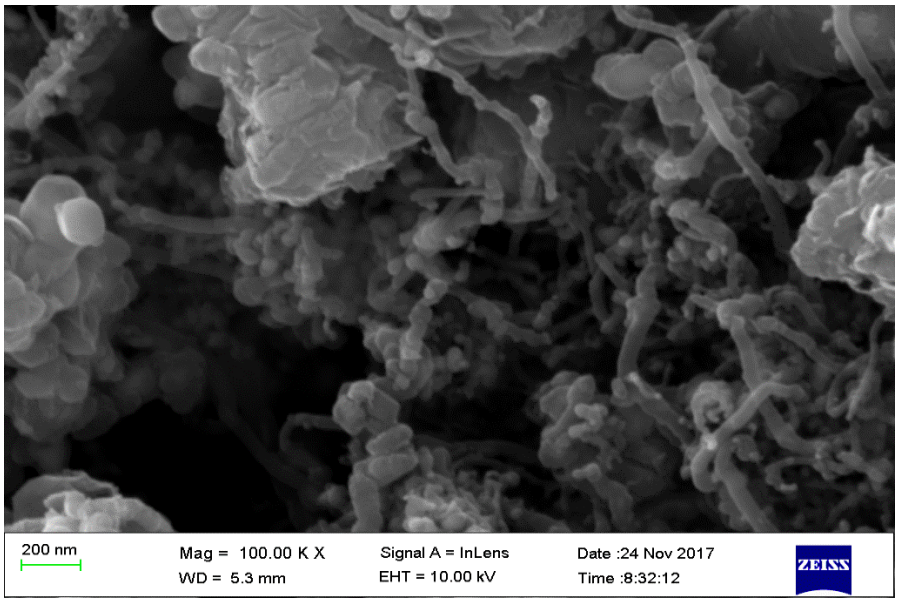


Figure 4.4:SEM image of CNTs produced at methane flow rate of 100 ml/min (950^{o}C)

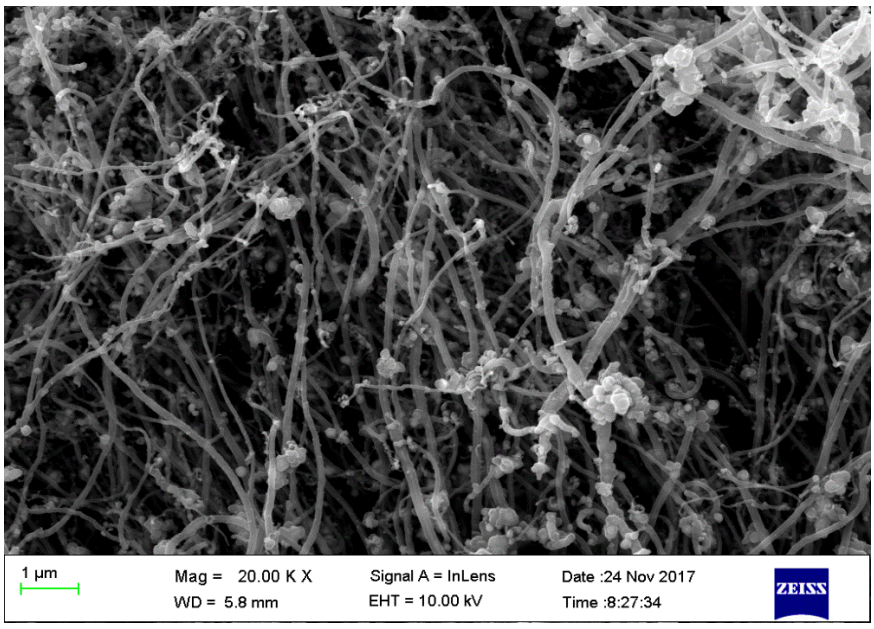


Figure 4.5:SEM image of CNTs produced at methane flow rate of 125 ml/min (950^{o}C)

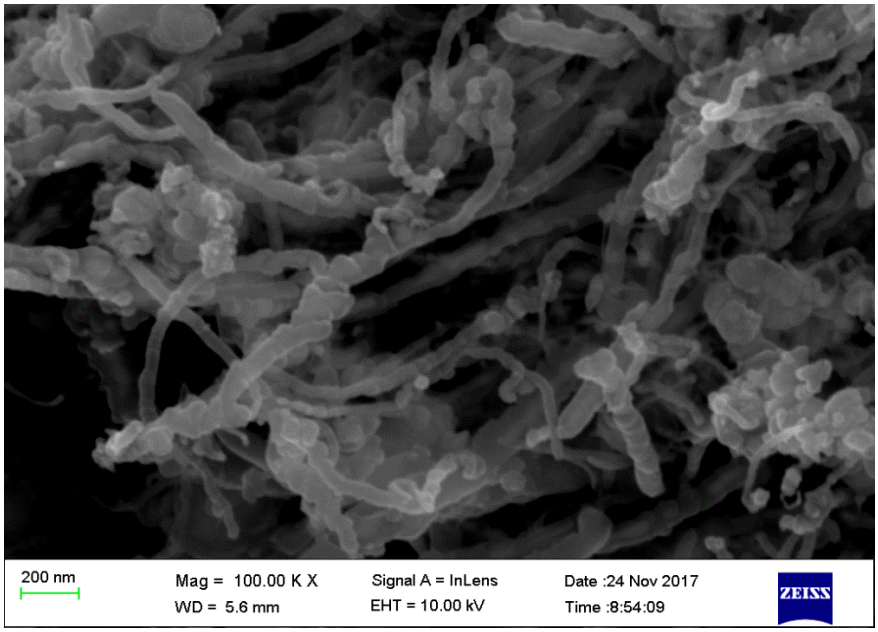


Figure 4.6:SEM image of CNTs produced at 150 ml/min methane flow rate (950^{o}C)

4.3.3. SEM images of CNTs produced at a reactor temperature of 1000^{o}C

The carbon nanotubes produced at methane flow rate of 100 ml/min are few as compared to the amorphous carbon as shown in Figure 4.7. The image in Figure 4.8 is the carbon nanotube and amorphous carbon produced at a methane flow rate of 125 ml/min, the image shows 50% CNTs and 50% amorphous carbon. Figure 4.9 shows few carbon nanotube and significant amount of amorphous carbon. From Figure 4.9 it can be concluded that further increase in reactor temperature to 1000^{o}C from 950^{o}C results in less CNTs produced. However, the CNTs have better quality that the one produced at 900^{o}C. This result could be due to the fact that at higher reactor temperature the produced CNTs were pyrolyzed and this finding agrees with literature (Tripathi et al, 2017).

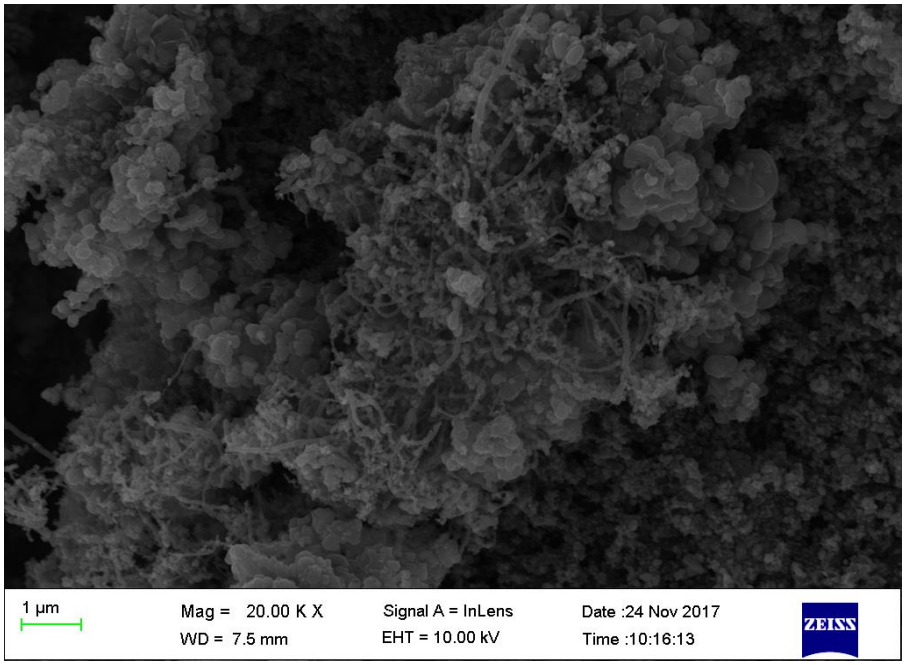


Figure 4.7: SEM image of CNTs produced at 100 ml/min methane flow rate (1000^{o}C)

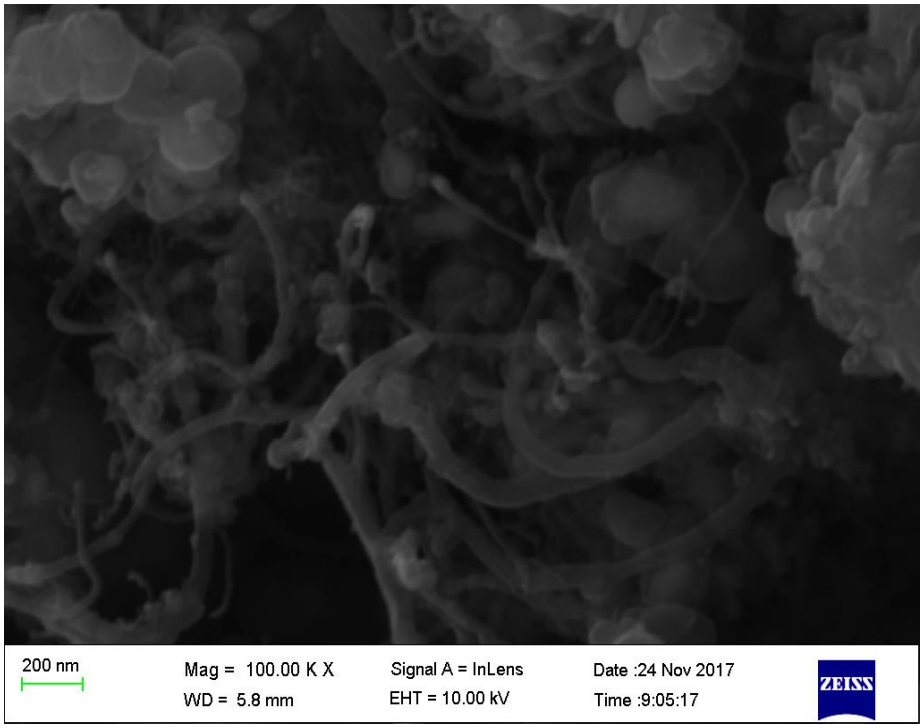


Figure 4.8: SEM images of CNTs produced at 125 ml/min methane flow rate(1000^{o}C)

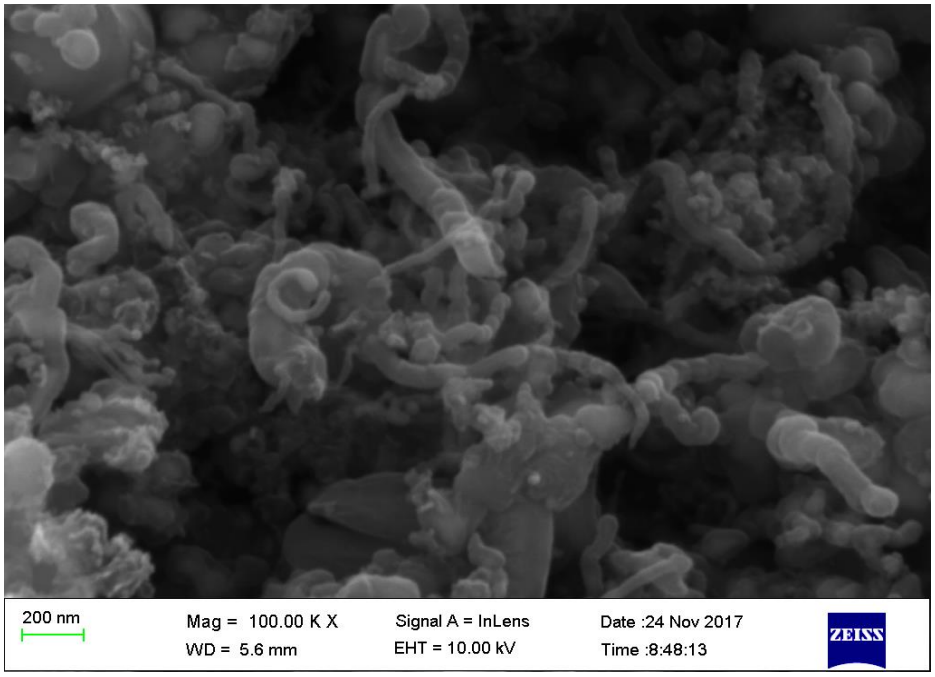


Figure 4.9:SEM image of CNTs produced at 150 ml/min methane flow rate (1000^{o}C).

4.3.4. Effect of methane flow rate on quality of CNTs obtained at 900^{o}C

At 900^{o}C, CNTs were produced at a methane flow rate of 100 ml/min as shown in Figure 4.10. Catalyst particles are shown in the inner core of the tube (Dark spot on the TEM image). The average diameter of the tube was 88.23 nm. Figure 4.11 shows a long smooth carbon nanotube produced at methane concentration of 125 ml/min. The image shows that there are catalyst particles that are embedded at the inner core of the tubes, but they are less. The CNTs at this condition have the diameter of about 53.70 nm. In Figure 4.12, the carbon nanotubes produced have the average diameter of 84.9 nm, these carbon nanotubes were produced at a methane flow rate of 150 ml/min. The TEM image clearly shows the catalyst particles trapped inside of CNTs structure as well as the amorphous carbon deposited at the surface of some tubes. The average diameter of tubes produced at reactor temperature of 900^{o}C has less than 100 nm but more than 20 nm indicating the presence of MWCNTs in the samples.

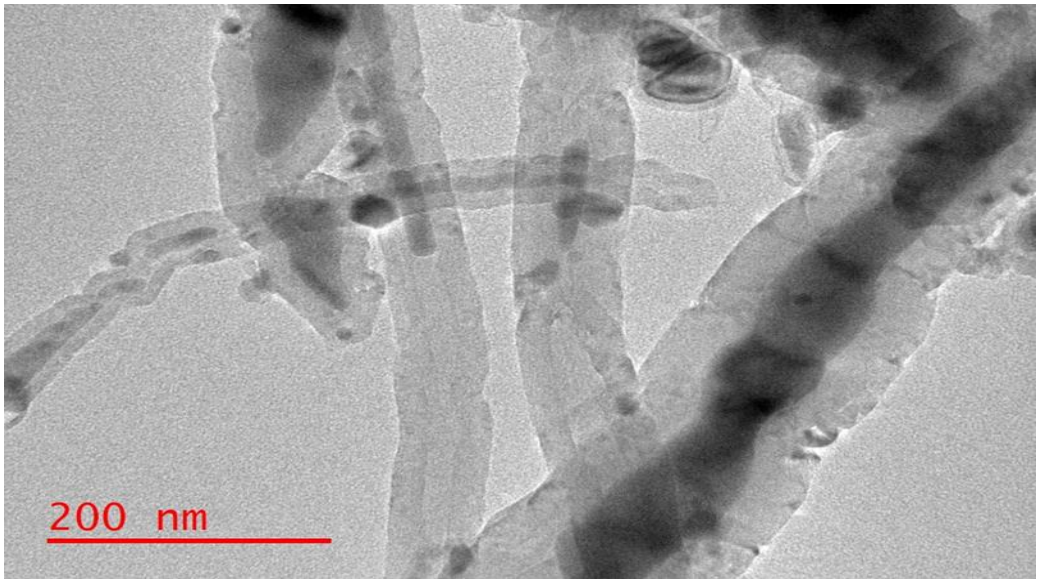


Figure 4.10:TEM image of CNTs produced at methane flow rate of 100 ml/min (900^{o}C).

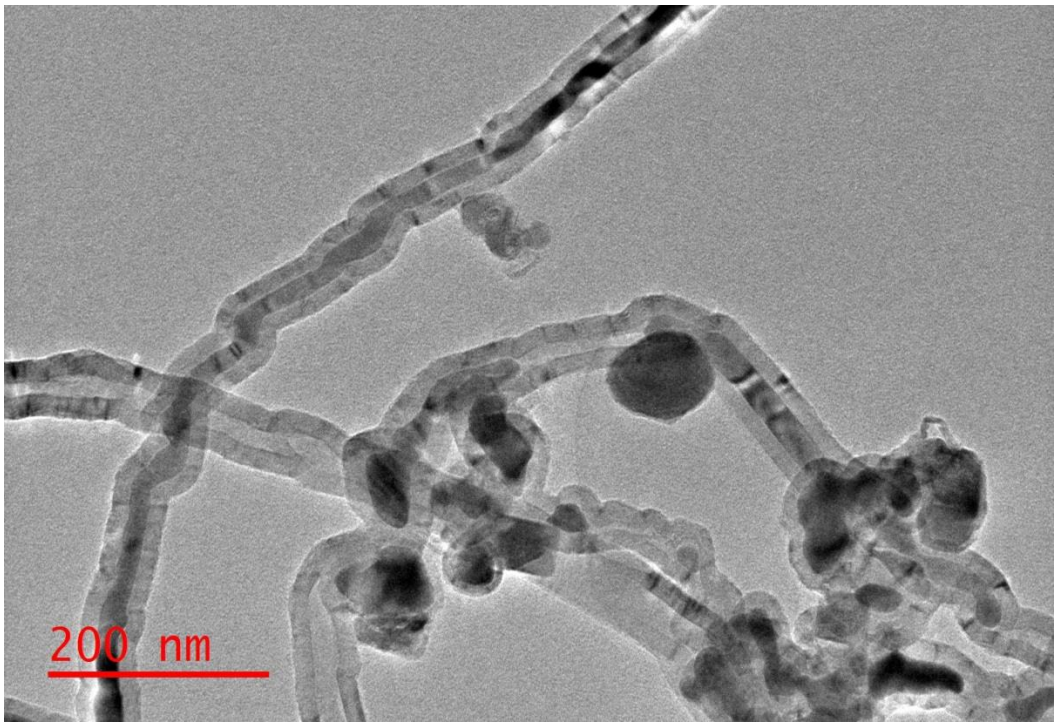


Figure 4.11: TEM images of CNTs produced at methane flow rate of 125 ml/min (900^{o}C).

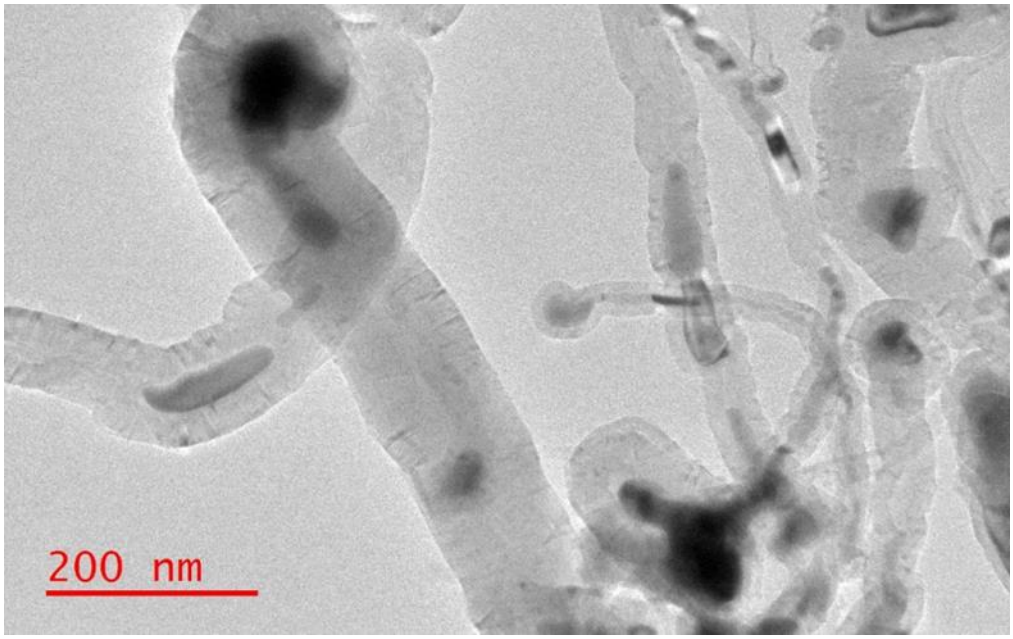


Figure 4.12: TEM image of CNTs produced at methane flow rate of 150 ml/min (900^{o}C).

4.3.5. TEM images of CNTs produced at a reactor temperature of 950^{o}C

Figure 4.13 displays the TEM image of CNTs produced at methane flow rate of 100 ml/min. The image shows the catalyst particles in inside of CNTs, the average diameter of this tubes was 84 nm. The catalyst nanoparticles inside the tip of the CNT produced at methane flow rate of 125 ml/min is visible in the TEM image shown in Figure 4.14. The smooth tube, as shown by the image, has a diameter of 17 nm. Figure 4.15 shows the CNTs produced using methane flow rate of 150 ml/min. The tube has some catalyst in it and has an average diameter of 76 nm. At a reaction temperature of 950^{o}C, the average diameter of CNTs produced at methane flow rate of 100 ml/min (Fig 4.13) and 150 ml/min (Fig 4.15) was 84 and 76 nm, respectively, indicating the presence of MWCNTs. For CNTs produced at methane flow rate of 125 ml/min (Fig 4.14) the average diameter was less than 20 nm showing the presence of SWCNTs.

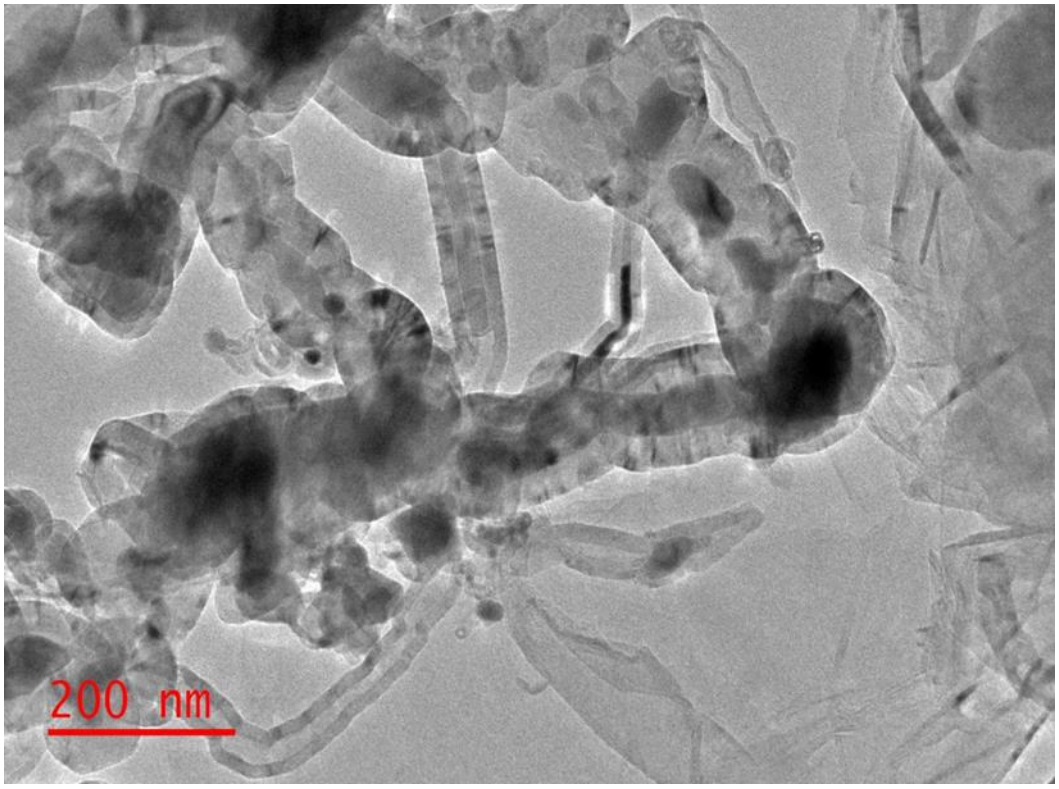


Figure 4.13: TEM image of CNTs produced at methane flow rate of 100 ml/min (950^{o}C).

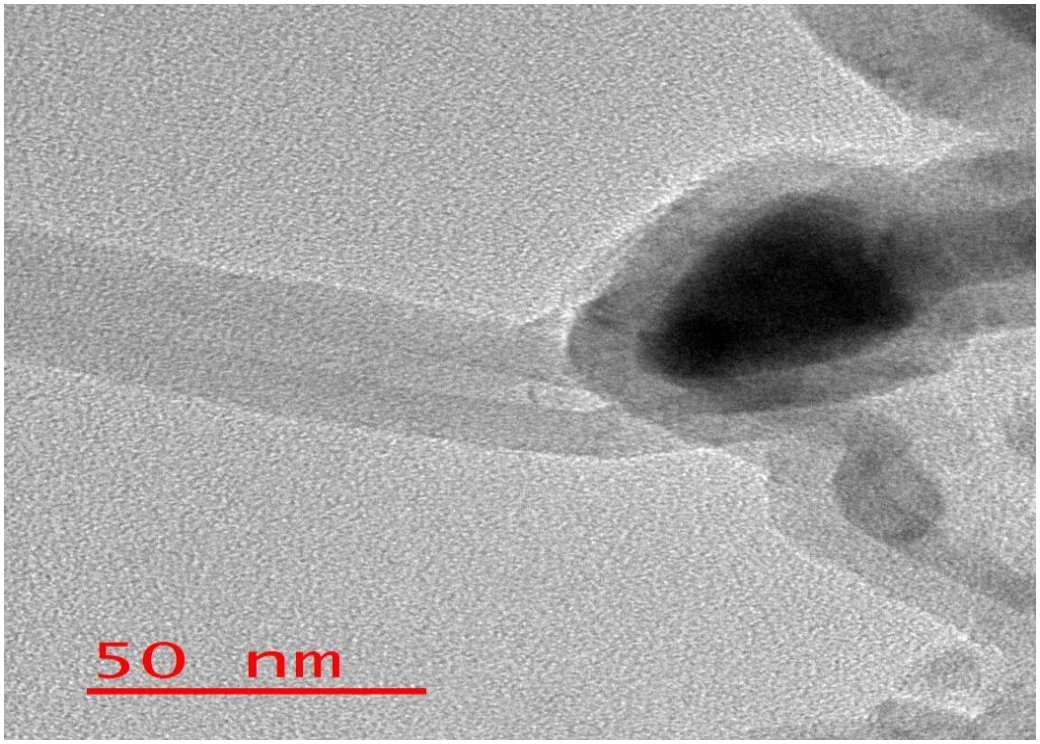


Figure 4.14: TEM image of CNTs produced at methane flow rate of 125 ml/min (950^{o}C).

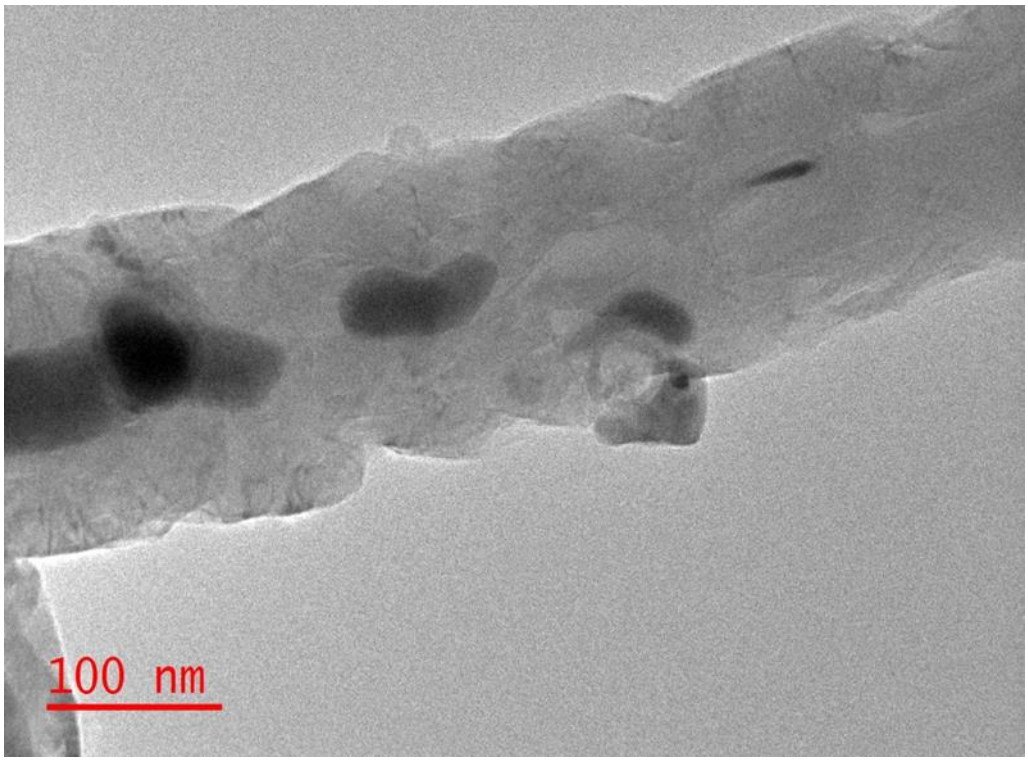


Figure 4.15: TEM image of CNTs produced at methane flow rate of 150 ml/min (950^{o}C).

4.3.6. TEM images of CNTs produced at a reactor temperature of 1000^{o}C

The diameter of CNTs produced at 100 ml/min was approximately 161.36 nm. These nanotubes were contaminated by catalyst nanoparticles as shown by TEM image in Figure 4.16. The TEM image in Figure 4.17 shows CNTs with average diameter of 71.42 nm produced at methane flow rate of 125 ml/min. The image shows CNTs with catalyst particles contained in the inner core of the tube as well as the amorphous carbon at the surface of the tubes. Figure 4.18 is the TEM image of CNTs produced at 150 ml/min of methane gas. The Tube has a diameter of 108.82 nm and the image also shows the trace of catalyst particle in the inner part of the tube. The average diameter of CNTs produced at a reactor temperature of 1000^{o}C is greater than 20 nm showing the presence of MWCNTs in the samples.

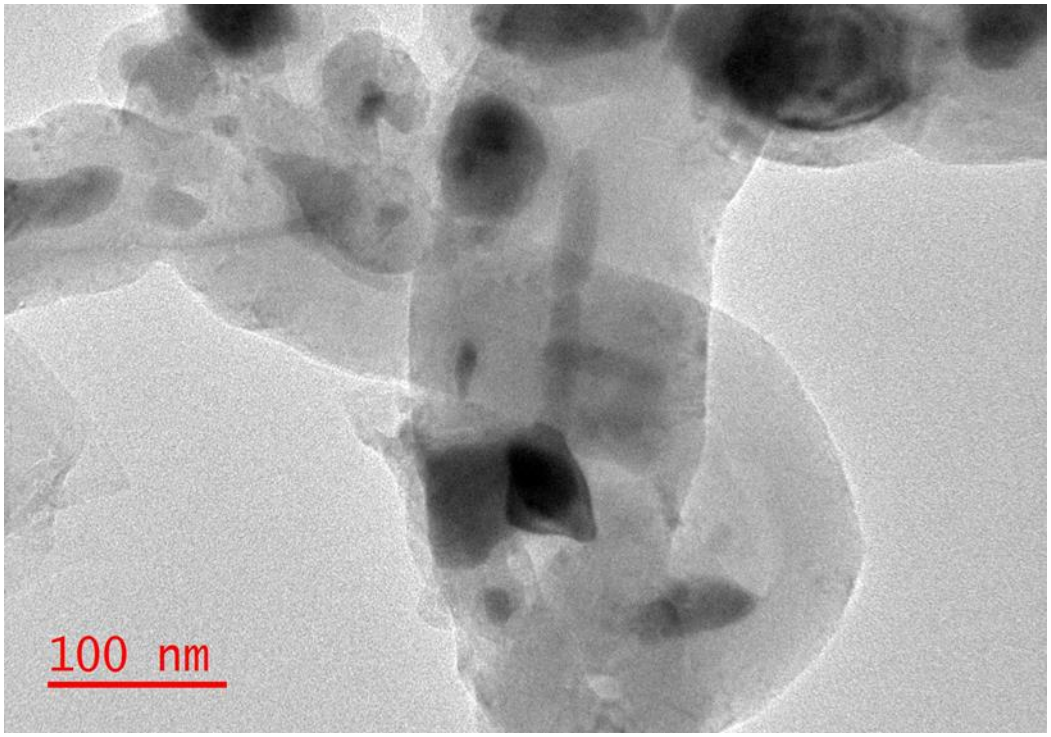


Figure 4.16:TEM mage of CNTs produced at methane flow rate of 100 ml/min (1000ºC).

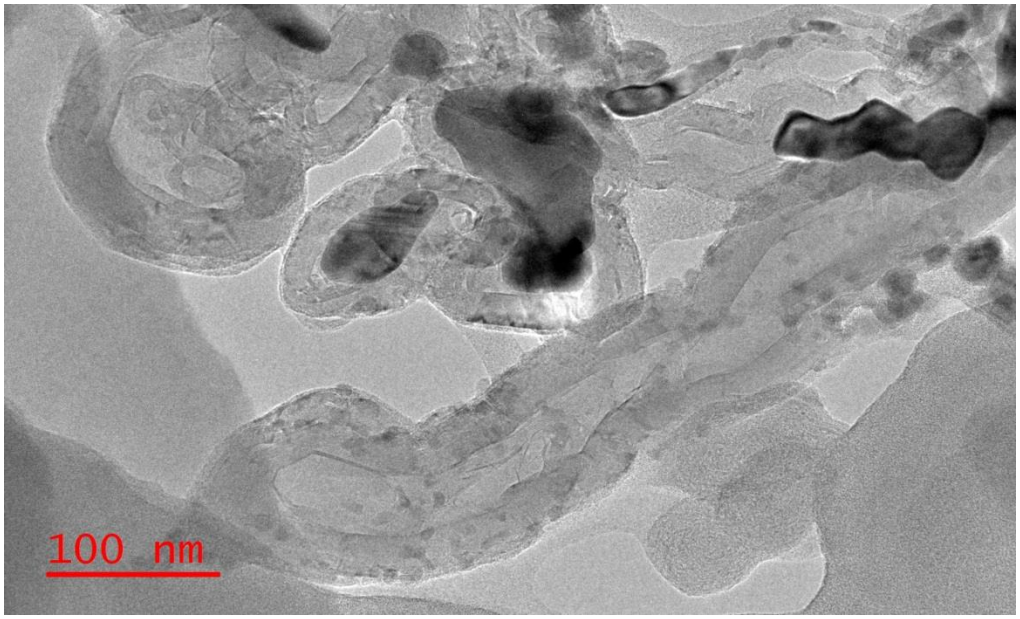


Figure 4.17: TEM image of CNTs produced at methane flow rate of 125 ml/min (1000ºC).

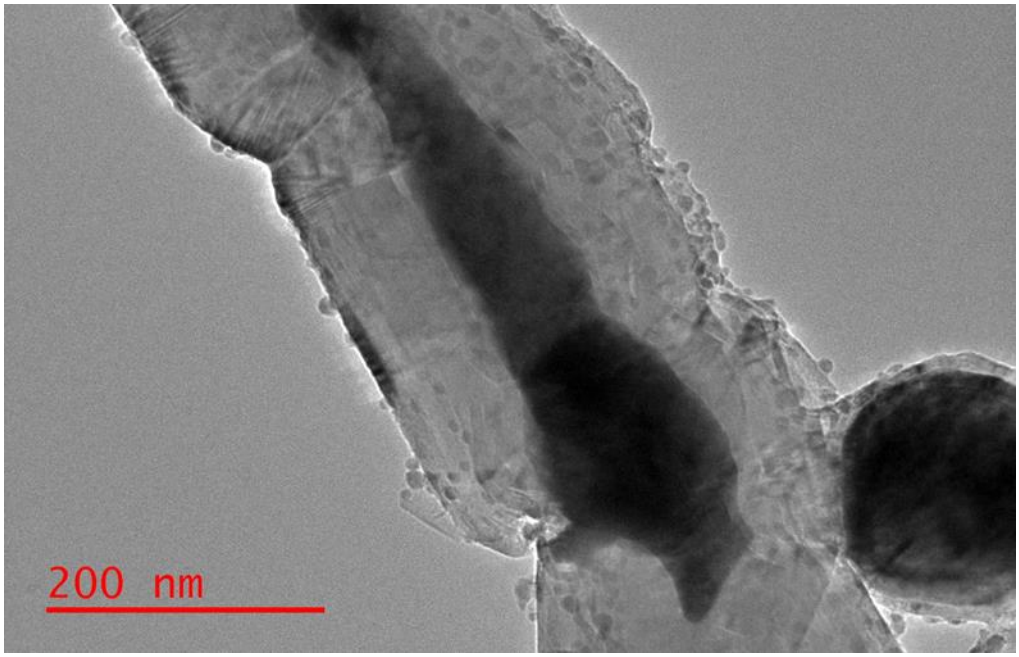


Figure 4.18: TEM image of CNTs produced at methane flow rate of 150 ml/min (1000^{o}C).

4.3.7. Raman Spectrometer Results

Figure 4.19 to Figure 4.21 depict the Raman spectra of Carbon Nanotubes produced at different reactor temperature. The I_G/I_D ratio in Table 4.1 to Table 4.3, clearly indicate that the CNTs produced at methane flow rate of 125 ml/min is lower than those produced at 100 and 150 ml/min at all the three temperatures. Comparing the I_G/I_D ratio at the best methane flow rate (125 ml/min), the ratio of 0.38, 0.18 and 0.29 were obtained for temperature of 900, 950 and 1000^{o}C, respectively. These ratios show that the as-produced CNTs have an incredible crystallinity as the temperature increased to 950^{o}C. However, a further increase of temperature to 1000^{o}C also increased the degree of deformation. This good ratio shows that the raw CNTs have less defect on the structure with a smooth surface.

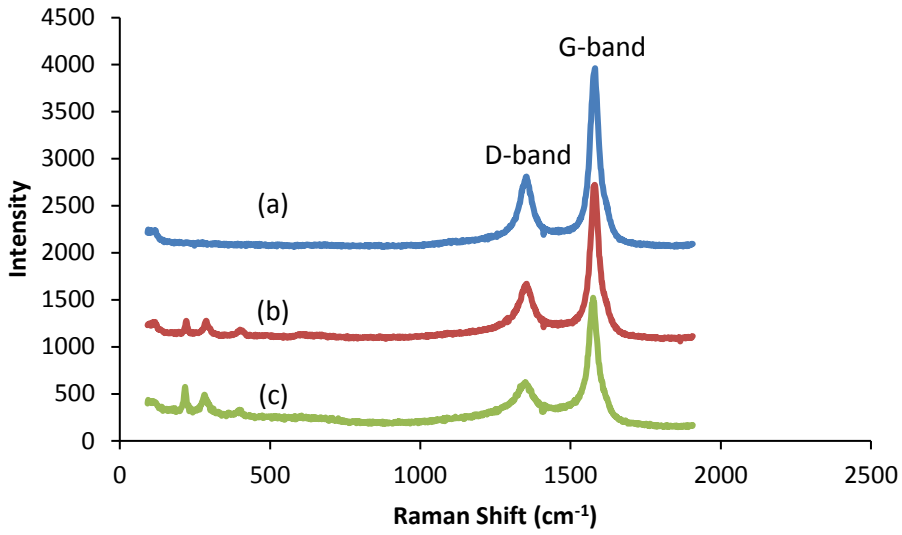


Figure 4.19:Raman shift of CNTs produced at 900°C and methane flow rate of (a) 100 ml/min; (b)125 ml/min (c); 150 ml/min.

All three spectra in Figure 4.19 have peaks that denote the presence of carbon nanotubes. The D-band, which is represented by the first peak, is between 1300 cm^{-1} and 1400 cm^{-1}. The G-band, which is signified by the second peak, is situated between 1500 cm^{-1} and 1700 cm^{-1}. The shoulder on the three graphs at 100 cm^{-1} shows the present of SWCNTs. Spectra (b) and (c) show the RBM peak at 200 and 400 cm^{-1} is a result of hematite caused by iron catalyst. These are the Raman Spectra of carbon nanotubes produced at different methane concentration and constant temperature of 900°C.

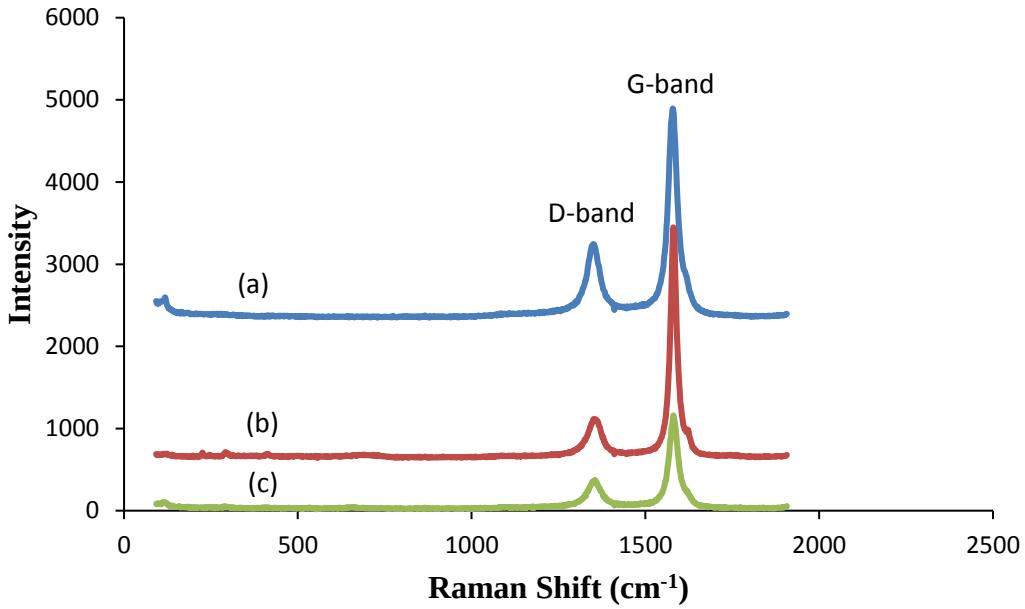


Figure 4.20:Raman shift of CNTs produced at 950°C and methane flow rate of (a) 100 ml/min; (b) 125 ml/min; (c) 150 ml/min.

The D-band of all the three spectra is located between 1300 cm^{-1} and 1400 cm^{-1} and the G-band is situated between 1500 cm^{-1} and 1700 cm^{-1} as shown in Figure 4.20. All the three Raman spectra are of CNTs produced at reactor temperature of 950°C at different CH_4 concentration. The I_D/I_G ratio for Figure 4.20 are presented in Table 4.1.

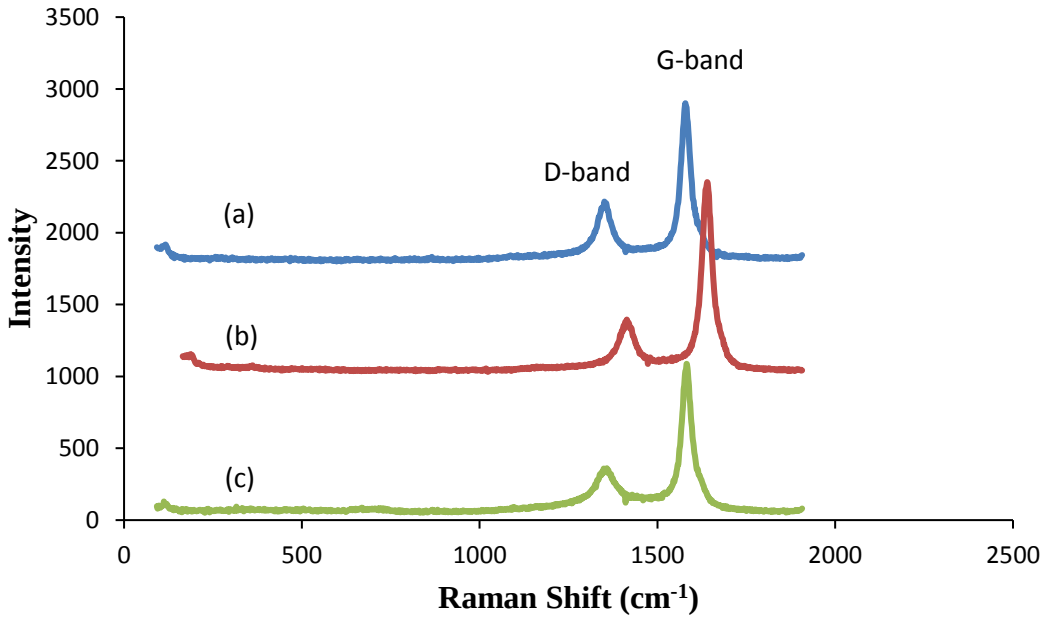


Figure 4.21: Raman shift of CNTs produced at 1000°C and methane flow rate of (a) 100 ml/min; (b)125 ml/min; (c) 150 ml/min.

At the reaction temperature of 1000°C the resulted CNTs produced at methane flow rate of 100, 125 and 150 ml/min shows Raman Spectra with the D-band located between 1200 cm^{-1} and 1500 cm^{-1}, the G-band appearing between 1500 cm^{-1} and 1800 cm^{-1} (Fig. 4.21). The shoulder for all the three spectra at about 100 cm^{-1} also appeared, representing the presence of SWCNTs. The I_D/I_G were calculated and reported as shown in Table 4.1.

The I_D/I_G ratio of CNTs at different reaction condition are summarised in the Table 4.1. The values in the table shows that CNTs produced at 125ml/min have low degree of deformation and high degree of graphitisation as compared the CNTs produced at 150ml/min and 100 ml/min at all the temperatures studied.

Table 4.1:I_D/I_G ratio of CNTs produced at reactor temperature of 900°C, 950°C and 1000°C.

Temp [°C]	CH_4 Flow rate [ml/min]	I_D/I_G
900	100	0.41
	125	0.38
	150	0.40
950	100	0.36
	125	0.18
	150	0.32
1000	100	0.37
	125	0.29
	150	0.33

4.3.8. Analysis by Gas Chromatogram

Gas chromatograms of all the experiments that were conducted during the production of Carbon nanotubes are shown in Table 4.2. The results show there was indeed methane decomposition to form hydrogen in addition to the carbons that were formed before carbon nanotubes as confirmed by the TEM, SEM and Raman spectroscopy. Reactor temperature of 900 to 1000°C is sufficient for decomposition of methane gas in the presence of catalyst to form carbon and hydrogen gas. Refer to Appendix 5 for a sample of chromatogram used for Table 4.2.

Table 4.2: Gas Chromatogram analysis of the outlet gas from CVD reactor.

Reaction Temperature [^oC]	CH_4 flow rate [ml/min]	Inlet Gas	Outlet Gas
900	100	CH_4 Ar	7.122%H_2 20.010%Ar 50.563%CH_4
900	125	CH_4 Ar	8.159% H_2 23.145% Ar 68.696% CH_4
900	150	CH_4 Ar	9.470% H_2 20.469% Ar 70.058% CH_4
950	100	CH_4 Ar	10.434% H_2 2.791% Ar 86.776% CH_4
950	125	CH_4 Ar	12.990% H_2 0.076% Ar 86.925% CH_4
950	150	CH_4 Ar	15.028% H_2 22.093% Ar 62.879% CH_4
1000	100	CH_4 Ar	17.341% H_2 17.954% Ar 64,705% CH_4
1000	125	CH_4 Ar	23.628% H_2 10.872% Ar 65.500% CH_4
1000	150	CH_4 Ar	38.020% H2 28.181% Ar 33.799% CH_4

Table 4.2 shows that the best decomposition temperature for Methane gas is 1000^{o}C as it has higher percentage of hydrogen gas in the outlet gas. Therefore, it can be concluded that when the reactor temperature increases, the decomposition of CH_4 to hydrogen and carbon also increases.

4.3.9. Kinetic Modelling

The equilibrium constant and reaction constant for the derived kinetic model (Equation 21 under Section 4.2.2) was estimated using Solver tool in excel. The kinetic parameters for the reaction at a temperature of 900^{o}C and Methane flow rate was found to be as follows:

$$K_1 = 1.13x10^4$$

$$K_2 = 6.72x10^6$$

$$k_3 = 4.16x10^6$$

The final model at temperature of 900ºC and methane flow rate of 125 ml/min is as follows:

$$\frac{d[CNT]}{dt} = \frac{(1.13x10^4)(6.72x10^6)(4.16x10^6)[CH_4][*]_0}{(1.13x10^4)[CH_4][H_2]^2 + (1.13x10^4)(6.72x10^6)[CH_4] + [H_2]^2}$$

The following graphs (Figure 4.22, Figure 4.23 & Figure 4.24) are a comparison between experiment data and simulated data (Using equation 21 under Section 4.22) for the production rate of carbon nanotubes produced at different methane concentration.

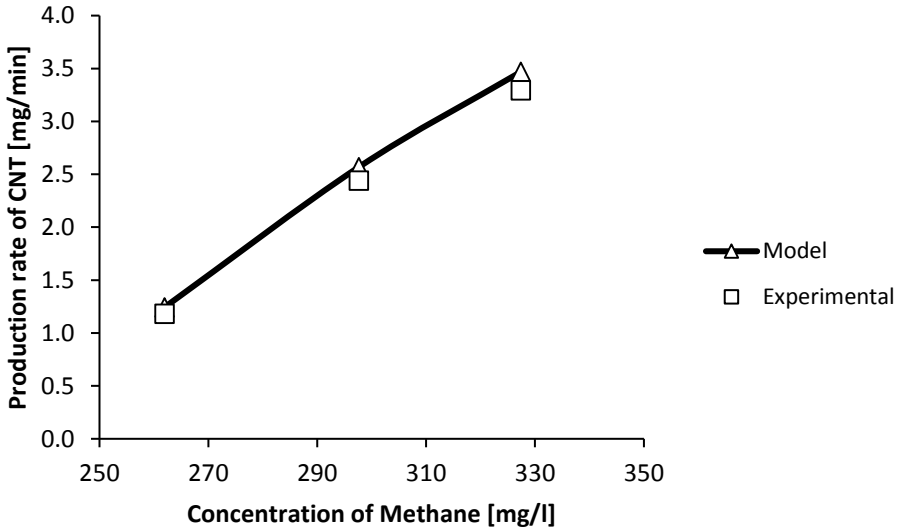


Figure 2.22: Experimental and simulated production rate of CNTs produced at 900ºC

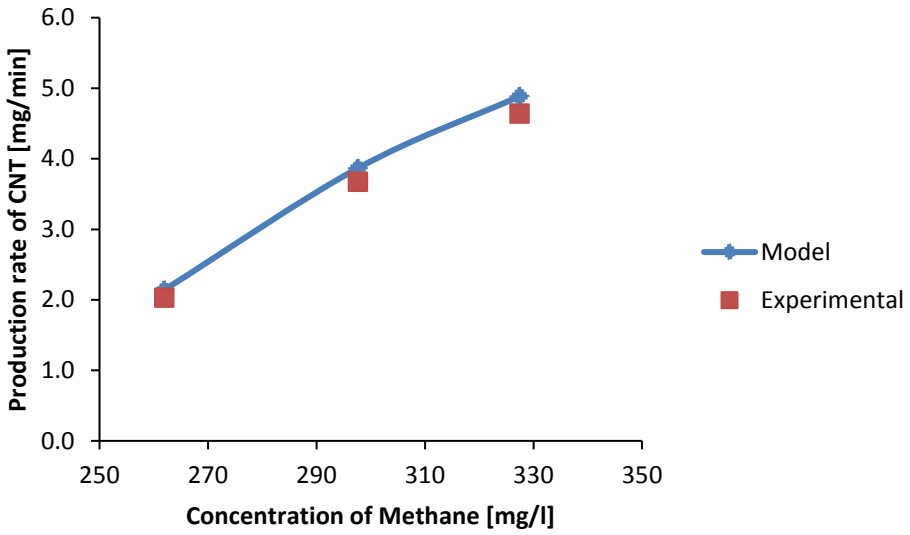


Figure 4.23: Experimental and simulate d production rate of CNTs produced at 950^{o}C

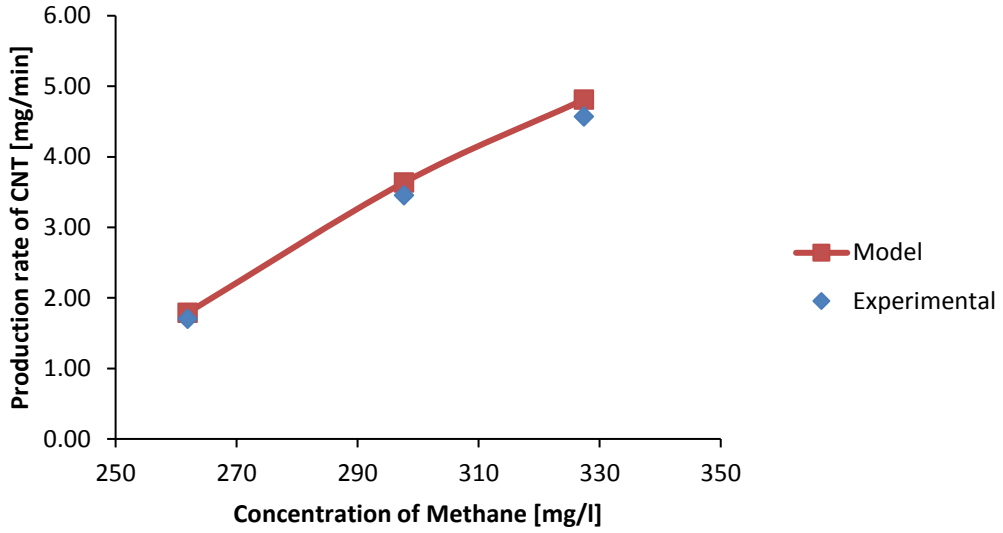


Figure 4.24: Experimental and simulated production rate of CNTs produced at 1000^{o}C

At any given concentration or volumetric flow rate of methane, the derived kinetic model (equation 21) can be utilised to predict the amount of CNTs that will be produced. Here, we discuss the effect of methane concentration on the yield of CNTs and the simulated results are compared with the experimental results. Volumetric flow rates of methane were converted into concentration (mg/l), taking into account the presence of argon gas during reaction. Figure 4.22 to Figure 4.24 depicts the experimental and simulated production rate of carbon nanotubes synthesized at different methane concentration, and a constant reactor temperature. From the

derived model the values of K_1, K_2 and k_3 at different methane concentration were calculated using solver tool in excel. The value of initial concentration of catalyst active site was 6.18×10^{-7} mol/min.mg (Blaser et al., 1997). This value was determined from literature because ferrocene is volatile and chermisorption could not be done on it. The concentration of hydrogen gas from the reaction was determined by the Gas chromatography. Figure 4.22 to Figure 4.24 shows that the production rate of CNTs increases from with the increase in methane concentration. These results also agree with other studies (Iyuke et al., 2007; Valles et al 2009). The increase in CNTs yield with the increase in concentration could be a result of high carbon concentration in the feedstock. Appendix 2 shows how the values of K_1, K_2 and k_3 were determined using 95% confidence interval.

4.4. Summary

The morphological characteristics of as-produced CNTs are shown in Figure 4.1 to 4.9. The images show that, the reactor temperature of 900, 950 and 1000^{o}C at methane flow rate of 100, 125 and 150 ml/min is capable of producing carbon nanotubes. All images show the presence of amorphous carbon and other impurities that may be attributed by the remaining of catalyst particle that are trapped inside the tubes. The TEM images in Figure 4.10 to Figure 4.18 clearly confirm that the deposited carbon are indeed carbon nanotubes. The tube of the as-produced CNTs ranged in average diameter across all the samples as shown by TEM images. The Raman spectra as shown in Figure 4.19 to Figure 4.21 confirm that the CNTs were synthesized during all the experiments as confirmed by SEM and TEM results. Derived Kinetic model is in 95% confidence interval with the experimental results at different reactor temperatures. In general, the overall CNTs characterisation shows that the high quality CNTs were produced at methane flow rate of 125 ml/min. Therefore, CNT yarn was only produced at different reactor temperature and methane flow rate of 125 ml/min.

CHAPTER FIVE

5.0. Thermodynamic properties and electrical conductivity of CNT yarn

5.1. Introduction

Currently there is a great effort by researchers to fabricate CNT yarn to make use of CNTs remarkable properties. These properties make CNT yarn a suitable material to consider in different application, such as, incandescent lamp filament (Jian et al., 2002), supercapacitor (Dalton et al., 2003), solar cell (Jeon et al., 2018), artificial muscle (Aliev et al., 2009), conductive wire for electricity (Yu et al., 2017), biosensors (Zhu et al.,2010) and many more. CNTs macrostructure such as yarn can be produced using different methods (Vigolo, 2000; Ericson,2004; Zhang,2004; Li, 2004). Surfactant-based coagulation spinning, direct spinning, forest spinning, and liquid crystalline spinning are the four most studied methods of manufacturing yarn from CNTs. Surfactant-based coagulation involves injecting a binder which is polymeric between CNTs to produce a yarn. During direct spinning method CNTs and yarns get produced at the same time. In forest spinning, CNTs that are grown on a substrate get drawn and twisted to form a yarn. Liquid-crystalline spinning involves spinning the suspension of CNTs to form a wet-crystalline suspension. Out of all four methods, direct spinning method was found to be advantageous for continuous mass production. It was also found to be the most effective method in producing yarn with good mechanical and electrical properties (Koziol et al., 2007; Vigolo, 2000). CNT yarn in this study was produced using direct spinning method. When using a direct spinning method, a study by Aberefa and his co-workers (Aberefa et al., 2018) shows that reactor temperature of 1000^{o}C and acetylene flow rate of 135 ml/min could produce CNT yarn. They also discovered that yarn produced at reactor temperature of 1000^{o}C has higher electrical conductivity and less defect as compared to yarn produced at rector temperature of 900^{o}C. Effect of production temperature on the conductivity of yarn is investigated in this study. Studies of thermodynamic properties of a material provide important information for classification of the energy state of the material, sorption, functionalization, calculation of equilibria, etc. Therefore, thermophysical quantities need to be considered when studying material. Investigation of thermophysical quantities of individual CNTs has gained interest and their study are being reported in open literature. The source of calculating these thermodynamic properties is by obtaining experimental heat capacities. Since CNT yarns will be used in different environmental conditions, their thermophysical quantities are crucial to determine their capabilities. Heat capacities of material are required in areas such

as physics, chemical engineering and in chemistry to determine phase transition, mass balance, entropy and enthalpy. Heat capacities of SWCNTs were found to be higher than that of MWCNTs at a temperature below 275 K. However, at a temperature above 275 K, MWCNTs have higher heat capacities than SWCNTs (Nan et al., 2009). A study by Muratov et al showed that the heat capacity of MWCNTs is almost the same as that of graphite at a temperature of 298.15K although the value of graphite is slightly higher (Muratov et al., 2012). However, as far as could be ascertained, there are no heat capacities and other thermodynamic properties of CNT yarn that are reported in the open literature. Hence this study considered the investigation of thermodynamic properties of yarn produced at different reactor temperatures using direct spinning method. The effect of production temperature on the thermophysical quantities of the yarn was investigated as well.

5.2. Experimental procedure

Based on TEM, SEM and Raman Spectra results as detailed in Chapter 4, the optimum Methane flow rate was found to be 125 ml/min. Therefore, CNT yarn was produced at this flow rate and different reactor temperature. Thermodynamic parameters of as-produced CNT yarn were studied using Thermal Gravimetric Analyser (TGA). Detailed experimental procedure is explained in Chapter 3.

5.3. Results and Discussion

5.3.1. Morphology of the produced yarn

The SEM images in Figure 5.1, Figure 5.3 and Figure 5.5 clearly indicate that the presence of CNT yarn produced at methane flow rate of 125ml/min and temperature of 900^{o}C, 950^{o}C and 1000^{o}C, respectively. The EDX spectra for CNT yarns are also presented in Figure 5.2, Figure 5.4 and Figure 5.6. More images are presented in Appendix 1.

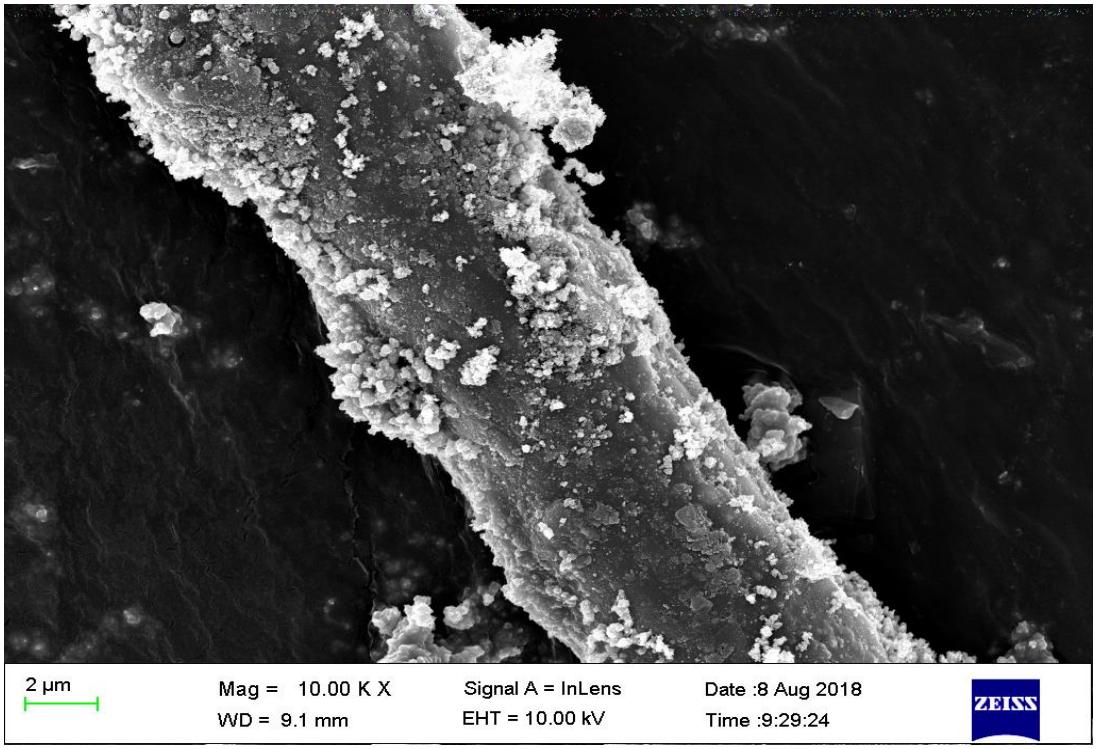


Figure 5.1:SEM image of CNT yarn produced at 900^{o}C

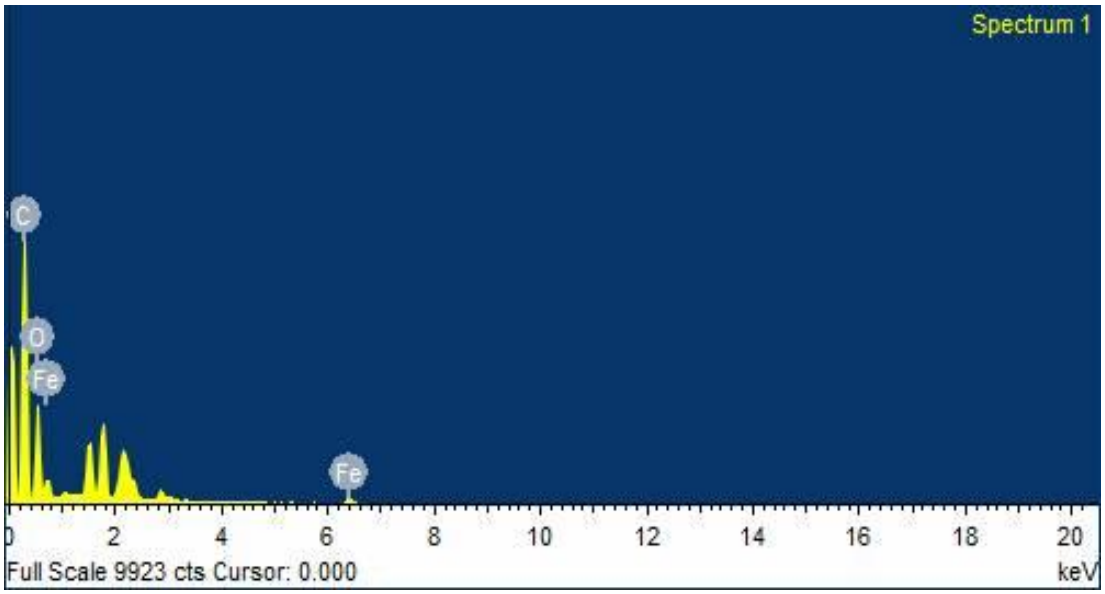


Figure 5.2: EDX spectrum of CNT yarn produced at 900^{o}C

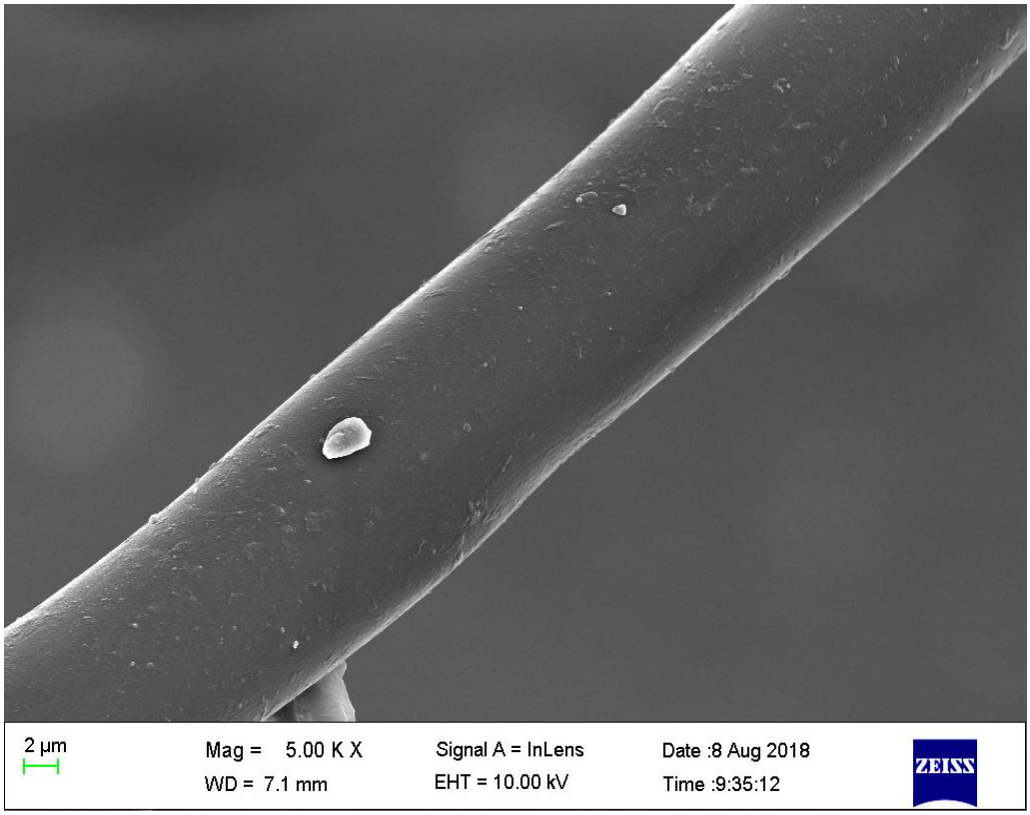


Figure 5.3:SEM image of CNT yarn produced at 950^{o}C

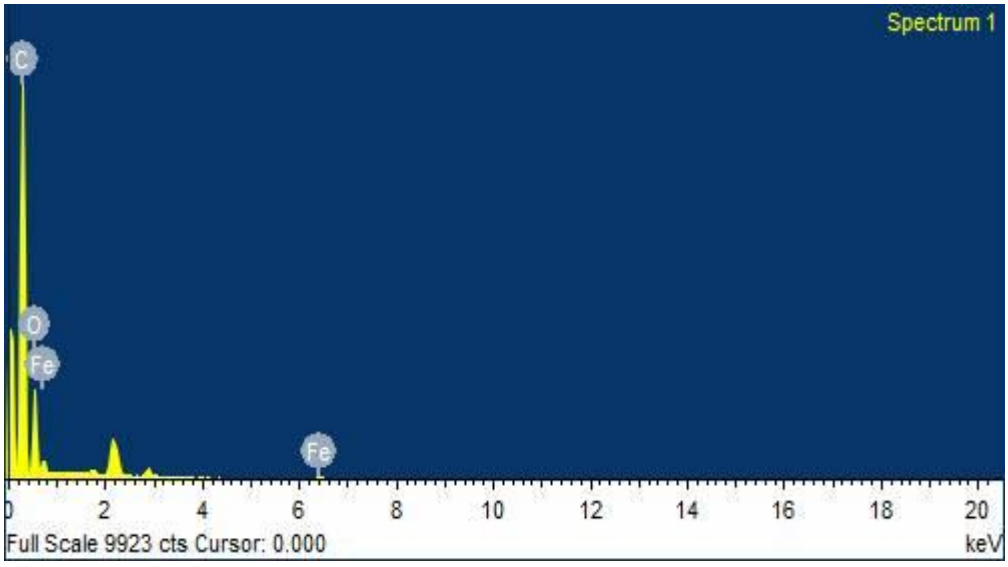


Figure 5.4:EDX spectrum of CNT yarn produced at 950^{o}C

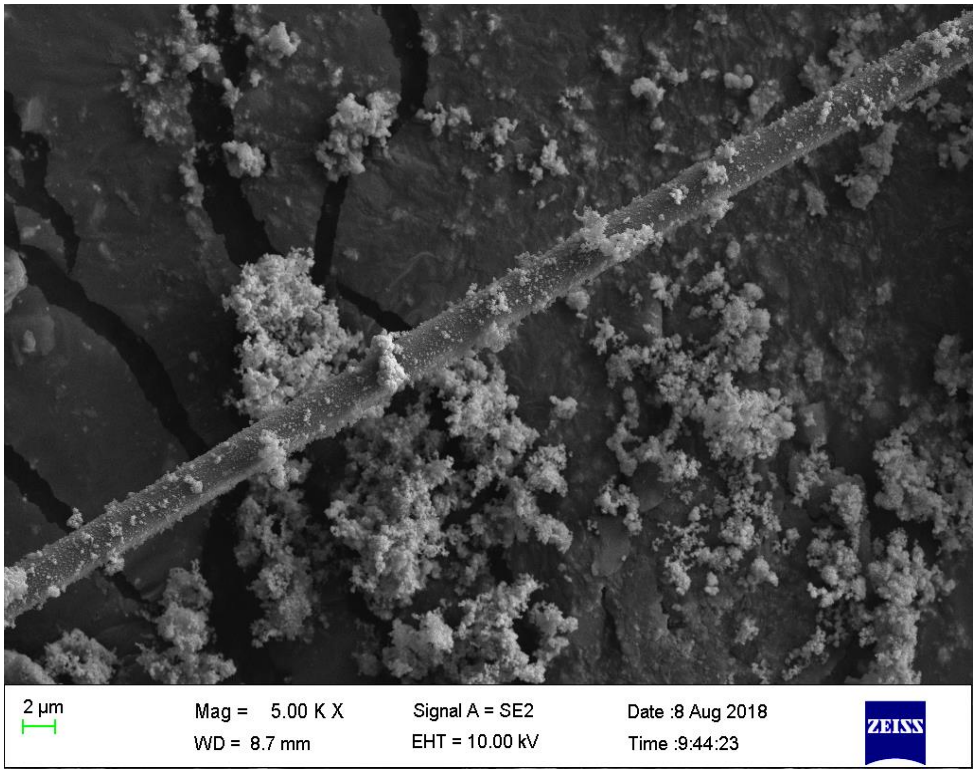


Figure 5.5:SEM image of CNT yarn produced at 1000^{o}C

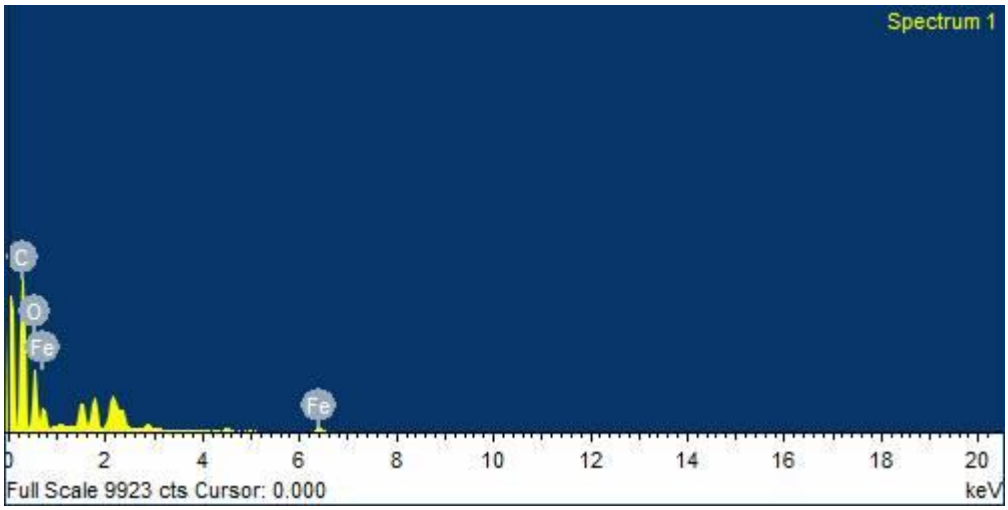


Figure 5.6: EDX spectrum of CNT yarn produced at 1000^{o}C

Figure 5.1 shows the SEM image with the fibrous structure. It can be concluded that the structure is a CNT yarn based on the EDS spectrum (Fig 5.2) of the sample, which clearly indicate that the sample consist of mainly carbon. The fibrous structure in Figure 5.3 bears a resemblance to that of a yarn like wool or human hair. The image shows that the structure has

high degree of alignment throughout the thickness of the fibre. Figure 5.4 is evidence that this is a CNT yarn, because the sample comprises predominantly by carbon and in addition the CNTs are presence. In Figure 5.5, a long and continuous fibrous structure is observed with high degree of alignment throughout the length of the structure, this is also a CNT yarn as evidenced by Figure 5.6, which indicate that the sample has more of carbon as compared to other impurities such as iron (Fe) and Oxygen (O).

5.3.2. Electrical conductivity

As-produced CNTs and CNT yarn produced at methane flow rate of 125 ml/min and different temperature of 900, 950 and 1000^{o}C was tested for conductivity using Four-Probe Method. The Current-Voltage characteristics of the sample was directly measured during Four Probe method. All six graphs (Fig.5.7, Fig5.8 & Fig.5.9) show linear ohmnic behaviour revealing that all the samples were electrically conductive and metallic. The calculated average electrical conductivity is shown Figure 5.10, Calculations are in Appendix.

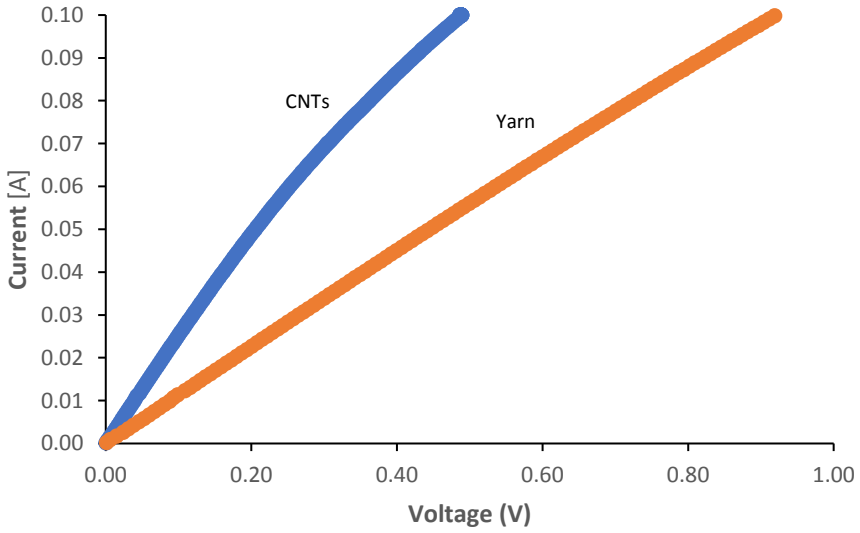


Figure 5.7:Current-voltage relationship for CNTs and CNT yarn produced at 900^{o}C

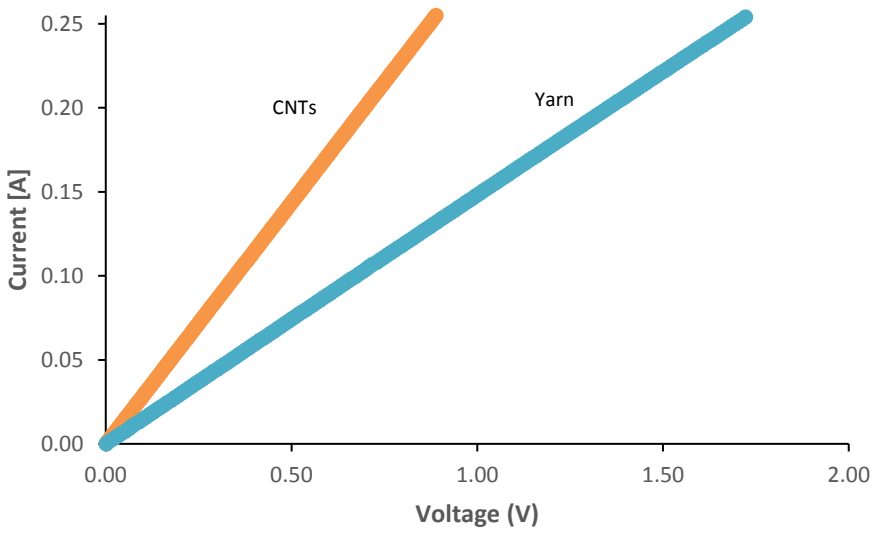


Figure 5.8:Current-voltage relationship for CNTs and CNT yarn produced at 950^{o}C

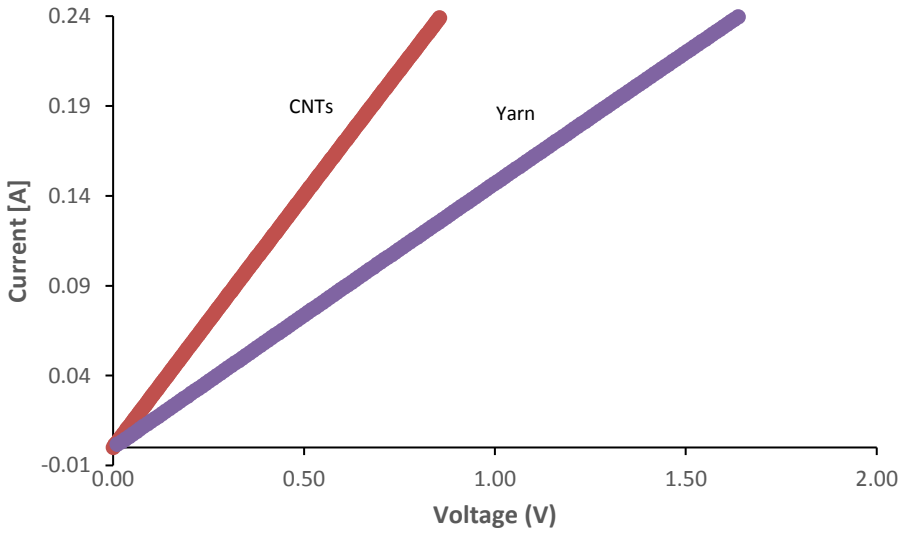


Figure 5.9:Current-voltage relationship for CNTs and CNT yarn produced at 1000^{o}C

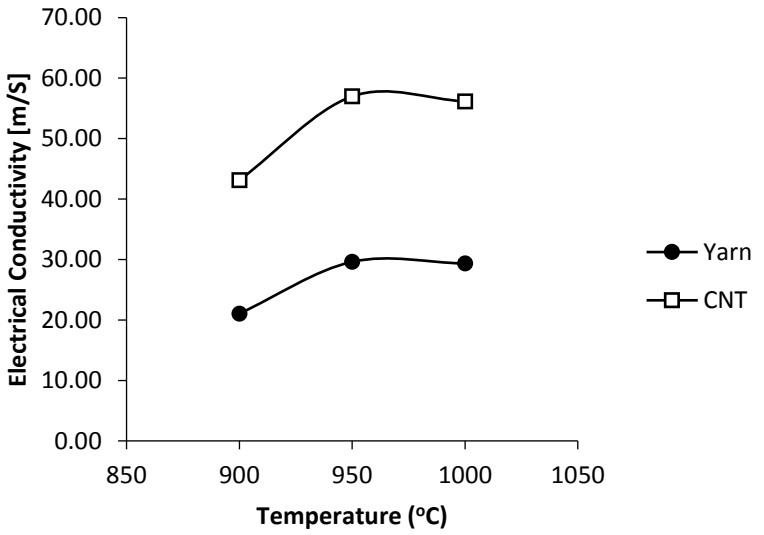


Figure 5.10: Electrical conductivity of CNTs and CNT yarn produced at different temperature

Upon the measurement by Four Probe method, the slopes given by Current-Voltage characteristics of CNTs sample is higher than the respective yarn as shown in all three graphs (Figure 5.7 to Figure 5.9). The calculated Electrical Conductivity of CNTs is higher than the Electrical Conductivity of their yarn as indicated in Figure 5.10. This could be attributed to the amorphous carbon and impurities that formed part of CNTs yarn (Dai et al., 1996; Bachtold et al., 1998). The Electrical Conductivity of as-produced CNTs is approximately twice than that of yarn. Yarn and CNTs produced at reactor temperature of 950^{o}C has higher Electrical Conductivity than the yarn and CNTs produced at 900^{o}C and 1000^{o}C. This agrees with the results from TEM, SEM and EDS, whereby the morphology and structure of CNTs and Yarn where properly aligned and mainly consist of SWCNTs. It is also in accordance with literature that SWCNTs results in higher Electrical Conductivity than MWCNTs (Bettinger, 2004). Furthermore, the Raman spectra analysis of CNTs produced at 950^{o}C has lower degree of defect. In general, reactor temperature of 950^{o}C gives a CNTs or CNT yarn that has higher Electrical conductivity followed by yarn or CNTs produced at reactor temperature of 1000^{o}C. The overall Electrical Conductivity of yarns produced in this study is lower than that of typical yarn that are reported in the literature. Such could be a result of impurities that our sample are contaminated with such as catalyst impurities and Amorphous carbon (lekawa-Raus et al., 2014) as observed in EDX, TEM and Raman Spectroscopy analysis for the yarns. Other factors that result in lower Electrical Conductivity could be misalignment of CNTs in our sample as observed in SEM micrographs. However, the electrical conductivity of yarn produced in this

study shows improvement from the one produced using acetylene at different flow rate (Aberefa et al.,2018).

5.3.3. Thermodynamic Properties

The Thermoanalytical measurements carried out using TGA/DSC analyser for CNT yarn produced at a reactor temperature of 900°C, 950°C and 1000°C are present in Figure 5.11 to Figure 5.13.

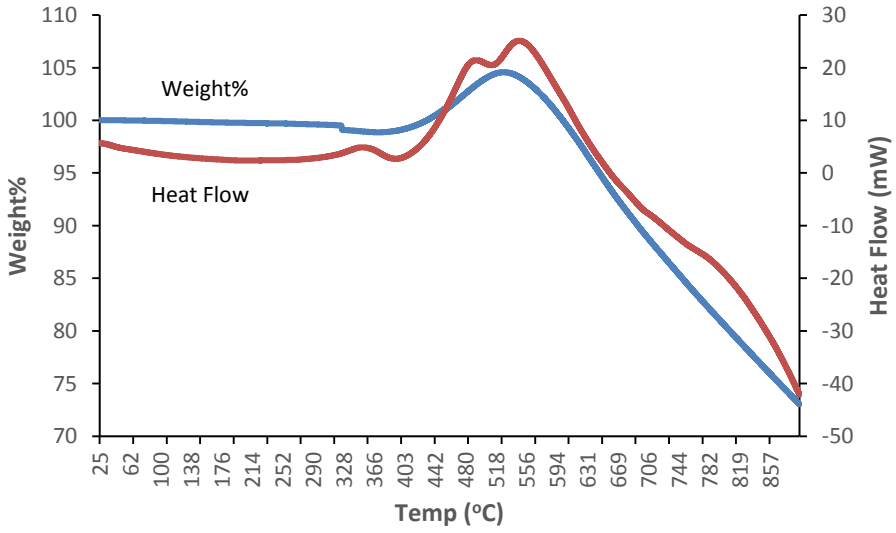


Figure 5.11: Thermoanalytical curve of yarn produced at 900°C

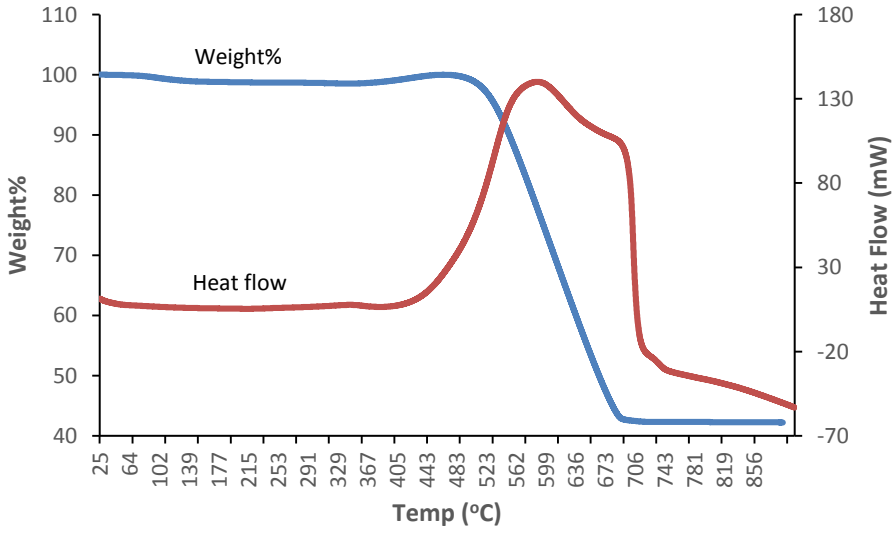


Figure 5.12: Thermoanalytical curve of yarn produced at 950°C

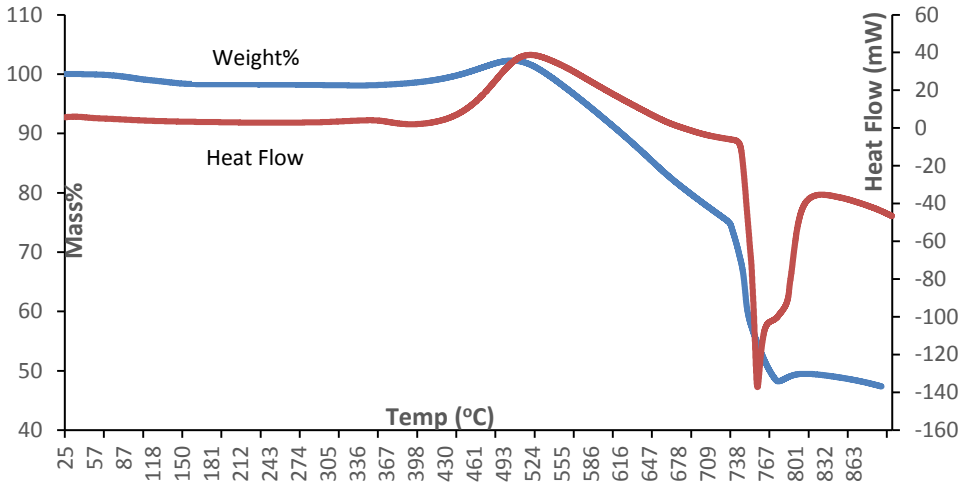


Figure 5.13:Thermoanalytical curve of yarn produced at 1000°C

Figure 5.11 weight% graph shows the thermal stability of yarn produced at a reactor temperature of 900°C, the initial mass during DSC/TGA analysis was approximately 10mg. The sample was stable at a temperature of 200 to 265°C as indicated by the mass% graph. Yarn produced at 950°C shows to be thermal stable at a temperature range of 200 to 330°C as shown in Figure 5.12. The initial mass of the sample was about 10 mg. Figure 5.13 shows the thermal stability of yarn produced at a reactor temperature of 1000°C. The initial mass for TGA/DSC analysis was about 10 mg. The sample shows to be stable at about 200 to 265°C. The mass% loss was about 15%, 58% and 52% for yarn produced at reactor temperature of 900,950 and 1000°C, respectively, when the TG temperature was $T \leq 856$°C. The TG curve also shows the thermal stability over the range of 200-265, 200-330 and 200-265°C for yarn produced at reactor temperature of 900,950 and 1000°C, respectively, meaning that at that stability temperature there was no phase change, association or thermal decomposition that took place.

The heat flow of yarns at thermal stable state was used to calculate the heat capacity and presented in Figure 5.14.

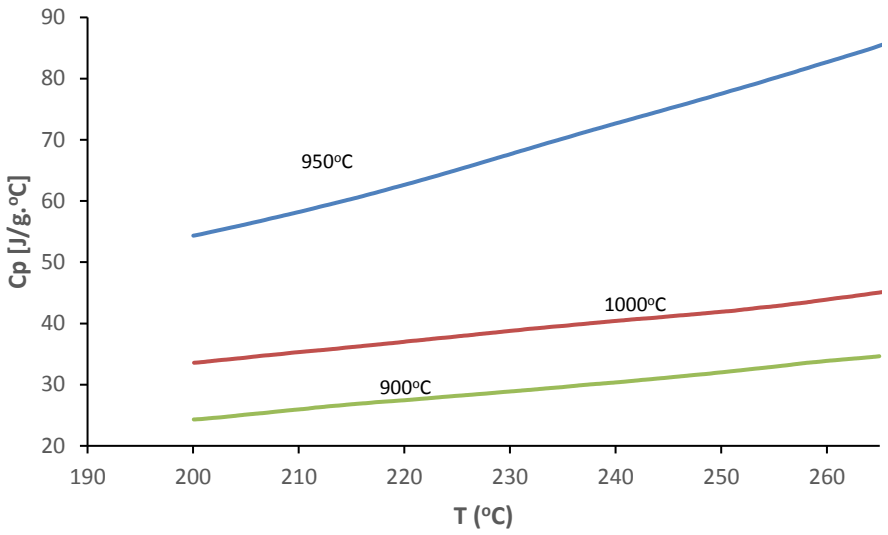


Figure 5.14:Specific heat capacities of yarn produced at different reactor temperature

By using DSC curve of heat flow one can calculate the specific heat capacity of sample (Morintale & Harabou, 2013: Degeratu et al., 2009) Figure 5.14 depicts that the specific heat capacity with respect to DSC temperature, are different for yarn produced at different reactor temperature. The polynomial equation of heat capacity at DSC temperature of 200 to 265°C (yarn stable temperature) were obtained using least square method. Equation 1 is for yarn produced at reactor temperature of 900°C.

$$C_p[J/g.\ ^oC] = 0.0003T^2 + 0.0394T + 6.5472 \quad (1)$$

Polynomial model to predict heat capacity for yarn produced at reactor temperature of 950°C is shown in equation (2).

$$C_p[J/g.\ ^oC] = 0.002T^2 - 0.4512T + 66.099 \quad (2)$$

For yarn produced at reactor temperature of 1000°C, the predictive model for heat capacity at different DSC temperature is shown in equation (3).

$$C_p[J/g.\ ^oC] = 0.0007T^2 - 0.1418T + 35.154 \quad (3)$$

Using equation (1), (2) and (3), average smoothed heat capacities of yarn at different temperature was obtained as presented in Table 5.1, 5.2 and 5.3 respectively. Thermodynamic functions such as Change in Enthalpy (ΔH) and change in Entropy(ΔS) were also calculated using equations as detailed in chapter 3 Section 3.3. Refer to Appendix 6 for detailed values. Change in entropy increases with the increase in temperature meaning the degree of disorder of material increase with temperature. Change in enthalpy increases with the increase in temperature, meaning the heat content of material increases with increase in temperature. This behaviour is in agreement with other studies for CNTs (Nan et al., 2009; Kabo et al., 2016).

Table 5.1: Average heat capacities and thermodynamic function of yarn produced at 900°C

Temp Range [°C]	Average Cp [J/°C.g]	Average ΔH [J/g]	Average ΔS [J/°C.g]
200-205	26.8	4 762.5	56.1
206-211	27.8	5 102.6	59.0
212-217	28.8	5 458.6	61.9
218-223	29.8	5 830.7	64.9
224-229	30.9	6 219.4	68.0
230-235	31.9	6 625.1	71.2
336-241	33.0	7 048.1	74.5
242-247	34.1	7 488.9	77.8
248-253	35.2	7 947.8	81.2
254-259	36.4	8 425.3	84.7
260-265	37.6	8 921.7	88.3

Table 5.2: Average heat capacities and thermodynamic function of yarn produced at 950°C

Temp Range [°C]	Average Cp [J/°C.g]	Average ΔH [J/g]	Average ΔS [J/°C.g]
200-205	56.7	10 074.1	118.7
206-211	59.0	10 822.9	125.1
212-217	61.3	11 625.7	131.9
218-223	63.9	12 485.1	139.0
224-229	66.5	13 403.6	146.6
230-235	69.3	14 383.9	154.6
336-241	67.4	13 723.4	149.2
242-247	75.3	16 540.2	171.8
248-253	78.6	17 721.3	181.1
254-259	82.0	18 974.6	190.8
260-265	85.5	20 302.6	201.0

Table 5.3: Heat capacities and thermodynamic function of yarn produced at 1000°C

Temp Range [°C]	Average Cp [J/°C.g]	Average ΔH [J/g]	Average ΔS [J/°C.g]
200-205	35.1	6 238.8	73.5
206-211	36.0	6 610.3	76.4
212-217	36.9	7 001.9	79.4
218-223	37.9	7 414.5	82.6
224-229	38.9	7 848.9	85.8
230-235	40.0	8 306.1	89.3
336-241	39.3	7 998.7	87.0
242-247	42.3	9 292.5	96.5
248-253	43.6	9 823.5	100.4
254-259	44.8	10 380.8	104.4
260-265	46.2	10 965.5	108.6

5.4. Summary

Figure 5.2, 5.4 and Figure 5.6 indicates that the produced yarns are mainly composed of carbon (C) followed by Fe which is deposited by catalyst. It can then be concluded that all three experiment at different reactor temperature (900,950 and 1000°C) successfully resulted in CNTs that has been spun and aligned to form a yarn. All three produced yarn are found to be electrically conductive. The yarns produced in this study have higher conductivity than the one produced using acetylene as carbon source.

The specific heat capacity of 26.4, 55.9 and 34.8 J/g.°C is obtained at a temperature of 200°C for yarn produced at 900,950 and 1000°C respectively. This is an evident that yarn produced at 950°C has higher specific heat capacity than that produced at either 900 or 1000°C. However, yarn produced at 1000°C has higher specific heat flow than that produced at 900°C. Yarns produced in this study were found to have higher heat capacities than the CNTs as reported in the literature. At DSC temperature of 200°C, the specific heat capacity of yarn produced at 950°C was found to be 55 .9 J/°C.g which is higher than the specific heat capacity of both MWCNTs and SWCNTs which were reported to be 1.1852 J/g.K (Kabo et al., 2016) and 1.02 J/g.K (Pradhan et al., 2009), respectively. The capacities of yarn and heat CNTs were expected to be different because of their differences in diameter and purity. In practical application, it will be advisable to use yarn produced at 950°C as filament in incandescent bulb because its temperature will not change easily with the change in heat. Thermodynamic properties such as entropy and enthalpy were determined and reported to be used in different field such as Chemical engineering and Physics.

CHAPTER SIX

6.0. Conclusion and Recommendations

6.1. Conclusion

Carbon nanotubes at different CH_4 flow rate and reactor temperature were produced in a continuous catalytic CVD reactor and characterised in this Study. A kinetic model to predict the production rate of CNTs at a given CH_4 concentration was developed. Developed kinetic model is in 95% confidence interval with the experimental results. The increase in CH_4 concentration as carbon source for CNTs production results in increase in production rate of CNTs. However, the quality of CNTs was optimum at CH_4 flow rate of 125 ml/min further increase in flow rate results in deteriorating of CNTs quality. Therefore, a well-aligned and high quality CNTs were obtained when the methane flow rate is 125 ml/min.

The CH_4 flow rate of 125 ml/min was used to produce CNTs yarn at different reactor temperature (900,950 and 1000^oC). The results showed that all three reactor temperatures were capable of producing yarn. The electrical conductivity tested on yarn produced at different temperature shows that all three samples were electrically conductive. Although it was found that yarn produced at 1000^oC was more conductive than the yarn produced at 900^oC, Yarn produced at 950^oC have higher Electrical conductivity than that produced at 900 and 1000^oC. The electrical conductivity of CNTs was found to be approximately 2 times higher than those of their respective yarn.

Thermodynamic properties of yarn produced at different reactor temperature were reported. The results show that the reactor temperature in which the CNTs yarn was produced has a great impact on the thermodynamical function such as heat capacity, enthalpy and entropy. For yarn produced at different reactor temperature a polynomial model for predicting the heat capacities was developed.

Although it was possible to produce CNTs yarn that could be used in incandescent light bulb, their electrical conductivities are still lower than the typical yarn that is reported in the literature. It will still be interesting to improve the electrical conductivity of yarn.

6.2. Recommendations

Yarn produced in a continuous CVD reactor suffer the disadvantage of encapsulating the catalyst particle in its structure, resulting in low quality yarn. A study to purify the yarn from catalyst particle and any amorphous carbon that may adhere on the surface of yarn need to be conducted. To further improve the conductivity of the yarn, the produced CNTs need to be controlled and consists only of SWCNTs.

For kinetic model, the equilibrium constants K_1 and K_2 changes with change in temperature, according to Le-Chateliers principle, the reactants concentration does not affect the equilibrium constant and it should stay constant. Thorough investigation needs to be undertaken in this regard.

REFERENCES

Abatemarco, T., Stickel, J., Belfort, J., Frank, B. P., Ajayan, P. M., & Belfort, G. (1999). Fractionation of multiwalled carbon nanotubes by cascade membrane microfiltration. *The Journal of Physical Chemistry B, 103*(18), 3534-3538.

Aberefa, O., Bedasie, K., Madhi, S., Daramola, M. O., & Iyuke, S. E. (2018). Production of carbon nanotube yarn from swirled floating catalyst chemical vapour deposition: a preliminary study. *Advances in Natural Sciences: Nanoscience and Nanotechnology*, 9(3), 035009.

Agboola, A. E., Pike, R. W., Hertwig, T. A., & Lou, H. H. (2007). Conceptual design of carbon nanotube processes. *Clean Technologies and Environmental Policy, 9*(4), 289-311

Bachtold, A., Henny, M., Terrier, C., Strunk, C., Schönenberger, C., Salvetat, J. P., ... & Forro, L. (1998). Contacting carbon nanotubes selectively with low-ohmic contacts for four-probe electric measurements. *Applied Physics Letters*, 73(2), 274-276.

Bandow, S., Asaka, S., Zhao, X., & Ando, Y. (1998). Purification and magnetic properties of carbon nanotubes. *Applied Physics A: Materials Science & Processing*, *67*(1), 23-27.

Bepete, G., Tetana, Z. N., Lindner, S., Rümmeli, M. H., Chiguvare, Z., & Coville, N. J. (2013). The use of aliphatic alcohol chain length to control the nitrogen type and content in nitrogen doped carbon nanotubes. *Carbon*, 52, 316-325.

Bethune, D. S., Kiang, C. H., De Vries, M. S., Gorman, G., Savoy, R., Vazquez, J., & Beyers, R. (1993). Cobalt-catalysed growth of carbon nanotubes with single-atomic-layer walls. *Nature*, *363*(6430), 605.

Bettinger, H. F. (2004). Carbon Nanotube - Basic Concepts and Physical Properties. By S. Reich, C. Thompsen, J. Maultzsch. *ChemPhysChem, 5*(12), 1914-1915.

Blanchard, F., Reymond, J. P., Pommier, B., & Teichner, S. J. (1982). On the mechanism of the Fischer-Tropsch synthesis involving unreduced iron catalyst. *Journal of Molecular Catalysis*, 17(2-3), 171-181.

Blaser, H. U., Baiker, A., & Prins, R. (Eds.). (1997). Heterogeneous catalysis and fine chemicals IV (Vol. 108). *Elsevier*.

Cantoro, M., Hofmann, S., Pisana, S., Scardaci, V., Ducati, C., Ferrari, A.C., Blackburn, A.M., & Robertson, J.(2006). Catalytic Chemical Vapor deposition of single-wall carbon Nanotubes at low temperatures. *Nano Letters*, 6(6), 1107-1112.

Chang, H., & Bard, A. J. (1991). Scanning tunneling microscopy studies of carbon-oxygen reactions on highly oriented pyrolytic graphite. *Journal of the American Chemical Society*, 113(15), 5588-5596.

Chen, X. H., Chen, C. S., Chen, Q., Cheng, F. Q., Zhang, G., & Chen, Z. Z. (2002). Non-destructive purification of multi-walled carbon nanotubes produced by catalyzed CVD. *Materials Letters, 57*(3), 734-738.

Chen, Y. K., Green, M. L., Griffin, J. L., Hammer, J., Lago, R. M., & Tsang, S. C. (1996). Purification and opening of carbon nanotubes via bromination. *Advanced Materials, 8*(12), 1012-1015.

Chiang, I. W., Brinson, B. E., Huang, A. Y., Willis, P. A., Bronikowski, M. J., Margrave, J. L., Smalley, R. E., & Hauge, R. H. (2001). Purification and characterization of single-wall carbon nanotubes (SWNTs) obtained from the gas-phase decomposition of CO (HiPco process). *The Journal of Physical Chemistry B, 105*(35), 8297-8301.

Choo, H., Jung, Y., Jeong, Y., Kim, H. C., & Ku, B. (2012). Fabrication and Applications of Carbon Nanotube Fibers. *Carbon letters*, 13(4), 191-204.

Choudhary, V., Singh, B. P., & Mathur, R. B. (2013). Carbon nanotubes and their composites. In *Syntheses and applications of carbon nanotubes and their composites (pp.193-222).* InTech.

Ci, L., Wei, J., Wei, B., Liang, J., Xu, C., & Wu, D. (2001). Carbon nanofibers and single-walled carbon nanotubes prepared by the floating catalyst method. *Carbon, 39*(3), 329-335.

Colbert, D. T., Zhang, J., McClure, S. M., Nikolaev, P., Chen, Z., Hafner, J. H., Owens, D.W., Kotula, P.G., Carter, C.B., Weaver, J.H., & Rinzler, A. G. (1994). Growth and sintering of fullerene nanotubes. *Science*, *266*(5188), 1218-1222.

Colomer, J. F., Piedigrosso, P., Fonseca, A., & Nagy, J. B. (1999). Different purification methods of carbon nanotubes produced by catalytic synthesis. *Synthetic Metals, 103*(1-3), 2482-2483.

Corrias, M., Caussat, B., Ayral, A., Durand, J., Kihn, Y., Kalck, P., & Serp, P. (2003). Carbon nanotubes produced by fluidized bed catalytic CVD: first approach of the process. *Chemical Engineering Science*, 58(19), 4475-4482.

Daenen, M., de Fouw, R.D., Hamers, B., Janssen, P.G.A., Schouteden,K., Veld, M.A.J. (2003). The Wondrous World of Carbon Nanotubes, a review of current carbon nanotube technologies (Interfaculty Project). *Eindhoven University of Technology*.

Dai, H., Wong, E. W., & Lieber, C. M. (1996). Probing electrical transport in nanomaterials: conductivity of individual carbon nanotubes. *Science*, *272*(5261), 523-526.

Degeratu, S., Rotaru, P., Manolea, G., Manolea, H., & Rotaru, A. (2009). Thermal characteristics of Ni–Ti SMA (shape memory alloy) actuators. *Journal of Thermal Analysis and Calorimetry*, *97*(2), 695-700.

Delpeux, S., Szostak, K., Frackowiak, E., & Béguin, F. (2005). An efficient two-step process for producing opened multi-walled carbon nanotubes of high purity. *Chemical Physics Letters*, *404*(4-6), 374-378.

Dillon, A. C., Gennett, T., Jones, K. M., Alleman, J. L., Parilla, P. A., & Heben, M. J. (1999). A simple and complete purification of single-walled carbon nanotube materials. *Advanced Materials*, *11*(16), 1354-1358.

Ding, F., Larsson, P., Larsson, J. A., Ahuja, R., Duan, H., Rosén, A., & Bolton, K. (2008). The importance of strong carbon− metal adhesion for catalytic nucleation of single-walled carbon nanotubes. *Nano Letters*, *8*(2), 463-468.

Dresselhaus, M. S., Dresselhaus, G., Eklund, P. C., & Rao, A. M. (2000). Carbon nanotubes. In *The Physics of Fullerene-Based and Fullerene-Related Materials* (pp. 331-379). Springer, Dordrecht.

Dresselhaus, M. S., Lin, Y. M., Rabin, O., Jorio, A., Souza Filho, A. G., Pimenta, M. A., Saito, R., & Dresselhaus, G. (2003). Nanowires and nanotubes. *Materials Science and Engineering: C*, *23*(1-2), 129-140.

Duesberg, G. S., Graupner, R., Downes, P., Minett, A., Ley, L., Roth, S., & Nicoloso, N. (2004). Hydrothermal functionalisation of single-walled carbon nanotubes. *Synthetic Metals*, *142*(1-3), 263-26

Dujardin, E., Ebbesen, T. W., Krishnan, A., & Treacy, M. M. (1998). Purification of single-shell nanotubes. *Advanced Materials*, *10*(8), 611-613.

Ebbesen, T. W., & Ajayan, P. M. (1992). Large-scale synthesis of carbon nanotubes. *Nature*, *358*(6383), 220.

Eklund, P. C., Pradhan, B. K., Kim, U. J., Xiong, Q., Fischer, J. E., Friedman, A. D., Holloway, B. C., Jordan, K. & Smith, M. W. (2002). Large-scale production of single-walled carbon nanotubes using ultrafast pulses from a free electron laser. *Nano Letters*, *2*(6), 561-566.

Engel-Herbert, R., Pforte, H., & Hesjedal, T. (2007). CVD synthesis and purification of single-walled carbon nanotubes using silica-supported metal catalyst. *Materials Letters*, *61*(11-12), 2589-2593.

Ericson, L. M. (2004). Macroscopic, Neat, Single-Walled Carbon Nanotube Fibers. *Science*, 305(5689), 1447-1450.

Flahaut, E., Bacsa, R., Peigney, A., & Laurent, C. (2003). Gram-scale CCVD synthesis of double-walled carbon nanotubes. *Chemical Communications*, (12), 1442-1443.

Friel, J. J. (1994). X-ray and image analysis in electron microscopy. Princeton Gamma-Tech, Incorporated pp. 16–40.

Gökçen, T., Dateo, C. E., & Meyyappan, M. (2002). Modeling of the HiPco process for carbon nanotube production. II. Reactor-scale analysis. *Journal of Nanoscience and Nanotechnology*, *2*(5), 535-544.

Govindaraj, A., & Rao, C. N. R. (2002). Organometallic precursor route to carbon nanotubes. *Pure and Applied Chemistry*, *74*(9), 1571-1580.

Guo, T., Nikolaev, P., Rinzler, A. G., Tomanek, D., Colbert, D. T., & Smalley, R. E. (1995). Self-assembly of tubular fullerenes. *The Journal of Physical Chemistry*, *99*(27), 10694-10697.

Hafner, J. H., Bronikowski, M. J., Azamian, B. R., Nikolaev, P., Rinzler, A. G., Colbert, D. T., Smith, K. A., & Smalley, R. E. (1998). Catalytic growth of single-wall carbon nanotubes from metal particles. *Chemical Physics Letters*, *296*(1-2), 195-202.

Hernandez, C. D., Zhang, M., Fang, S., Baughman, R. H., Gates, T. S., & Kahng, S. K. (2006). Multifunctional characteristics of carbon nanotube (CNT) yarn composites. In *ASME 2006 Multifunctional Nanocomposites International Conference* (pp. 247-251). American Society of Mechanical Engineers.

Hou, P. X., Liu, C., & Cheng, H. M. (2008). Purification of carbonnanotubes. *Carbon*, *46*(15), 2003-2025.

Hsieh, C. T., Lin, Y. T., Lin, J. Y., & Wei, J. L. (2009). Synthesis of carbon nanotubes over Ni-and Co-supported CaCO3 catalysts using catalytic chemical vapor deposition. *Materials Chemistry and Physics*, *114*(2-3), 702-708.

Hu, H., Zhao, B., Itkis, M. E., & Haddon, R. C. (2003). Nitric acid purification of single-walled carbon nanotubes. *The Journal of Physical Chemistry B*, *107*(50), 13838-13842.

lijima, S. (1991). Helical microtubules of graphitic. *Nature*, *354*(6348), 56-58.

Iijima, S., & Ichihashi, T. (1993). Single-shell carbon nanotubes of 1-nm diameter. *Nature*, *363*(6430), 603.

Iijima, T., Oshima, H., Hayashi, Y., Suryavanshi, U. B., Hayashi, A., & Tanemura, M. (2011). Morphology control of a rapidly grown vertically aligned carbon-nanotube forest for fiber spinning. *Physica Ptatus Solidi (a)*, *208*(10), 2332-2334.

Igarashi, H., Murakami, H., Murakami, Y., Maruyama, S., & Nakashima, N. (2004). Purification and characterization of zeolite-supported single-walled carbon nanotubes catalytically synthesized from ethanol. *Chemical Physics Letters*, *392*(4-6), 529-532.

Iyuke, S. E., Abdulkareem, S. A., Afolabi, S. A., & vZ Piennar, C. H. (2007). Catalytic production of carbon nanotubes in a swirled fluid chemical vapour deposition reactor. *International Journal of Chemical Reactor Engineering*, *5*(1), 1-9.

Iyuke, S.E., Mamvura, T.A., Liu, K., Sibanda, V., Meyyappan, M., &. Varadan, V.K (2009). Process synthesis and optimization for the production of carbon nanostructures. *Nanotechnology, 20*(37), 375602.

Jakubinek, M. B., Johnson, M. B., White, M. A., Jayasinghe, C., Li, G., Cho, W., Schulz, M.J., & Shanov, V. (2012). Thermal and electrical conductivity of array-spun multi-walled carbon nanotube yarns. *Carbon, 50*(1), 244-248.

Jeynes, J. C. G., Mendoza, E., Chow, D. C., Watts, P. C., McFadden, J., & Silva, S. R. P. (2006). Generation of Chemically Unmodified Pure Single-Walled Carbon Nanotubes by Solubilizing with RNA and Treatment with Ribonuclease A. *Advanced Materials, 18*(12), 1598-1602.

Jiang, K., Wang, J., Li, Q., Liu, L., Liu, C., & Fan, S. (2011). Superaligned carbon nanotube arrays, films, and yarns: a road to applications. *Advanced Materials, 23*(9), 1154-1161.

Jose-Yacaman, M., Miki-Yoshida, M., Rendon, L., & Santiesteban, J.G. (1993). Catalytic growth of carbon microtubules with fullerene structure. *Applied Physics Letters,* 62(6), 657-659.

Journet, C., Maser, W. K., Bernier, P., Loiseau, A., de La Chapelle, M. L., Lefrant, D. S., ... & Fischer, J. E. (1997). Large-scale production of single-walled carbon nanotubes by the electric-arc technique. *Nature, 388*(6644), 756.

Kabo, G. J., Paulechka, E., Blokhin, A. V., Voitkevich, O. V., Liavitskaya, T., & Kabo, A. G. (2016). Thermodynamic properties and similarity of stacked-cup multiwall carbon nanotubes and graphite. *Journal of Chemical & Engineering Data, 61*(11), 3849-3857.

Khavarian, M., Chai, S. P., Tan, S. H., & Mohamed, A. R. (2009). Floating catalyst cvd synthesis of carbon nanotubes using iron (III) Chloride: Influences of the growth parameters. *Nano, 4*(06), 359-366.

Kim, N. S., Lee, Y. T., Park, J., Ryu, H., Lee, H. J., Choi, S. Y., & Choo, J. (2002). Dependence of the vertically aligned growth of carbon nanotubes on the catalysts. *The Journal of Physical Chemistry B, 106*(36), 9286-9290.

Kim, Y., & Luzzi, D. E. (2005). Purification of pulsed laser synthesized single wall carbon nanotubes by magnetic filtration. *The Journal of Physical Chemistry B, 109*(35), 16636-16643.

Kokai, F., Takahashi, K., Yudasaka, M., Yamada, R., Ichihashi, T., & Iijima, S. (1999). Growth dynamics of single-wall carbon nanotubes synthesized by CO_2 laser vaporization. *The Journal of Physical Chemistry B, 103*(21), 4346-4351.

Kunii, D., & Levenspiel, O. (1991). Fluidization and mapping of regimes. *Fluidization engineering*, 2(3), 61-94.

Lee, C. J., Park, J., & Jeong, A. Y. (2002). Catalyst effect on carbon nanotubes synthesized by thermal chemical vapor deposition. *Chemical Physics Letters, 360*(3-4), 250-255.

Lekawa-Raus, A., Patmore, J., Kurzepa, L., Bulmer, J., & Koziol, K. (2014). Electrical properties of carbon nanotube based fibers and their future use in electrical wiring. *Advanced Functional Materials, 24*(24), 3661-3682.

Li, J., Papadopoulos, C., & Xu, J. (1999). Nanoelectronics: Growing y-junction carbon nanotubes. *Nature*, 402(6), 253-254.

Li, Y. (2004). Direct Spinning of Carbon Nanotube Fibers from Chemical Vapor Deposition Synthesis. *Science*, 304(5668), 276-278.

Liu, K., Sun, Y., Zhou, R., Zhu, H., Wang, J., Liu, L., Fan, S., & Jiang, K. (2009). Carbon nanotube yarns with high tensile strength made by a twisting and shrinking method. *Nanotechnology*, 21(4), 045708.

Lu, K. L., Lago, R. M., Chen, Y. K., Green, M. L. H., Harris, P. J. F., & Tsang, S. C. (1996). Mechanical damage of carbon nanotubes by ultrasound. *Carbon, 34*(6), 814-816.

Maphutha, S.K. (2010). Thermodynamic study of Carbon nanotube production from greenhouse gases during syngas synthesis (Doctoral dissertation). From University of the Witwatersrand Johannesburg.

Maser, W. K., Munoz, E., Benito, A. M., Martınez, M. T., De La Fuente, G. F., Maniette, Y., Anglaret, E., & Sauvajol, J. L. (1998). Production of high-density single-walled nanotube material by a simple laser-ablation method. *Chemical Physics Letters, 292*(4-6), 587-593.

Miao, M. (2013). Yarn spun from carbon nanotube forests: Production, structure, properties and applications. *Particuology, 11*(4), 378-393.

Mohanapriya, S., & Lakshminarayanan, V. (2007). Simultaneous purification and spectrophotometric determination of nickel present in as-prepared single-walled carbon nanotubes (SWCNT). *Talanta, 71*(1), 493-497.

Mohlala, M. S., Liu, X. Y., Robinson, J. M., & Coville, N. J. (2005). Organometallic precursors for use as catalysts in carbon nanotube synthesis. *Organometallics, 24*(5), 972-976.

Morîntale, E., & Harabou, A. (2013). Use of heat flows from DSC curve for calculation of specific heat of the solid materials. *Physics AUC, 23*, 89-94.

Motta, M., Moisala, A., Kinloch, I., & Windle, A. (2007). High Performance Fibres from 'Dog Bone' Carbon Nanotubes. *Advanced Materials*, 19(21), 3721-3726.

Munoz, E., Maser, W. K., Benito, A. M., Martınez, M. T., De La Fuente, G. F., Maniette, Y., Righi, A., Anglaret, E., & Sauvajol, J. L. (2000). Gas and pressure effects on the production of single-walled carbon nanotubes by laser ablation. *Carbon, 38*(10), 1445-1451.

Nan, Z., Wei, C., Yang, Q., & Tan, Z. (2009). Thermodynamic properties of carbon nanotubes. *Journal of Chemical & Engineering Data, 54*(4), 1367-1370.

Perez-Cabero, M., Rodrıguez-Ramos, I., & Guerrero-Ruız, A. (2003). Characterization of carbon nanotubes and carbon nanofibers prepared by catalytic decomposition of acetylene in a fluidized bed reactor. *Journal of catalysis*, 215(2), 305-316.

Perez-Cabero, M., Romeo, E., Royo, C., Monzon, A., Guerrero-Ruiz, A., & Rodriguez-Ramos, I. (2004). Growing mechanism of CNTs: A kinetic approach. *Journal of Catalysis, 224*(1), 197-205.

Perry, J. H. (1950). Chemical engineers' handbook. Japan: *McGraw-Hill*

Philippe, R., Morançais, A., Corrias, M., Caussat, B., Kihn, Y., Kalck, P., ... & Serp, P. (2007). Catalytic Production of Carbon Nanotubes by Fluidized-Bed CVD. *Chemical Vapor Deposition*, 13(9), 447-457.

Philippe, R., Serp, P., Kalck, P., Kihn, Y., Bordère, S., Plee, D., Gaillard, P., Bernard, D., & Caussat, B. (2009). Kinetic study of carbon nanotubes synthesis by fluidized bed chemical vapor deposition. *AIChE Journal, 55*(2), 450-464.

Rafique, M. M., & Iqbal, J. (2011) Production of Carbon Nanotubes by different routes – A Review. *Journal of Encapsulation and Adsorption Sciences, 01*(02), 29-34.

Rahmandoust, M., & Öchsner, A. (2011). Buckling behaviour and natural frequency of zigzag and armchair single-walled carbon nanotubes. In *Journal of Nano Research* (Vol. 16, pp. 153-160). Trans Tech Publications

Raman, C. V., & Krishnan, K. S. (1928). A new type of secondary - radiation. Nature, 121(3048), 501.

Ramesh, P., Okazaki, T., Sugai, T., Kimura, J., Kishi, N., Sato, K., Ozeki, Y., & Shinohara, H. (2006). Purification and characterization of double-wall carbon nanotubes synthesized by catalytic chemical vapor deposition on mesoporous silica. *Chemical Physics Letters, 418*(4-6), 408-412.

Rao, A. M., Richter, E., Bandow, S., Chase, B., Eklund, P. C., Williams, K. A., Fang, S., Subbaswamy, K.R., Menon, M., Thess, A., & Smalley, R. E. (1997). Diameter-selective Raman scattering from vibrational modes in carbon nanotubes. *Science, 275*(5297), 187-191.

Robertson, J. (2004). Realistic applications of CNTs. *Materials Today, 7*(10), 46-52.

Russ, J. C. (2013). Fundamentals of Energy Dispersive X-Ray Analysis: Butterworths Monographs in Materials. Butterworth-Heinemann. pp.17-41.

Saito, R., Takeya, T., Kimura, T., Dresselhaus, G., & Dresselhaus, M. S. (1999). Finite-size effect on the Raman spectra of carbon nanotubes. *Physical Review B, 59*(3), 2388.

Salernitano, E., Giorgi, L., Makris, T. D., Giorgi, R., Lisi, N., Contini, V., & Falconieri, M. (2007). Purification of MWCNTs grown on a nanosized unsupported Fe-based powder catalyst. *Diamond and Related Materials, 16*(8), 1565-1570.

See, C. H., & Harris, A. T. (2007). A Review of Carbon Nanotube Synthesis via Fluidized-Bed Chemical Vapor Deposition. *Industrial & Engineering Chemistry Research, 46*(4), 997-1012.

Segura-Cardenas, E., Reyes-Reyes, M., & López-Sandoval, R. (2012). Effects of Varying the Content of Alcohol in the Reaction Mixture on the Graphitization of MWCNTs and Their Surface Functionalization. *The Journal of Physical Chemistry C, 116*(17), 9783-9792.

Sheshmani, S., Ashori,A., & Fashapoyeh,m. A. (2013) Wood plastic composite using graphene nanoplateles. *International Journal of Biological Micromolecules*, 58, 1-6.

Shelimov, K. B., Esenaliev, R. O., Rinzler, A. G., Huffman, C. B., & Smalley, R. E. (1998). Purification of single-wall carbon nanotubes by ultrasonically assisted filtration. *Chemical Physics Letters, 282*(5-6), 429-434

Shin, K. Y., Su, H. C., & Tsai, C. H. (2006). In situ growth of single-walled carbon nanotubes by bimetallic technique with/without dielectric support for nanodevice applications. *Journal of Vacuum Science & Technology B: Microelectronics and Nanometer Structures Processing, Measurement, and Phenomena, 24*(1), 358-361

Sivakumar, V. M., Abdullah, A. Z., Mohamed, A. R., & Chai, S. P. (2011). Optimized parameters for carbon nanotubes synthesis over Fe and Ni catalysts VIA methane CVD. Rev. Adv. Mater. Sci, 27, 25-30.

Simate, G. S., Moothi, K., Meyyappan, M., Iyuke, S. E., Ndlovu, S., Falcon, R., & Heydenrych, M. (2014). Kinetic model of carbon nanotube production from carbon dioxide in a floating catalytic chemical vapour deposition reactor. *RSC Advances, 4*(19), 9564-9572.

Suriani, A. B., Asli, N. A., Salina, M., Mamat, M. H., Aziz, A. A., Falina, A. N., Maryam, M., Shamsudin, M.S., Nor, R.M., Abdullah, S. & Rusop, M. (2013). Effect of iron and cobalt catalysts on the growth of carbon nanotubes from palm oil precursor. In IOP Conference Series: Materials Science and Engineering (Vol. 46, No. 1, p. 012014). IOP Publishing.

Szabó, A., Perri, C., Csató, A., Giordano, G., Vuono, D., & Nagy, J. B. (2010). Synthesis Methods of Carbon Nanotubes and Related Materials. *Materials*, 3(5), 3092-3140.

Tagmatarchis, N., Zattoni, A., Reschiglian, P., & Prato, M. (2005). Separation and purification of functionalised water-soluble multi-walled carbon nanotubes by flow field-flow fractionation. *Carbon*, *43*(9), 1984-1989.

Thess, A., Lee, R., Nikolaev, P., Dai, H ., Petit, P., Robert, J., Xu, C., Lee, Y.H., Kim, S.G., Rinzler, A.G., & Smalley, R. E. (1996). *Crystalline Ropes of Metallic Carbon Nanotubes. Science*, *273*(5274), 483-487.

Tripathi, P. K., Durbach, S., & Coville, N. J. (2017). Synthesis of Multi-Walled Carbon Nanotubes from Plastic Waste Using a Stainless-Steel CVD Reactor as Catalyst. *Nanomaterials*, *7*(10), 284.

Ummartyotin, S., Juntaro, J., Wu, C., Sain, M., & Manuspiya, H. (2011). Deposition of PEDOT: PSS nanoparticles as a conductive microlayer anode in OLEDs device by desktop inkjet printer. *Journal of Nanomaterials*, 2011, 26.

Vallés, C., Pérez-Mendoza, M., Maser, W. K., Martinez, M. T., Alvarez, L., Sauvajol, J. L., & Benito, A. M. (2009). Effects of partial and total methane flows on the yield and structural characteristics of MWCNTs produced by CVD. *Carbon*, *47*(4), 998-1004.

Venegoni, D., Serp, P., Feurer, R., Kihn, Y., Vahlas, C., & Kalck, P. (2002). Parametric study for the growth of carbon nanotubes by catalytic chemical vapor deposition in a fluidized bed reactor. *Carbon*, 40(10), 1799-1807.

Vigolo, B. (2000). Macroscopic Fibers and Ribbons of Oriented Carbon Nanotubes. *Science*, 290(5495), 1331-1334.

Vigolo, B., Poulin, P., Lucas, M., Launois, P., & Bernier, P. (2002). Improved structure and properties of single-wall carbon nanotube spun fibers. *Applied Physics Letters*, 81(7), 1210-1212.

Wei, J., Zhu, H., Wu, D., & Wei, B. (2004). Carbon nanotube filaments in household light bulb. *Applied Physics Letters*, *84*(24), 4869-4871.

Xiang, R., Luo, G. H., Qian, W. Z., Wang, Y., Wei, F., & Li, Q. (2007). Large area growth of aligned CNT arrays on spheres: towards large scale and continuous production. *Chemical Vapor Deposition*, 13(10), 533-536.

Xu, F., Sadrzadeh, A., Xu, Z., & Yakobson, B. I. (2013). Can carbon nanotube fibers achieve the ultimate conductivity? – Coupled-mode analysis for electron transport through the carbon nanotube contact. *Journal of Applied Physics*, *114*(6), 063714.

Yang, C., Hu, X., Wang, D., Dai, C., Zhang, L., Jin, H., & Agathopoulos, S. (2006). Ultrasonically treated multi-walled carbon nanotubes (MWCNTs) as PtRu catalyst supports for methanol electrooxidation. *Journal of Power Sources*, 160(1), 187-193.

Zaporotskova, I. V., Polikarpova, N. P., & Vil'keeva, D. E. (2013). Sensor Activity of Carbon Nanotubes with a Boundary Functional Group. *Nanoscience and Nanotechnology Letters*, *5*(11), 1169-1173.

Zhang, J., Zou, H., Qing, Q., Yang, Y., Li, Q., Liu, Z., Guo, x., & Du, Z. (2003). Effect of chemical oxidation on the structure of single-walled carbon nanotubes. *The Journal of Physical Chemistry B, 107*(16), 3712-3718.

Zhang, M. (2004). Multifunctional Carbon Nanotube Yarns by Downsizing an Ancient Technology. *Science*, 306(5700), 1358-1361.

Zhang, M., & Li, J. (2009). Carbon nanotube in different shapes. *Materials Today*, 12(6), 12-18.

Zhang, X., Jiang, K., Feng, C., Liu, P., Zhang, L., Kong, J., Zhang, T., Li, Q., & Fan, S. (2006). Spinning and processing continuous yarns from 4-inch wafer scale super-aligned carbon nanotube arrays. *Advanced Materials, 18*(12), 1505-1510.

Zimmerman, J. L., Bradley, R. K., Huffman, C. B., Hauge, R. H., & Margrave, J. L. (2000). Gas-phase purification of single-wall carbon nanotubes. *Chemistry of Materials, 12*(5), 1361-1366.

APPENDIX

Appendix 1: SEM Images

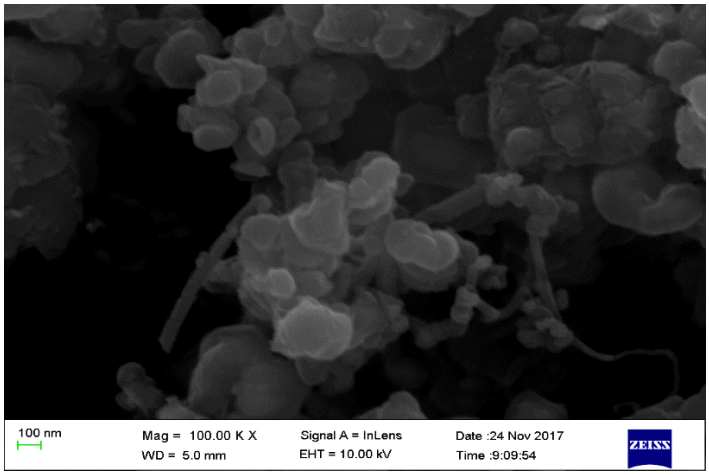


Figure 0.1:CNTs produced at methane flow rate of 100 ml/min and 900^{o}C

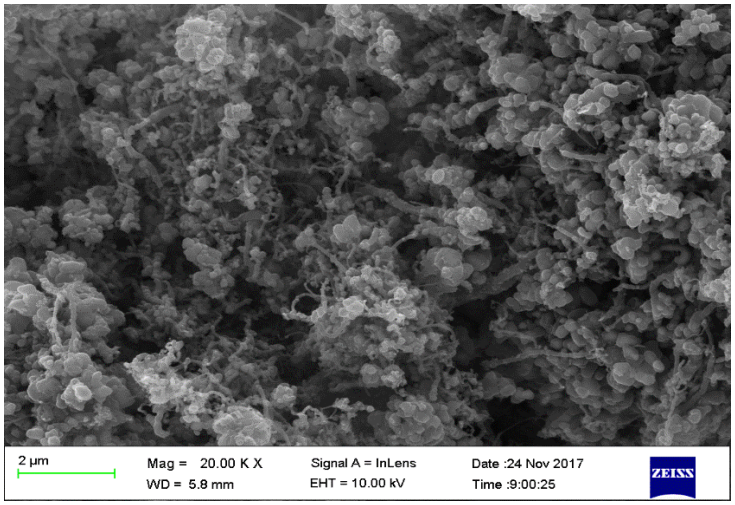


Figure 0.2:CNTs produced at methane flow rate of 125 ml/min and 900^{o}C

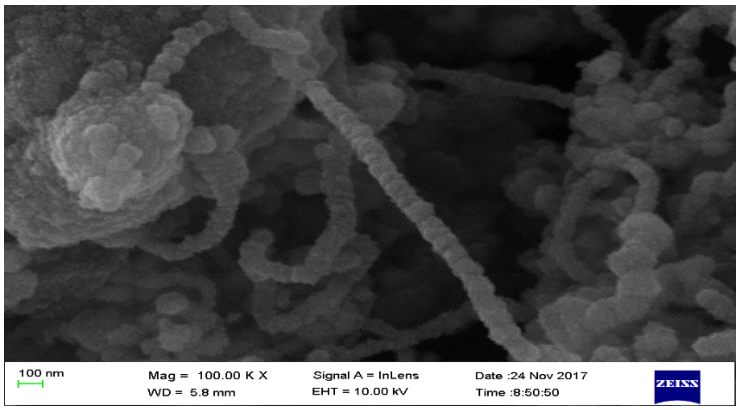


Figure 0.3:CNTs produced at methane flow rate of 150 ml/min and 900^{o}C

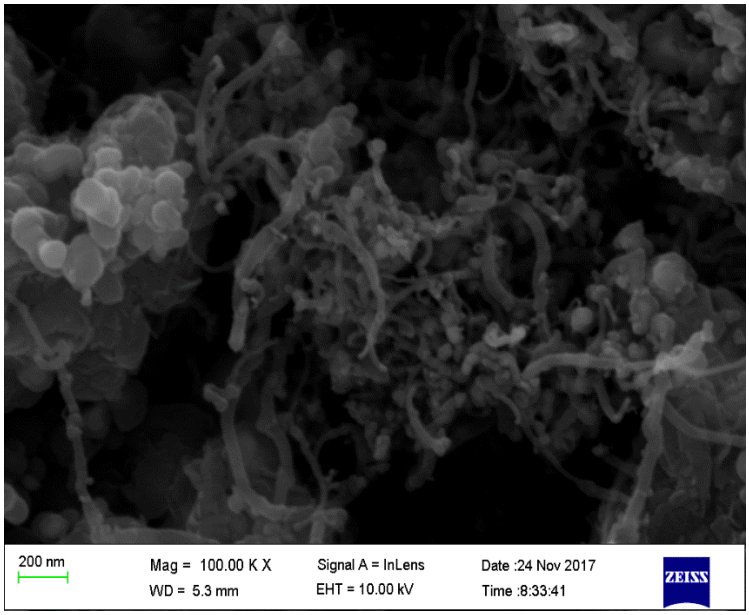


Figure 0.4: CNTs produced at methane flow rate of 100 ml/min and 950^{o}C

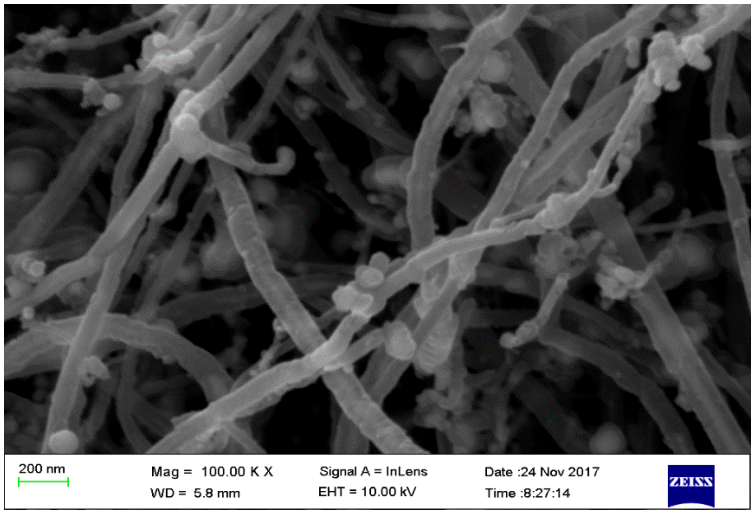


Figure 0.5: CNTs produced at methane flow rate of 125 ml/min and 950^{o}C

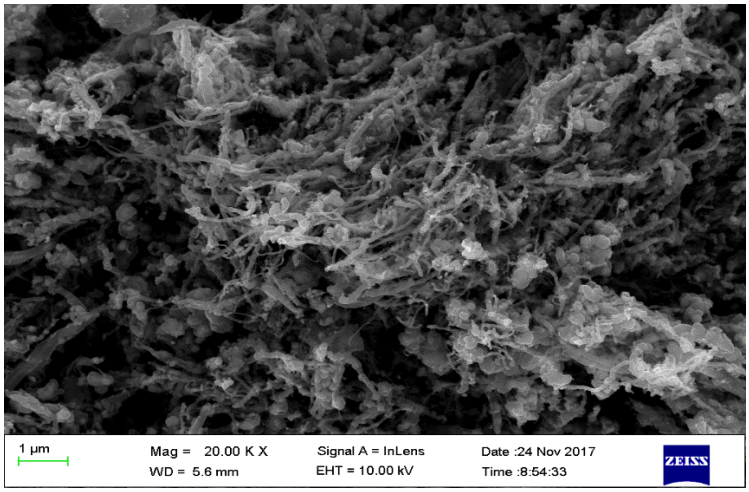


Figure 0.6: CNTs produced at methane flow rate of 150 ml/min and 950^{o}C

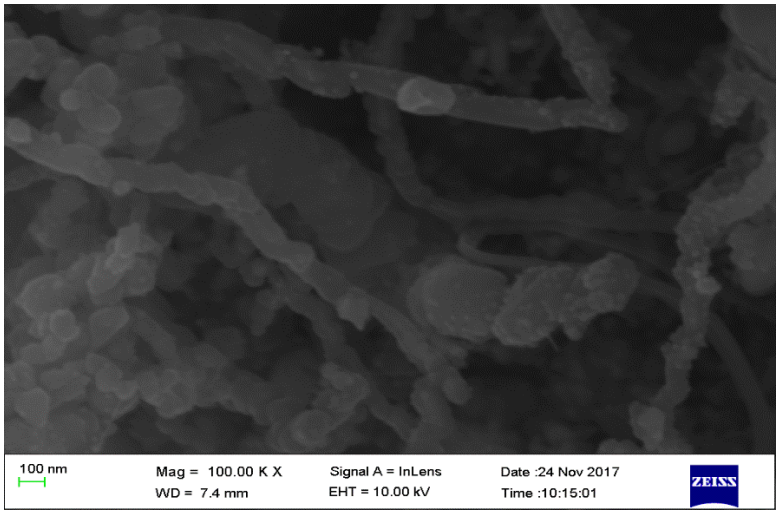


Figure 0.7:CNTs produced at methane flow rate of 100 ml/min and 1000^{o}C

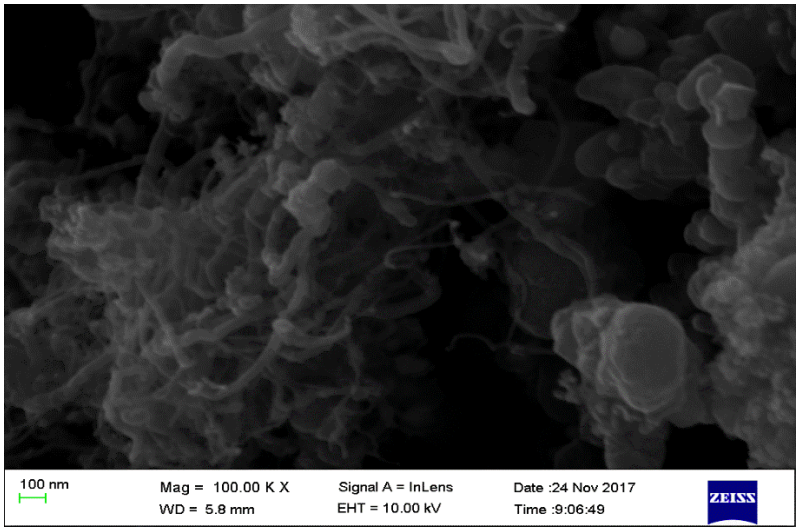


Figure 0.8:CNTs produced at methane flow rate of 125 ml/min and 1000^{o}C

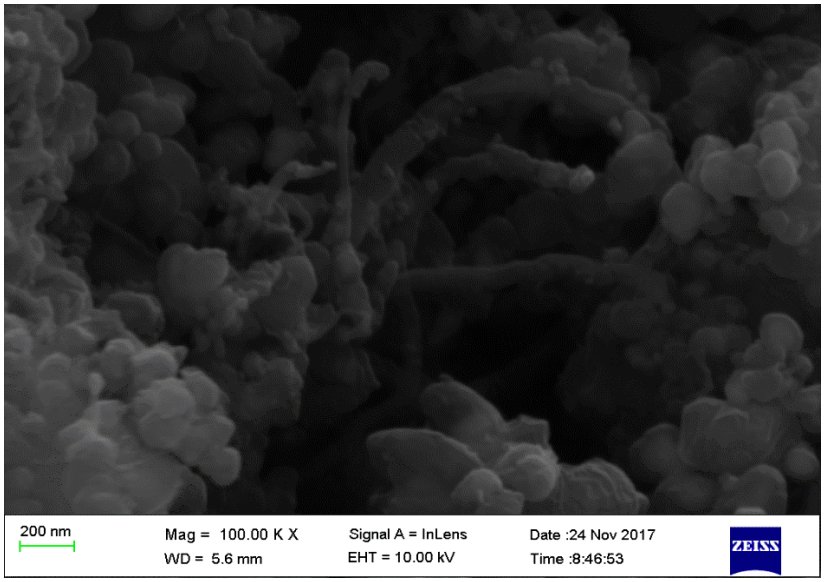


Figure 0.9:CNTs produced at methane flow rate of 150 ml/min and 1000^{o}C

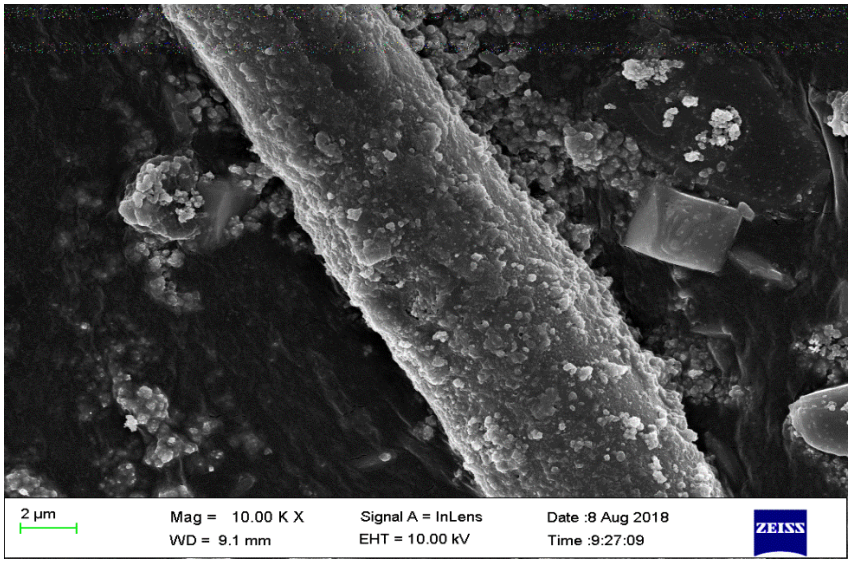


Figure 0.10:SEM image of yarn produced at 900^{o}C

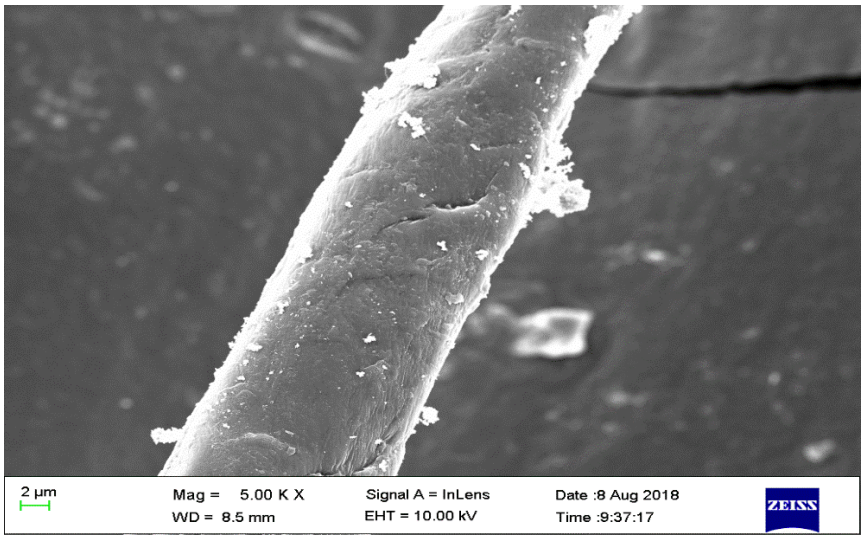


Figure 0.11: SEM images of yarn produced at 950^{o}C

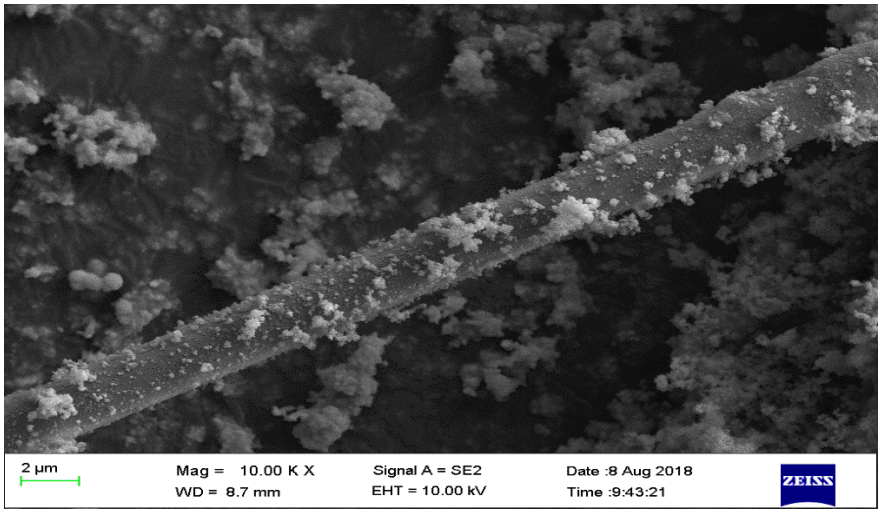


Figure 0.12:SEM image of yarn produced at 1000^{o}C

Appendix 2: Calculating rate for kinetic model

Reactor conditions

Reaction Temperature = 900°C

Methane Flow rate = 150 ml/min

Reference Hydrogen gas (H_{2F}) for calibrating GC equipment

Density = 0.08988 g/L

Concentration = 99%

GC peak area = 19248.8 µV/min

$$Response\ factor = \frac{H_{2F} Peak\ area}{[H_{2F}]}$$

$$= \frac{19248.8}{0.99}$$

$$= 192.5\%$$

Hydrogen gas from reaction (H_{2R})

Peak area = 9342.5 µV/min

$$\%[H_{2R}] = \frac{Peak\ H_{2R}\ Area}{H_{2F}\ Response\ factor}$$

$$= \frac{9342.5}{192.5}$$

$$= 48.53\%$$

Concentration in mg/l

$$[H_{2R}] = \frac{([H_{2R}]\%)}{100} * (H_{2F}\ density * 1000)$$

$$= \frac{(48.53)}{100} * (0.08988 * 1000)$$

$$= 43.62\ mg/l$$

$[H_{2R}]^2 = (43.62)^2 = 1902.6$

Derived kinetic model:

$$\frac{d[CNT]}{dt} = \frac{K_1 K_2 k_3 [CH_4][*]_0}{K_1[CH_4][H_2]^2 + K_1 K_2 [CH_4] + [H_2]^2}$$

$[*]_0 = 6.18\ x\ 10^{-7} mol/min.mg$

From experiment: $\frac{d[CNT]}{dt} = 2.44\ mg/min$

Methane flow rate = 125m*l*/min

Converting CH_4 flow rate to concentration [mg/*l*]

Conversion factor of gases from ppm to mg/*l* = 0.0409

Argon (Ar) flow rate = 150 m*l*/mil

Molecular weight of CH_4 = 16.01 g/mol

$$[CH_4] = \frac{\frac{125\ X\ 10^6}{125 + 150} x0.0409x16.01}{1000}$$

$$= 297.64\ mg/l$$

Using the model to determine kinetic constants:

$$3.295 = \frac{K_1 K_2 k_3 (327.4)(6.18x10^{-7})}{K_1(327.4)(353.838) + K_1 K_2 (327.4) + (1902)}$$

Using solve tool in excel the value of $K_1 K_2 k_3$ was estimated as follows:

$$K_1 = 1.62x10^4$$

$$K_2 = 1.06x10^7$$

$$k_3 = 5.61x10^6$$

Using $K_1 K_2 k_3$ estimated the value of $\frac{d[CNT]}{dt} = 3.468\ mg/l$ was obtained which is in 95% confidence interval with the experimental value of 3.296 mg/*l*

Reactor conditions

Reaction Temperature = 900^{o}C

Methane Flow rate = 125 ml/min

Reference Hydrogen gas (H_{2F}) for calibrating GC equipment

Density = 0.08988 g/L

Concentration = 99%

GC peak area = 19248.8 µV/min

$$Response\ factor = \frac{H_{2F} Peak\ area}{[H_{2F}]}$$

$$= \frac{19248.8}{0.99}$$

$$= 192.5\%$$

Hydrogen gas from reaction (H_{2R})

Peak area = 4028.9 µV/min

$$\%[H_{2R}] = \frac{Peak\ H_{2R}\ Area}{H_{2F}\ Response\ factor}$$

$$= \frac{4028.9}{192.5}$$

$$= 20.92\%$$

Concentration in mg/l

$$[H_{2R}] = \frac{([H_{2R}]\%)}{100} * (H_{2F}\ density * 1000)$$

$$= \frac{(20.92)}{100} * (0.08988 * 1000)$$

$$= 18.81\ mg/l$$

$[H_{2R}]^2 = (18.81)^2 = 353.81$

Derived kinetic model:

$$\frac{d[CNT]}{dt} = \frac{K_1 K_2 k_3 [CH_4][*]_0}{K_1[CH_4][H_2]^2 + K_1 K_2 [CH_4] + [H_2]^2}$$

$[*]_0 = 6.18\ x\ 10^{-7} mol/min.mg$

From experiment: $\frac{d[CNT]}{dt} = 2.44\ mg/min$

Methane flow rate = 125m*l*/min

Converting CH_4 flow rate to concentration [mg/*l*]

Conversion factor of gases from ppm to mg/l = 0.0409

Argon (Ar) flow rate = 150 ml/mil

Molecular weight of CH_4 = 16.01 g/mol

$$[CH_4] = \frac{\frac{125\ X\ 10^6}{125 + 150} x 0.0409 x 16.01}{1000}$$

$$= 297.64\ mg/l$$

Using the model to determine kinetic constants:

$$2.440 = \frac{K_1 K_2 k_3 (297.64)(6.18x10^{-7})}{K_1(297.64)(353.838) + K_1 K_2 (297.64) + (353.838)}$$

Using solve tool in excel the value of $K_1 K_2 k_3$ was estimated as follows:

$$K_1 = 1.13x10^4$$

$$K_2 = 6.72x10^6$$

$$k_3 = 4.16x10^6$$

Using $K_1 K_2 k_3$ estimated the value of $\frac{d[CNT]}{dt} = 2.568\ mg/l$ was obtained which is in 95% confidence interval with the experimental value of 2.44 mg/l

The above calculation was repeated for each experiment at different methane flow rate.

Appendix 3: Data for production rate plot

Table 0.1: Figure 2.22 data

Methane Concentration [mg/l]	Production Rate [mg/min]	
	Experimental	Model
261.9	1.180	1.242
297.6	2.440	2.568
327.4	3.295	3.468

Table 0.2:Figure 2.23 data

Methane Concentration [mg/l]	Production Rate [mg/min]	
	Experimental	Model
261.9	2.033	2.140
297.6	3.673	3.867
327.4	4.640	4.884

Table 0.3: Figure 2.24 data

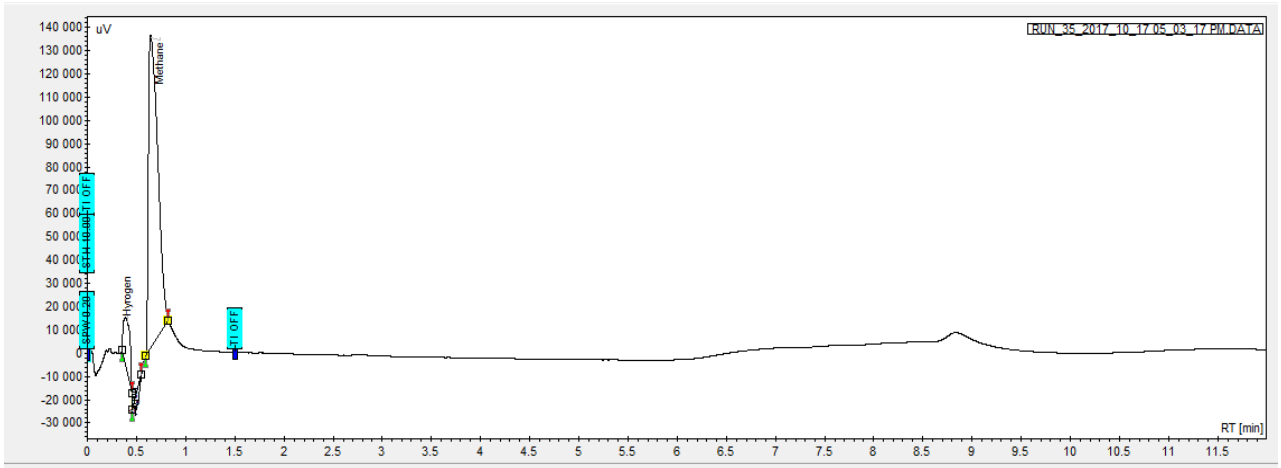
Methane Concentration [mg/l]	Production Rate [mg/min]	
	Experimental	Model
261.9	1.700	1.789
297.6	3.453	3.635
327.4	4.571	4.811

Appendix 4: Data for Electrical Conductivity calculations and plot

Table 0.4:Figure 4.25 data and calculations

Temperature[^{o}C]	**Resistance [Ω]**		**Resistivity [Ωm]**		**Electrical Conductivity [S/m]**	
	CNTs	*Yarn*	*CNT*	*Yarn*	*CNTs*	*Yarn*
900	4.638219	9.496676	0.0231911	0.047483	43.12	21.06
950	3.510004	6.752194	0.01755	0.033761	56.98	29.62
1000	3.561254	6.816633	0.0178063	0.034083	56.16	29.34
Length of Glass [m]	0.005					
Area of Glass [m^2]	0.000025					

Appendix 5: Sample Chromatogram



Name	Time [Min]	Quantity [% Area	Area [uV.Min]	Area % [%]
Hyrogen	0.41	10.43	1776.2	10.434
Argon	0.48	2.79	475.1	2.791
Methane	0.64	86.78	14772.6	86.776
		100.00	17023.9	100.000

Figure 0.13: Gas chromatogram of experiment at 950ºC and CH4 flow rate of 100 ml/min

Appendix 6: Thermodynamic Properties of yarn

Table 0.5: Detailed data for Table 5.1

Temp [ºC]	Cp [J/ºC.g]	ΔH [J/g]	ΔS [J/ºC.g]
200	26.4	4 624.8	55.0
201	26.6	4 679.3	55.4
202	26.7	4 734.3	55.9
203	26.9	4 789.6	56.4
204	27.1	4 845.5	56.8
205	27.2	4 901.7	57.3
206	27.4	4 958.4	57.8
207	27.6	5 015.5	58.3
208	27.7	5 073.1	58.7
209	27.9	5 131.0	59.2
210	28.1	5 189.5	59.7
211	28.2	5 248.3	60.2
212	28.4	5 307.7	60.7
213	28.6	5 367.4	61.2
214	28.7	5 427.6	61.7
215	28.9	5 488.3	62.2
216	29.1	5 549.4	62.7
217	29.2	5 611.0	63.2
218	29.4	5 673.0	63.7
219	29.6	5 735.4	64.2
220	29.7	5 798.4	64.7
221	29.9	5 861.8	65.2
222	30.1	5 925.6	65.7
223	30.3	5 989.9	66.2
224	30.4	6 054.7	66.7
225	30.6	6 119.9	67.2
226	30.8	6 185.7	67.8
227	30.9	6 251.8	68.3
228	31.1	6 318.5	68.8
229	31.3	6 385.6	69.3
230	31.5	6 453.2	69.9
231	31.7	6 521.3	70.4
232	31.8	6 589.9	70.9
233	32.0	6 658.9	71.5
234	32.2	6 728.5	72.0
235	32.4	6 798.5	72.5
236	32.6	6 869.0	73.1
237	32.7	6 940.0	73.6
238	32.9	7 011.4	74.2
239	33.1	7 083.4	74.7
240	33.3	7 155.9	75.3

241	33.5	7 228.9	75.8
242	33.7	7 302.3	76.4
243	33.8	7 376.3	76.9
244	34.0	7 450.7	77.5
245	34.2	7 525.7	78.1
246	34.4	7 601.2	78.6
247	34.6	7 677.1	79.2
248	34.8	7 753.6	79.8
249	35.0	7 830.6	80.4
250	35.1	7 908.1	80.9
251	35.3	7 986.1	81.5
252	35.5	8 064.7	82.1
253	35.7	8 143.7	82.7
254	35.9	8 223.3	83.3
255	36.1	8 303.4	83.8
256	36.3	8 384.0	84.4
257	36.5	8 465.1	85.0
258	36.7	8 546.8	85.6
259	36.9	8 629.0	86.2
260	37.1	8 711.7	86.8
261	37.3	8 795.0	87.4
262	37.5	8 878.8	88.0
263	37.7	8 963.1	88.6
264	37.9	9 048.0	89.2
265	38.1	9 133.4	89.8

Table 0.6: Detailed data for Table 5.2

Temp [ºC]	Cp [J/ºC.g]	ΔH [J/g]	ΔS [J/ºC.g]
200	55.9	9 775.3	116.2
201	56.2	9 892.9	117.2
202	56.6	10 011.9	118.2
203	56.9	10 132.4	119.2
204	57.3	10 254.2	120.3
205	57.7	10 377.5	121.3
206	58.0	10 502.3	122.4
207	58.4	10 628.5	123.4
208	58.8	10 756.3	124.5
209	59.2	10 885.5	125.6
210	59.5	11 016.2	126.7
211	59.9	11 148.4	127.8
212	60.3	11 282.2	129.0
213	60.7	11 417.5	130.1
214	61.1	11 554.4	131.3
215	61.5	11 692.8	132.4
216	62.0	11 832.8	133.6

217	62.4	11 974.4	134.8
218	62.8	12 117.6	136.0
219	63.2	12 262.4	137.2
220	63.6	12 408.8	138.4
221	64.1	12 556.9	139.6
222	64.5	12 706.6	140.9
223	64.9	12 858.0	142.1
224	65.4	13 011.1	143.4
225	65.8	13 165.8	144.6
226	66.3	13 322.2	145.9
227	66.7	13 480.4	147.2
228	67.2	13 640.3	148.5
229	67.7	13 801.9	149.8
230	68.1	13 965.2	151.2
231	68.6	14 130.3	152.5
232	69.1	14 297.2	153.9
233	69.5	14 465.9	155.2
234	70.0	14 636.3	156.6
235	70.5	14 808.6	158.0
236	71.0	14 982.6	159.4
237	71.5	15 158.6	160.8
238	72.0	15 336.3	162.2
239	72.5	15 515.9	163.7
240	73.0	15 697.4	165.1
241	73.5	15 880.7	166.6
242	74.0	16 065.9	168.1
243	74.6	16 253.1	169.6
244	75.1	16 442.1	171.1
245	75.6	16 633.1	172.6
246	76.1	16 826.0	174.1
247	76.7	17 020.9	175.6
248	77.2	17 217.7	177.2
249	77.8	17 416.5	178.7
250	78.3	17 617.3	180.3
251	78.8	17 820.1	181.9
252	79.4	18 024.8	183.5
253	80.0	18 231.7	185.1
254	80.5	18 440.5	186.7
255	81.1	18 651.4	188.3
256	81.7	18 864.3	190.0
257	82.2	19 079.4	191.6
258	82.8	19 296.5	193.3
259	83.4	19 515.6	195.0
260	84.0	19 736.9	196.7
261	84.6	19 960.4	198.4
262	85.2	20 185.9	200.1

263	85.8	20 413.6	201.8
264	86.4	20 643.4	203.6
265	87.0	20 875.4	205.3

Table 0.7: Detailed data for Table 5.3

Temp [ºC]	Cp [J/ºC.g]	ΔH [J/g]	ΔS [J/ºC.g]
200	34.8	6 089.0	72.4
201	34.9	6 148.2	72.8
202	35.1	6 208.0	73.3
203	35.2	6 268.3	73.8
204	35.4	6 329.1	74.2
205	35.5	6 390.5	74.7
206	35.6	6 452.4	75.2
207	35.8	6 514.8	75.7
208	35.9	6 577.8	76.2
209	36.1	6 641.4	76.6
210	36.2	6 705.5	77.1
211	36.4	6 770.2	77.6
212	36.6	6 835.4	78.1
213	36.7	6 901.3	78.6
214	36.9	6 967.7	79.2
215	37.0	7 034.7	79.7
216	37.2	7 102.2	80.2
217	37.3	7 170.4	80.7
218	37.5	7 239.1	81.2
219	37.7	7 308.5	81.8
220	37.8	7 378.4	82.3
221	38.0	7 449.0	82.8
222	38.2	7 520.1	83.4
223	38.3	7 591.9	83.9
224	38.5	7 664.3	84.5
225	38.7	7 737.3	85.0
226	38.9	7 810.9	85.6
227	39.0	7 885.2	86.1
228	39.2	7 960.1	86.7
229	39.4	8 035.7	87.2
230	39.6	8 111.9	87.8
231	39.8	8 188.7	88.4
232	39.9	8 266.2	89.0
233	40.1	8 344.3	89.5
234	40.3	8 423.1	90.1
235	40.5	8 502.6	90.7
236	40.7	8 582.7	91.3
237	40.9	8 663.5	91.9
238	41.1	8 745.0	92.5

239	41.2	8 827.2	93.1
240	41.4	8 910.0	93.7
241	41.6	8 993.6	94.3
242	41.8	9 077.8	95.0
243	42.0	9 162.7	95.6
244	42.2	9 248.4	96.2
245	42.4	9 334.7	96.8
246	42.6	9 421.8	97.5
247	42.8	9 509.5	98.1
248	43.0	9 598.0	98.8
249	43.2	9 687.2	99.4
250	43.5	9 777.2	100.1
251	43.7	9 867.8	100.7
252	43.9	9 959.2	101.4
253	44.1	10 051.4	102.0
254	44.3	10 144.2	102.7
255	44.5	10 237.9	103.4
256	44.7	10 332.3	104.1
257	44.9	10 427.4	104.7
258	45.2	10 523.3	105.4
259	45.4	10 620.0	106.1
260	45.6	10 717.4	106.8
261	45.8	10 815.6	107.5
262	46.1	10 914.6	108.2
263	46.3	11 014.4	108.9
264	46.5	11 114.9	109.6
265	46.7	11 216.3	110.3